Study on Charge Transport Properties through DNA by Nanoscale Electrical Measurements

A Dissertation
Presented to the Faculty of the Graduate School of Science
Osaka University

In Candidacy for the Degree of
Doctor of Science

by
Yoichi Otsuka

Dissertation Director: Professor Tomoji Kawai

"Genius was 1 percent inspiration and 99 percent perspiration."

Thomas Edison (1847 - 1931)

“Imagination is more important than knowledge."

Albert Einstein (1879 – 1955)

Acknowledgement

This thesis is dedicated to my parents

This work was carried out at the Institute of Science and Industrial Research, Department of Chemistry at the Osaka University during years 2000 – 2006.

I am deeply grateful to colleague at the laboratory, friends and my family. I definitely think it was impossible to accomplish this work without their existence.

I especially would like to express my gratitude to my supervisor, Professor Tomoji Kawai for supporting this work. His idea always inspired me to pursue challenging study.

I am also indebted to Professor Hitoshi Tabata and Professor Takuya Matsumoto for supporting this work. Professor Hitoshi Tabata gave me valuable advice on the analysis of results from a physical standpoint. Professor Takuya Matsumoto gave me valuable information especially for the development of measurement device.

I believe all their advice and guidance resulted in this productive result.

I would like to thank Dr. Hea-Yeon Lee for her help of my first study. I also would like to thank Dr. Yasuhisa Naitoh and Dr. Wataru Mizutani for collaboration. It was essential study to establish the fabrication method of electrodes for this work.

I would like to thank everyone in laboratory for his or her kind help and cooperation, especially Dr. Akihiko Takagi, Dr. Kaoru Ojima, Dr. Masateru Taniguchi, Dr. Shin-ichi Tanaka, Dr. Jian-hua Gu and Dr. Takashi Kanno and Satomi Tabuchi for their significant help and advice. I also would like to Professor Hidekazu Tanaka, Dr. Takeshi Yanagida, Dr. Teruo Kanki, Dr. Yasushi Hotta, Dr. Yohei Yamamoto, and Dr. Munetoshi Seki for enjoyable discussion regardless of the area of specialization. I want to thank Tomoko Yakabe, Tomohiko Nakamura, Kazumichi Yokota, Takuya Takahashi, Fumihiko Yamada, Dr. Toshihiko Matsuura, Dr. Eriko Mikamo, Hitomi Yamaguchi and Chiemi Takamori for cooperation and help.

I want to thank all my friends who helped me to go through these years. It would be impossible to brace myself to this challenging but formidable work without their enjoyable discussion. I especially thank to Shingo Tanaka, Nobuyuki Bokui, Shuhei Nakano, Makoto Omoto, Masayoshi Kawaguchi, Kazunobu Moriguchi, and Toshiko Miyazaki for our invaluable friendship.

I want to thank Mai Ikuma for her warm heart. Her kind attention always gives me repose, and encouragement sets me forward-looking person.

I would like to thank the Foundation Advanced Technology Institute and the Japan Society for the Promotion of Science for financial support.

Lastly, I dedicate this thesis to my father and mother, for teaching the importance of conceiving and acquiring knowledge by myself.

Abstract

Study on Charge Transport Properties through DNA by Nanoscale Electrical Measurements

Yoichi Otsuka
Osaka University
2006

DNA is very unique macromolecule not only from the viewpoint of biology, but also from that of physical chemistry. As for the structure of DNA, it was found that base molecules (A, T, G, C) inside double helix form the specific complementary hydrogen bonding[1]. The base sequence contains the essential information for the synthesis of compounds to maintain the living things. As the plane of π-conjugated base molecules connected by hydrogen bond are stacked each other through the strand, it was proposed that charge migration might occur through π–stacked base sequences[2].

The charge migration along DNA is treated as "the damaging of base sequences" from both of the biological and chemical viewpoints. The base molecules are oxidized in the charge migration process. Hence, the "charge transfer" of DNA in solution has been studied.

On the other hand, the charge migration is treated as "electrical conductivity" from both of the physical and chemical viewpoints. As the size of DNA is so small, extremely small electrical circuits may be fabricated if DNA can be utilized as molecular wire, switch and memory. Hence, the "charge transport" of DNA under dried state has been studied. However, various controversial results are reported so far. This would indicate various factors are involved in the experimental results.

This thesis focuses on the controlled direct electrical measurements of DNA with the "Electrode – DNA – Electrode" configuration in order to study the origin of discrepant results. Different methods are employed and / or newly developed, and electrical measurements are performed.

As a result, the electrical properties of DNA are measured under both of the condition that

[1] J. Watson, F, Crick, *Nature* **171**, 737 (1953).
[2] D.D Eley, D.I. Spivey, *Trans. Faraday. Soc.* **58**, 411 (1962).

the structure of DNA at the interface between electrodes and DNA is maintained and that counter ions exist around DNA. The temperature dependence of electrical property indicates the formation of electrical carrier due to counter ions and it is transported through the localized state along DNA. The conduction mechanism varies by both of the temperature and electric field between electrodes. These mechanisms are as follows; 1: Hopping Conduction at low electric field ($V < 0.1$V) and high temperature ($T > 150$K). 2: Frenkel-Poole Conduction at high electric field and high temperature. 3: Trap assisted tunneling at high electric field and low temperature.

The information obtained from these experiments is that the electrical properties of DNA are too much sensitive to the change of environment. Therefore, it was essentially needed to work out the proper measurement method. This method would be applicable not only to DNA, but also other soft materials in the next step.

Contents

List of Tables

List of Figures

DNA strands in the film was placed perpendicularly to electrodes and measured in the atmosphere, (2) the same film as (1) was measured in vacuum at 0.1 mmHg, and (3) DNA strands in the film was placed parallel to electrodes both in vacuum and atmosphere. (From the report by Y. Okahata, T. Kobayashi, H. Nakyama, K. Tanaka, *Supramolecular Science* 5, 317 (1998).)

Figure 1.2-6 *I-V* characteristic of 600-nm-long DNA rope. (From H.W. Fink, C. Schönenberger, *Nature* 398, 407 (1999).)

Figure 1.2-7 (a) *I-V* characteristics of a DNA molecule immobilized between Pt electrodes under atmospheric condition at room temperature. (b) *I-V* charactericstics that show that transport is indeed measured on DNA. The solid curve is measured after trapping a DNA molecule as in (a). The dashed curve is measured after incubation of the same sample for 1 hour in a solution with DNAse I enzyme. (From D. Porath, A. Bezryadin, S. de Vries, C. Dekker, *Nature* 403, 635 (2000).)

Figure 1.2-8 AFM images of DNA assembled in various devices. For all these devices, we observe an absence of conduction. (a) Mixedsequence DNA between platinum electrodes spaced by 40 nm. Scale bar: 50nm. (b) Height image of Poly(dG)-Poly(dC) DNA bundles on platinum electrodes. The distance between electrodes is 200 nm, and the scale bar is 1 μm. (c) High magnification image of the device shown in (b). Several DNA bundles clearly extend over the two electrodes. Scale bar: 200 nm. (d) Poly(dG)-Poly(dC) DNA bundles on platinum electrodes fabricated on a mica substrate. Scale bar: 500 nm. (From A.J. Storm, J. van Noort, S. de Vries, C. Dekker, *Appl. Phys. Lett.* 79, 3881 (2001).)

Figure 1.2-9 (**A**) Schematic drawing of the measured sample. (**B**) AFM image showing DNA molecules combed on the Re/C bilayer. The large vertical arrow indicates the direction of the solution flow. The small arrows point toward the combed molecules. (**C**) DC resistance as a function of temperature on a large temperature scale, showing the power law behavior down to 1 K. (From the report by A.Y. Kasumov, M. Kociak, S. Gueron, B. Reulet, V.T. Volkov, D.V. Klinov, H. Bouchiat, *Science* 291, 280 (2001).)

Figure 1.2-10 (a) Schematic illustration of the. (b) Relationship between resistance and DNA length. The exponential fitting plots of data are also shown. (c) Typical *I-V*

curves of Poly(dG)-Poly(dC), the linear Ohmic behaviors on L = 100 nm at the repeat measurement of five samples. (d) Rectifying curves of Poly(dG)-Poly(dC) at L = 100 nm. (From the report by L. Cai, H. Tabata, T. Kawai, *Appl. Phys. Lett.* 77, 3105 (2000).)

Figure 1.2-11 Three-dimensional SFM image of the channel border, showing two DNA molecules in contact with the left gold electrode. It is also presented the scheme of the electrical circuit used to measure the DNA resistivity. (From the report by P.J. de Pablo, F. Moreno-Herrero, J. Colchero, J, Gomez Herrero, P. Herrero, A.M. Baro, P. Ordejon, J.M. Soler, E. Artacho, Phys. Rev. Lett. 85, 4992 (2002).)

Figure 1.2-12 (a) AFM images (scale bar, 10 nm) of a three-terminal single DNA molecule device at source–drain distance (d_{DS}); 25 nm are shown. NT, P1, P2 indicate SWCNT (gate), first CNT probe (source), and second one (drain), respectively. (b) I_{DS}–V_{DS} curves for various gate voltages (V_G)=0, 1, 2, 3, 4, and 5 V is shown. (From the report by H. Watanabe, C. Manabe, T. Shigematsu, K. Shimotani, M. Shimizu, *Appl. Phys. Lett.* 79, 1 (2001).)

Figure 1.2-13 (a) SEM Image of the nanogap electrode separated by 20 nm. (b) SEM image of a Poly(dG)-Poly(dC) DNA molecule trapped between two electrodes. (c), (d) The *I-V* curves measured at room temperature for various values of the gate voltage for Poly(dA)-Poly(dT) (c) and Poly(dG)-Poly(dC) (d). In the inset of (c), the conductance at V = 0 is plotted as a function of gate voltage for Poly(dA)-Poly(dT). The inset of (d) is the schematic diagram of electrode arrangement for gate dependent transport experiments. (From the report by K.-H. Yoo, D.H. Ha, J.-O. Lee, J.W. Park, J. Kim, J.J. Kim, H.-Y. Lee, T. kawai, H.Y. Choi, *Phys. Rev. Lett.* 87, 198102 (2001).)

Figure 1.2-14 *I-V* characteristics measured in vacuum at room temperature on *M*-DNA (○) and *B*-DNA (●) molecules. Lower inset shows a schematic experimental layout. (From the report by A. Ratkin, P. Aich, C. Papadopoulos, Y. Kobzar, A.S. Vedeneev, J.S. Lee, J.M. Xu, *Phys. Rev. Lett.* 86, 3670 (2001).)

Figure 1.2-15 The *I-V* characteristics of a Poly(dG)-Poly(dC) [(a) and (b)] and Poly(dA)-Poly(dT) [(c) and (d)] DNA films. The *I-V* curves in an air showed in (a) and (c), whose difference shows the typical fluctuations of our data. The data in an oxygen ambient exhibited (b) and (d). The distance between the

electrodes was about 100 nm. The *I-V* characteristics were measured several times, and the measured *I-V* curves were found to be quite reproducible. (From the report by H.-Y. Lee, H. Tanaka, Y. Otsuka, K.-H. Yoo, J.-O. Lee, T. Kawai, *Appl. Phys. Lett.* 80, 1670 (2002).)

Figure 1.2-16 *I-V* and the *dI*/*dV*–*V* characteristics measured from the electrodes with the gap of 20 nm after dropping the diluted DNA solution. There are clear staircases in the *I-V* and maxima are observed in the *dI*/*dV*–*V*. The inset shows the *I-V* measured between the 20 nm gap electrodes after dropping the DI water. (From the report by J.S. Hwang, K.J. Kong, D. Ahn, G.S. Lee, D.J. Ahn, S.W.Hwang, *Appl. Phys. Lett.* 81, 1134 (2002).)

Figure 1.2-17 (a) The schematic of the incorporation of deoxynucleoside triphosphates into lambda DNA sticky ends using the Klenow fragment. (b) *I-V* characteristics for a sample of lambda DNA bridging two parallel Au electrodes separated by 4 μm. The DNA was rinsed with NH_4Ac before the measurement to remove the buffer salt residue. The dashed line is a linear fit to the data. The inset shows the *I-V* curve for a test chip containing TE buffer solution (without DNA). The chip was dried in vacuum but not subject to NH_4Ac rinsing. The observed conductance is entirely from trace TE salt residue. Both measurements were done in vacuum at 295 K. (From the report by Y. Zhang, R.H. Austin, J. Kraeft, E.C. Cox, N.P. Ong, *Phys. Rev. Lett.* 89, 198102 (2002).)

Figure 1.2-18 (a) Above: the Au electrode geometry. Below: sketch of the disulfide-labeled lambda DNA molecules used in this work. The nicked DNA features a gap between the 3' and 5' nucleotides, where indicated. In the repaired DNA, the gaps were repaired using T4 DNA ligase. (b) *I-V* characteristics measured at room temperature on disulfide-labeled l-DNA molecules. Dashes: repaired DNA; dots: nicked DNA, swept from negative to positive potential; solid line: nicked DNA, swept from positive potential to negative potential. (From the report by B. Hartzell, B. McCord, D. Asare, H. Chen, J.J. Heremans, V. Soghomonian, *Appl. Phys. Lett.* 82, 4800 (2003).)

Figure 1.2-19 (a) AFM height image of several small DNA ropes contacted by gold leads separated by 1 μm. The scan width is 2.5 μm. (b) AFM height image of a dense DNA network contacted by 15-nm-thick, 12-μm-wide AuPd leads separated by 1 μm. The scan size is 8 μm. (c) *I-V* characteristics of a dense DNA network

position of electrodes is also noted, and it is correspond to the position of aligned electrode as shown in figure 2.3-3 (a).

Figure 2.3-6 (a) Molecular structure of TPPS. Left and right structure correspond to the free-base form and dianion form, respectively. (b) TPPS nanorods on sapphire substrate observed by AFM. (c) UV-Vis absorbance spectrum of TPPS molecules in solution and as nanorods. The straight line corresponds to the solution and the dotted line to a nanorod.

Figure 2.3-7 (a) Current-voltage characteristics of TPPS nanorods under the vacuum condition for seven samples. (b) Current change of TPPS nanorods under various conditions. (c) and (d) Current change in TPPS nanorod under oxygen and nitrogen gas conditions, respectively. The current was measured under 4 V of applied bias voltage.

Figure 2.3-8 CD spectrum of TPPS nanorod under various environmental conditions. Upper and lower graph show experimental results and differential results between different environmental conditions, respectively.

Figure 3.1-1 (a) SEM image of comb-shaped nanogap electrodes. Each electrodes are separated 100 nm, respectively. (b) Morphology of dried DNA films. Poly(dG)-Poly(dC) DNA formed dendrite structure. Concentration of DNAs is 1.25 μg/μl.

Figure 3.1-2 Typical *I-V* curves of DNA film (Poly(dG)-Poly(dC)). Squares and triangles indicate the *I-V* curve measured in vacuum and the atmospheric condition at the relative humidity of 28%, respectively.

Figure 3.1-3 Relationship between relative humidity and resistance of DNA film. Resistances are estimated from the *I-V* measurements at the voltage of –2 V under each relative humidity condition.

Figure 3.1-4 (a) Cole-Cole plot of DNA at 83% relative humidity. Solid line and dotted line indicate the measured result and the fitted curve, respectively. The equivalent circuit adopted for fitting is shown in the inset. R_S, R1 and C1 are calculated to be $3.2\times10^{2}\,\Omega$, $1.5\times10^{3}\,\Omega$ and 1.6×10^{-10} F, respectively. ◆ (83%), ▼ (70%) and ● (50%). (b) AC measurement of capacitance vs. frequency of applied electric field (25 mV) under various relative humidities.

Figure 3.2-1 (a) Topographic image of DNA network on mica substrate. The gold electrode

List of Abbreviations and Symbols

A	Adenine
A	Acceptor
Å	angstrom
AC	alternating current
Ac	acetyl group
AFM	Atomic Force Microscope
Al	Alminum
Al_2O_3	aluminum oxide
APS	aminopropyltrimethoxysilane
ArF	argon-fluorine
Au	Gold
β	characteristic decay parameter
bp	base pair
C	Cytosine
CD	circular dichroism
$CHCl_3$	chloroform
CM-AFM	contact mode atomic force microscope
CNT	carbon nanotube
Co	cobalt
Cr	chromium
D	donor
d	distance
DC	direct current
dATP	2'-Deoxyadenosine 5'-triphosphate
dGTP	2'-Deoxyguanosine 5'-triphosphate
℃	degree centigrade
DNA	deoxyribonucleic acid
E	electric field
Ea	activation energy
EB	electron beam
eV	electronvolt
ε_0	the vacuum dielectric constant
EDTA	ethylenediaminetetraacetic acid
EtOH	ethanol
G	Guanine
GΩ	gigaohm
H	Plank's constant
HCl	hydrogen chloride
HEPES	2-[4-(2-Hydroxyethyl)-1-piperazinyl] ethanesulfonic Acid
HOMO	highest occupied molecular orbital
HOPG	highly oriented pyrolytic graphite
Hz	Hertz
H_3PO_4	orthophosphoric acid

I	current
J	joule
K	Kelvin
KCl	potassium chloride
LEEPS	low-energy electron point source
LUMO	lowest unoccupied molecular orbital
M	mega
M	molarity
mbar	millibar
$MgCl_2$	magnesium chloride
$MgSO_4$	magnesium sulfate
mmHg	millimeter mercury column
μm	micrometer
μl	microliter
mV	millivolt
MWCNT	multi walled carbon nanotube
m*	effective mass
N	Newton
N_2	nitrogen
Na	sodium
NaCl	sodium chloride
nm	nano meter
nN	nano newton
O_2	oxygen
Ω	ohm
%	percent
Pa	pascal
pA	picoamper
PC-AFM	point contact atomic force microscope
PCI-AFM	point-contact current-imaging atomic force microscope
pH	hydrogen-ion concentration exponent
Pt	platinum
q	electric charge
R	resistance
REG	regulate
Rh	rhodium
RHEED	reflection high-energy electron diffraction
RMS	root square measn
Ru	ruthenium
ρ	resistivity

S	siemens
S	sulfur
sec	second
SEM	scanning electron microscope
Si	silicon
SiO_2	silicon dioxide
SnO_2	tin oxide
STM	scanning tunneling microscope
SRM	spreading resistance mode
SWCNT	single walled carbon nanotube
T	Tymine
T	tera
T	temperature
TCE	top-contacted geometry electrode
TE	Tris – EDTA
Ti	titanium
TM-AFM	tapping mode atomic force microscope
TPPS	5,10,15,20 - tetraphenyl - 21H, 23H - porphyrine tetrasulfonic acid
TPS	trimethoxypropylsilane
TTL	transistor transistor logic
Tris	tris-(hydroxymethyl) aminomethane
dTTP	2'-Deoxythymidine 5'-triphosphate
UV	ultraviolet radiation
V	voltage
W	tungsten
Zn	zinc

Chapter1

General Introductions

1.1. Structure of DNA

Deoxyribonucleic acid (DNA) is a biological molecule that contains generic information to maintain organisms. The synthesis of amino acid, that is essential to build an organ, is based on the information derived from the sequence of base molecules. Base molecules are classified into two compounds, pyrimidine and purine. Adenine (A) and guanine (G) are purine bases; thymine (T) and cytosine (C) are pyrimidine bases. (Figure 1.1.1 (a))

As it is not allowed to disarrange the order of base sequnece, the structure of DNA is found to be quite unique in order to protect them from external damage. Watson and Click found that the structure of DNA is double stranded [1]. The double stranded structure is composed of two DNA strands that are interacted in the antiparallel manner each other.

Single DNA strand is composed of polynucleotide in which the nucleotide is connected through the phosphodiester linkage. A nucleotide is composed of base, sugar and phosphate and connected each other in this order. (Figure 1.1.1 (b)) The specific feature of polynucleotide is the complementary interaction between base molecules. G bonds specifically to C and A bonds to T through hydrogen bonds, respectively. Thus, these specific pairings of bases permit the duplication of genetic information (Figure 1.1.1 (c)). Moreover, as phosphate groups surround the double stranded structure, DNA is stable in water.

The structure of double helix is variable due to the freedom of the conformational change of nucleotide. The structure proposed by Watson and Click is referred to as B-form. The B-form is the most stable structure for a DNA with random sequence. On the other hand, different structures have been also characterized in a crystal structure. The A form is favored in many solutions that are relatively devoid of water. The DNA is still arranged in a right- handed double helix, but the helix is wider and the number of base pairs per helical turn is 11, rather than 10.5 as in B-DNA. Z-form DNA is quite different from the B structure; the most obvious distinction is the left-handed helical rotation. There are 12 base pairs per helical turn, and the structure appears more slender and elongated. The DNA backbone takes on a zigzag appearance. Certain nucleotide sequences fold into left-handed Z helices much more readily than others. These Z-DNA tracts may play a role (as yet undefined) in the regulation of the expression of some genes or in genetic recombination. (Figure 1.1.1 (d))

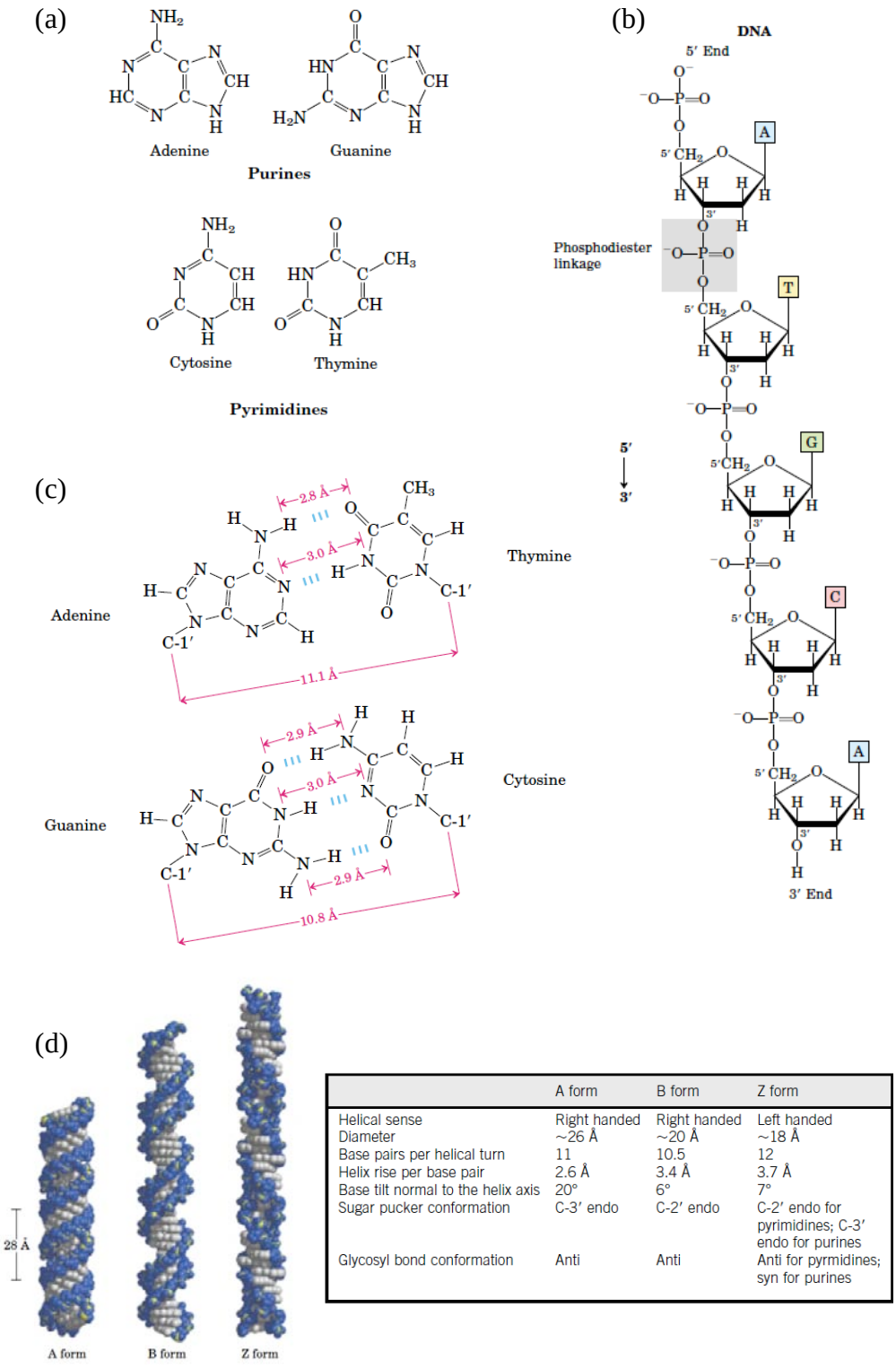

	A form	B form	Z form
Helical sense	Right handed	Right handed	Left handed
Diameter	~26 Å	~20 Å	~18 Å
Base pairs per helical turn	11	10.5	12
Helix rise per base pair	2.6 Å	3.4 Å	3.7 Å
Base tilt normal to the helix axis	20°	6°	7°
Sugar pucker conformation	C-3′ endo	C-2′ endo	C-2′ endo for pyrimidines; C-3′ endo for purines
Glycosyl bond conformation	Anti	Anti	Anti for pyrmidines; syn for purines

Figure 1.1-1
(a) Molecular structure of base molecules. (b) Molecular structure of polynucleotide. (c) Complementary base pairs through hydrogen bonds. (d) Structure of double helix. (From *Lehninger Principles of Biochemistry, 3rd Ed.*)

1.2. Experimental Results

The paired base molecule (A-T and G-C pair) forms the plane of π–conjugated compounds (Figure 1.1-1 (c)). As these planes are stacked each other inside double helix, it has been proposed that charge migration might occur through π–stacked structure [2]. The *p* orbitals perpendicular to the plane of π–conjugated compounds form delocalized molecular orbitals. The delocalized molecular orbitals as a result of side-to-side overlap are classified into two kinds; π bonding and π^* antibonding molecular orbitals. The energy gap between two orbitals is around 4 eV [3]. Moreover, the strong coupling between adjacent base pairs may lead to extended states in the direction vertical to the plane of π–conjugated compounds. Therefore, it is expected the metallic behavior for the vanishing gap, or the semiconductive behavior in the case of a non-vanishing gap, with a possibility of doping by electrons or holes, in analogy with conventional semiconductors [4].

This idea has stimulated researchers to study the electrical properties of DNA enthusiastically from both of biological and physicochemical viewpoint.

As biological viewpoint, it is important to elucidate the electrical properties of DNA because the charge migration along π–stacked structure would cause the damage to base molecules due to the oxidative reaction. Hence, most study targets the measurement of DNA in solution. The phenomenon of charge migration along DNA in this system is usually noted as “charge transfer” because the charge migration occurs spontaneously according to the electrical potential difference between base molecules, and the distance of migration is relatively shorter than that of studied from the physicochemical viewpoint as noted next.

Then, as physicochemical viewpoint, it is important to elucidate the electrical properties of DNA because DNA might be encouraging material. Amid growing concern over the limitation of miniaturization technique of semiconductor, it is required to find novel materials to overcome this problem. As the size of DNA molecule is known to be 2 nm in diameter it may be possible to fabricate the smaller electrical circuits than conventional one. Moreover, as it is possible to synthesize DNA with controlled base sequences, it might be possible to control the electrical properties of DNA and fabricate elemental devices such as conductive wire and switching devices.

Based on these motivations, electrical measurements are mostly performed for dried DNA molecules that are connected to metal electrodes. The phenomenon of charge migration along DNA in this system is usually noted as “charge transport” because the distance of migration is

larger compared to the “charge transfer” phenomenon in solution, and/or the main driving force of charge is supplied by applying bias voltage between electrodes.

In this section, previous results both of “charge transfer” and “charge transport” are shown, and the reason of controversial results in “charge transport” studies is discussed.

Charge Transfer of DNA in solution

Charge transfer is already known as fundamental chemical process. The physics of charge transfer is often explained by the semi-classical Marcus theory [5]. This theory predicts the charge transfer efficiency in large molecules such as proteins that falls off as $e^{-\beta r}$ with $\beta = 1.5\,\text{Å}$. On the other hand, β-value for DNA was first reported to $\beta = 0.2\,\text{Å}$ [6]. This value was surprisingly smaller than expected, and the possibility of long rage charge transfer along DNA was shown. Therefore, charge transfer of DNA has been studied vigorously after the interesting results reported by Barton group at the beginning of 1990.

Measurement of charge transfer rate is performed for synthesized DNA in solution. The synthesized DNA molecules used for experiments are mainly classified into two cases.

One is based on the photochemical experiments. Donor (D) and acceptor (A) are incorporated in DNA and the excited-state quenching of D by A is measured. [7-12] For example, $Ru(phen)^{2+}_3$ was used for D and Co(III) and Rh(III) are used for A [13-15]. (Figure 1.2-1)

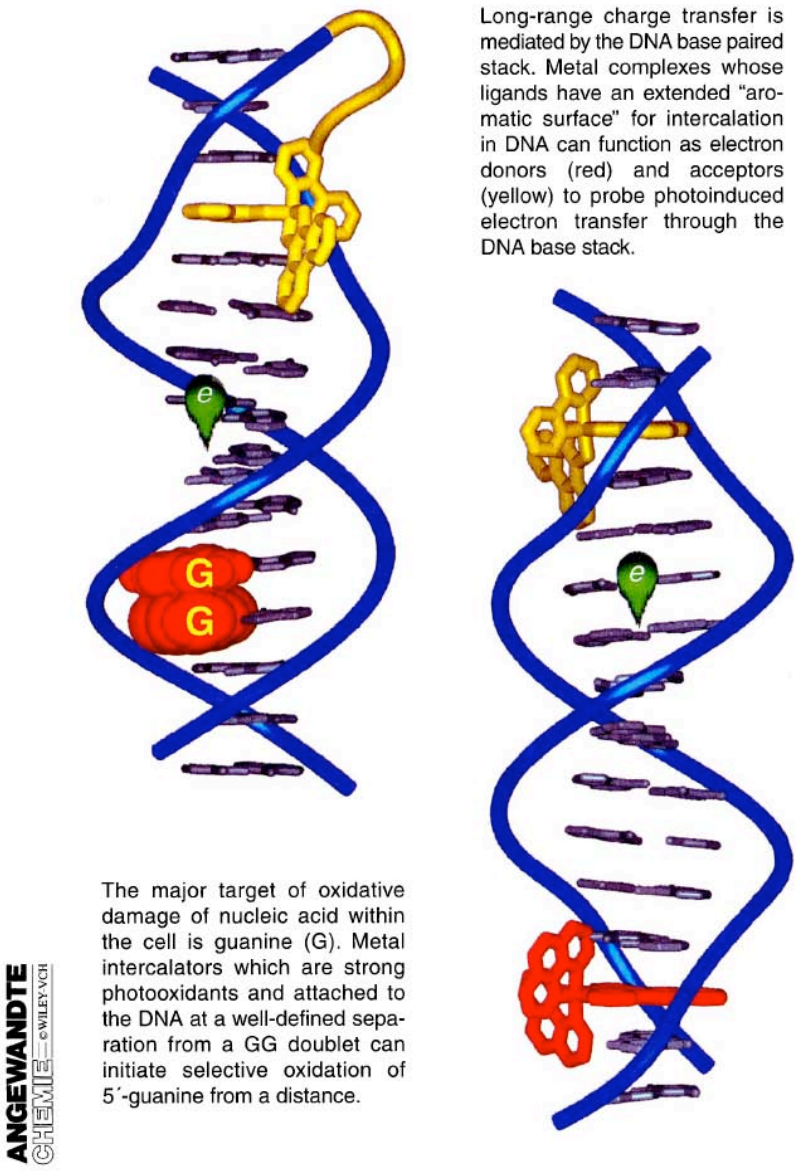

Figure 1.2-1
Illustration of the charge transfer between donor and acceptor bound to DNA. Electron donor and acceptor are $[Ru(phen)z(dppz)]^{2+}$ (red) and $[Rh(phi),(bpy)]^{3+}$ (yellow), respectively. (From the cover image of R.E. Holmlin, P.J. Dandliker, J.K. Barton, *Angew. Chem. Int. Ed. Engl.* 36, 2714 (1997).)

Other stydy is based on the synthetic chemistry. Guanine is selectively oxidized immediately after the formation of an adjacent deoxyribose radical cation by Norrish I cleavage of ketone (Figure 1.2-2 (a)). This is because G is the most favorable site for location of holes due to the order of the ionization potentials (G < A < T < C) [16-18]. (G is easy to be oxidized compared to other base molecules) After the formation of radical cation ($G^{+\cdot}$), it migrates along base sequences spontaneously, stops at GGG sequence and due to the formation of GGG^{+}. DNA with GGG^{+} was cleaved at the position GGG^{+} exist by the piperidine treatment. The amount of DNA with different length was measured by electrophoresis, and the relative rate coefficients of the charge transfer were estimated [19-21]. (Figure 1.2-2 (b))

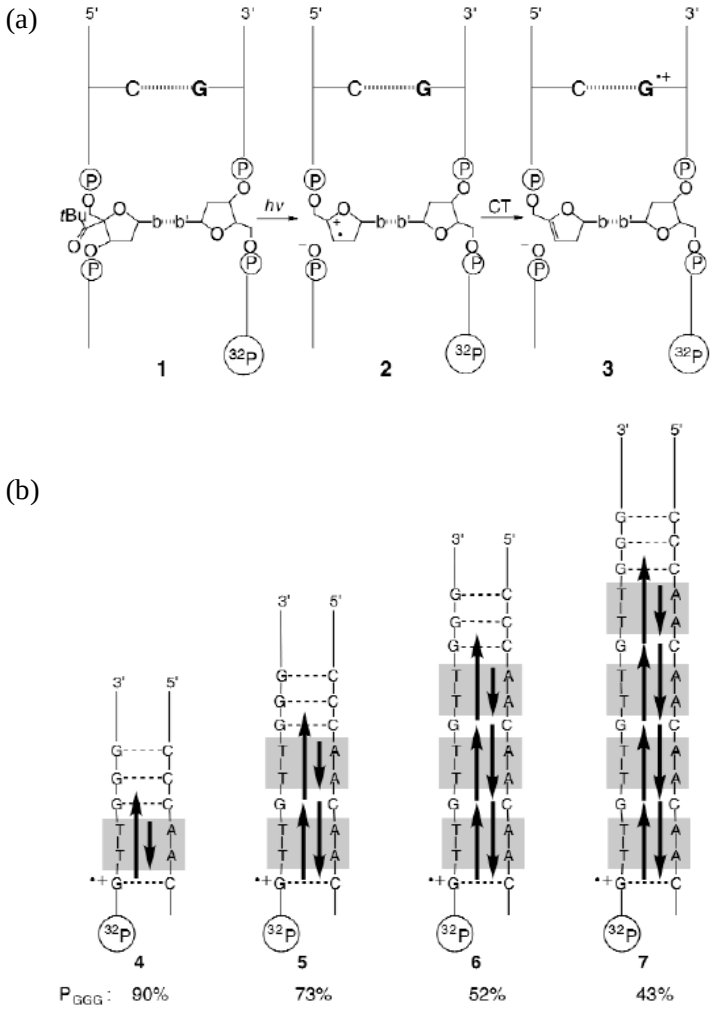

Figure 1.2-2
(a) Assay for the charge injection into a guanine. (b) Yield of H_2O-trapping products at the GGG sequence (P_{GGG}) in long-distance charge transfer by a hopping between guanines (G). (From B. Giese, M. Spichty, S. Wessely, *Pure Appl. Chem.* 73, 449 (2001).)

The rate of charge transfer is strongly affected by both of the length of DNA and base sequences. (Figure 1.2-3) The mechanism of charge transfer is a combination of "superexchange" and "multistep thermally induced hopping". In case the distance between $G^{+\cdot}$ and GGG is short, the rate-limiting step is "superexchange" that is coherent transfer. On the other hand, in case the distance is long, the rate-limiting step is "multistep thermally induced hopping" that is incoherent transfer [22]. Moreover, as the experiments target DNA in solution, there is an interaction between $G^{+\cdot}$ and water molecules. The reaction of $G^{+\cdot}$ to water molecules cause the oxidized guanine, and charge transfer stops. The rate of this reaction is two orders smaller than those of charge transfer, but may not in case the distance is long. Therefore the efficient distance for charge transfer is limited to be about a few tens of angstrom at most.

As summery, the charge transfer phenomenon is occurred along G site distributed in base sequences. This is because the HOMO of G is higher than other base molecules (A, T, C), and G is easily oxidized. The distance between G sites limits the transfer rate strongly. These relatively consistent results by chemical experiments indicated the evidence that charge can migrate along π-stacked base sequences. Followed by these findings, measurements of charge transport properties have been studied as noted in the next section.

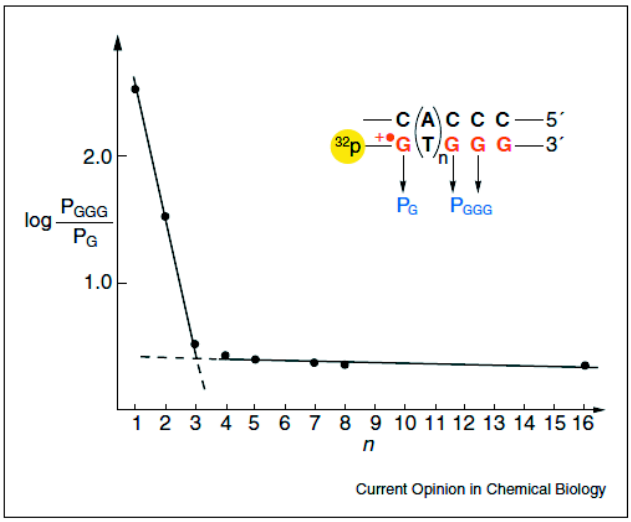

Figure 1.2-3

The relationship between the efficiency of charge transfer and the number of A:T base pairs that intervene between G and GGG sequence. The efficency is measured by the ratio of the cleavage products P_{GGG}/P_G that are formed by water trapping of the guanine radical cations. The A:T base pairs do not carry the charge, they are the bridge between the electron donor and electron acceptor. The flat line shows that at long (A:T)n sequences the distance dependence vanishes. This is explained by a change of the reaction mechanism where also the adenines act as charge carriers. (From B. Giese *Curr. Opin. Chem. Biol.* 6, 612 (2002).)

Charge Transport of DNA under solid state

The charge transport property of DNA has been studied after the findings of charge transfer phenomenon. The experimental approach to measure the charge transport property is fairly different from that of charge transfer property. Whereas DNA is present in the solution in the charge transfer study, DNA is present under solid (dried) state in the charge transport study.

One of the main motivations for this study is whether it is possible to conduct an electrical current through dried DNA molecules. This is because if it is possible to utilize DNA molecules as molecular electronic wire, highly integrated molecular-based computer might be emerged in the next-generation.

For this purpose, it is important to measure the electrical properties under the condition that DNA molecules are connected to metal electrodes on the substrate. Then, the electrical measurement of DNA with the "Electrode – DNA – Electrode" configuration has been performed so far. Then, the various results are shown in the next section.

Review of the electrical measurement of DNA

In 1998, Braun et al. performed the first electrical measurement. [23] (Figure 1.2-4) The electrical conductivity of 16-μm-long lambda DNA was studied. Lambda DNA was connected to the Au electrode fabricated on the glass substrate. The electrodes were separated by 12 - 16 μm. The connection between lambda DNA and electrodes were made by hybridizing two distant surface-bound 12-base oligonucleotides with a fluorescently labeled lambda DNA that contains two 12-base sticky ends, where each of the ends was complementary to one of the two different sequences attached to the Au electrodes. (Figure 1.2-4 (a)) Electrical measurements showed no observable current up to 10V. (Lower inset of figure 1.2-4 (b)) Hence it is concluded that DNA is insulative.

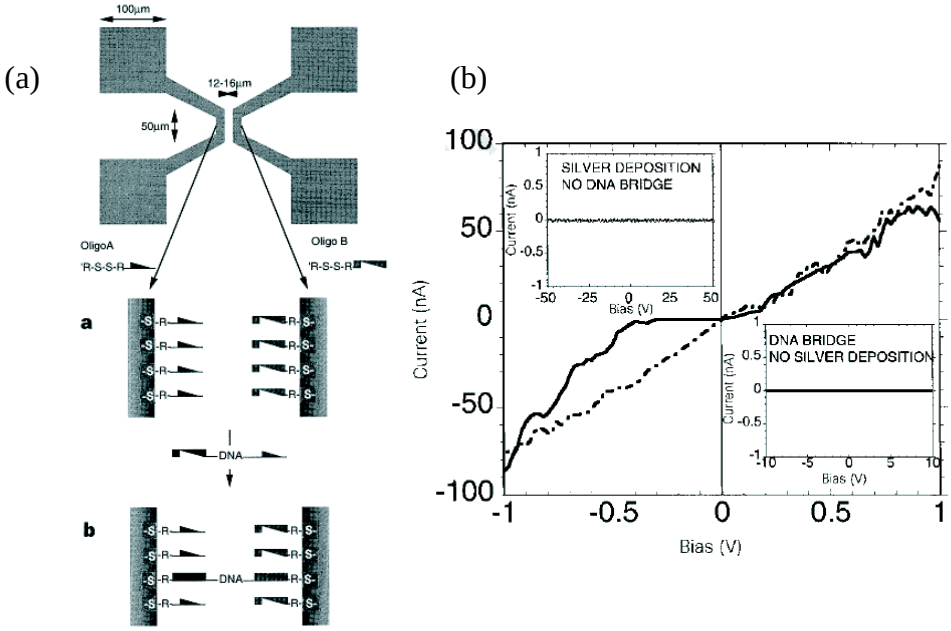

Figure 1.2-4
(a) The procedure of DNA immobilization between electrodes. First, 12-base oligonucleotides with two different sequences attached to the electrodes. Then lambda DNA is connected to electrodes by the hybridization with oligonucleatides. (b) *I-V* characteristics of fabricated samples. They are also measured the electrical properties of silver stained DNA nanowire. The main plot shows the *I-V* characteristic of silver nanowire. Please see the lower inset that shows the *I-V* characteristics of DNA moleucules connected to electrodes. (From E. Braun, Y. Eichen, U. Sivan, G. Ben-Yoseph, *Nature* 391, 775 (1998).)

In 1998, Okahata et al. reported the electrical conductivity of DNA-aligned cast film [24]. (Figure 1.2-5 (a)) DNA was taken from salmon testes and it was mixed with cationic amphiphiles. The polyion complex precipitates were gathered and freeze-dried. The white powder was only soluble in organic solvents. Then the powder was dissolved in the $CHCl_3$ / EtOH solution and it was deposited on the Teflon plate. After the solvent was evaporated, the transparent film was obtained. In the film of the DNA-lipid complex, DNA strands could be aligned in the same direction that the film was stretched. The stretched DNA film was put on the comb-shaped Au electrode, and DC conductivity was measured.

As shown in the figure 1.2-5 (b), the *I-V* characteristics of the DNA film in which DNA strands aligned perpendicular to the electrodes showed the large ohmic current under both of atmospheric and vacuum (10^{-1} mmHg (Torr)) condition. On the other hand, the *I-V* characteristics of the DNA film in which DNA strands aligned parallel to electrodes showed

observable current. Therefore, it was concluded that electric currents might pass through stacked base pairs of the aligned DNA strands. The conductivity was calculated to be 5.6×10^{-5} and 10^{-9} S cm^{-1} for parallel and perpendicularly immobilized DNA. This value was compared with fragile conductive polymers (polyacetylene and polyphenylene; 10^{-3} – 10^{-1}), and the value was found to be reasonable.

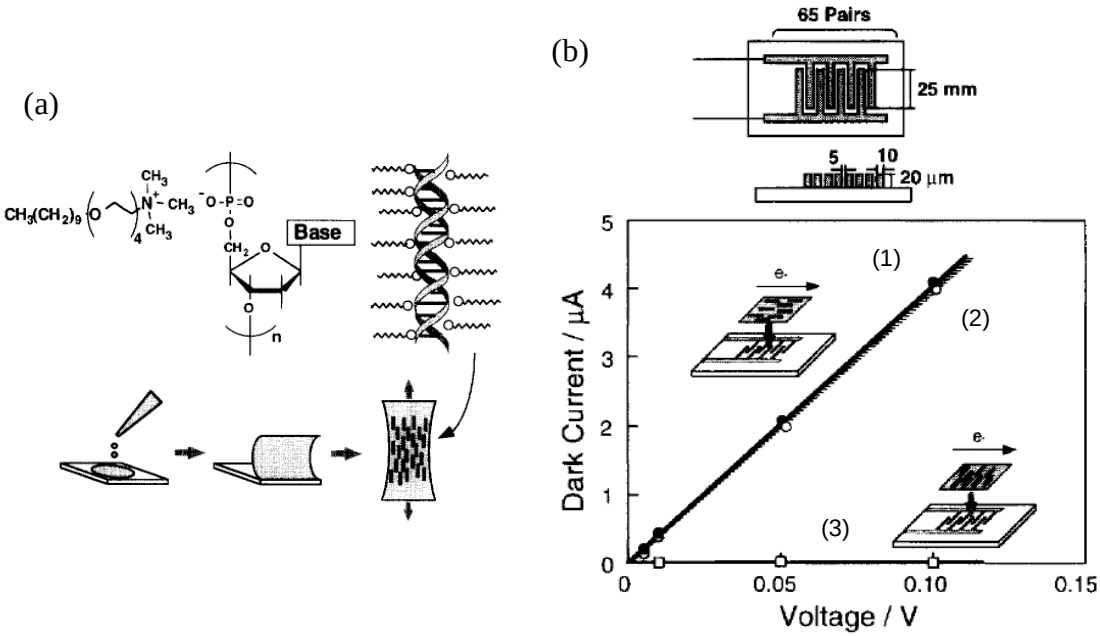

Figure 1.2-5
A schematic diagram and a photograph of DNA-lipid complex cast film. (b) Dark current of aligned-DNA films on comb-shaped electrodes at 25 ℃. (1) DNA strands in the film was placed perpendicularly to electrodes and measured in the atmosphere, (2) the same film as (1) was measured in vacuum at 0.1 mmHg, and (3) DNA strands in the film was placed parallel to electrodes both in vacuum and atmosphere. (From the report by Y. Okahata, T. Kobayashi, H. Nakyama, K. Tanaka, *Supramolecular Science* 5, 317 (1998).)

Nakayama et al. also reported the detailed study in 2001 [25]. They prepared the similar DNA-aligned cast film and its DC conductivity in a dry box was measured. Two different length of DNA taken from salmon testes were used. The stretched DNA film was put on the comb-shaped electrodes that were separated 5μm each other so as the direction of DNA strands were perpendicular to the electrodes.

In case the DNA film with long DNA (10 μm) was measured, a large ohmic current was again measured in the range of ±0.5 V. The conductivity was estimated to be 5×10^{-3} S cm^{-1}. On the other hand, in case the DNA film with short DNA (0.2 μm) was measured, very small

ohmic current was measured, but it diminished within 5 sec. Moreover, temperature dependence of Cole-Cole plots was studied. As for the DNA film with long DNA, the apparent resistances at the zero imaginary of impedance were constant at 400 Ω independent of temperature from 25 to 60 ℃. On the other hand, as for DNA film with short DNA, the resistance was increased to 100 – 650 kΩ depending on temperature, and semi-circle form was observed in the plot.

Thus it was concluded that temperature independent conductance of the film with long DNA indicates electron conductance along intramolecular DNA strands, and the temperature-dependent conductance of the film with short DNA indicated the small ionic transport between DNA molecules.

In 1999, on the other hand, Fink et al. reported nearly ohmic *I-V* characteristics through lambda DNA ropes [26]. (Figure 1.2-6) Lambda DNA ropes were first immobilized across the 2mm-wide holes in a Au-covered carbon grid by dropping DNA solution. DNA solution contains 0.3 μg/ml DNA, 10 μM Tris-HCl and 1 μM EDTA (pH 8). The ropes were then observed by low-energy electron point source (LEEPS) microscope. After the suitable ropes were found, manipulation tip (tungsten) that was introduced into the ultrahigh vacuum chamber (~10^{-7} mbar) was controlled to move to the position that the DNA ropes exits. Finally, the tip was contacted to the DNA ropes and electrical measurements were performed. As it was possible to control the length of DNA rope between Au-covered carbon grid and manipulation tip, *I-V* characteristics of different DNA ropes were measured.

In case of 600-nm-long DNA rope, linear and fluctuated *I-V* characteristics were measured at the bias voltage of within ± 20 mV and above this range, respectively. The estimated resistance was about 2.5 MΩ. In case of 900-nm-long DNA rope, the resistance was estimated to be 3.3 MΩ. It was also reported that the estimated values of resistance include the unknown contact resistance between metal electrode and DNA. Measurements were performed under vacuum condition, and hence the ionic conduction would not be applicable to the conduction mechanism. However, there was a room that the residual buffer, counter ions around DNA might affect the electrical properties of DNA. Moreover, even if the energy of imaging electrons are limited to be between 20 and 300 eV, there was still a room that such electrons irradiated to DNA ropes might cause contaminations around DNA ropes.

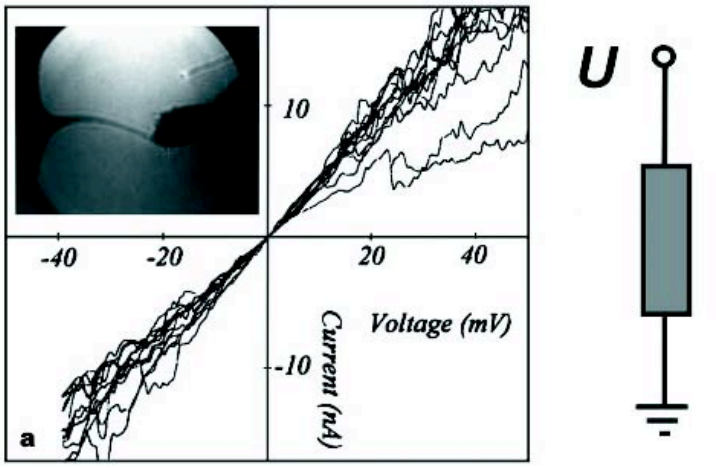

Figure 1.2-6
I-V characteristic of 600-nm-long DNA rope. (From H.W. Fink, C. Schönenberger, *Nature* 398, 407 (1999).)

In 2000, Porath et al. reported a different electrical property of synthesized DNA. [27] (Figure 1.2-7) The DNA was obtained by the hybridization between two different 30-base oligonucleotides. The base sequence was Polyd$(G)_{30}$ and Poly d$(C)_{30}$, respectively. DNA solution contains 300mM NaCl, 10mM Na citrate and 5mM EDTA. DNA was trapped between Pt electrodes by electrostatic trapping method. About one DNA molecule exist for $(100\ nm)^3$. The gap size between electrodes was controlled to be 8 nm.

Electrical measurements under atmospheric condition (relative humidity 50 %) showed nonlinear *I-V* characteristics with threshold voltage about a few volts for 20 different samples. After such characteristics were measured, DNA immobilized electrodes were incubated in a solution containing DNAse I, an enzyme that specifically cut double-stranded DNA. After this treatment, no significant current was measured. Hence it was suggested that the electrical property was actually originated from DNA immobilized between electrodes. Moreover, temperature dependence of electrical properties was also studied under the range from 4 K to 300 K. The differential conductance *dI/dV* versus *V* exhibited a peak structure, with a peak spacing of 0.1 to 0.5 eV. The *I-V* curves for tree different samples showed the voltage gap at low temperature, and the width of the gap was increased with increasing temperature.

Authors concluded that Poly(G)-Poly(C) DNA is a large-bandgap semiconductor, and the electrical contact between metal electrodes and DNA would be originate from the offset between the Fermi level of electrodes and the molecular energy bands of DNA molecule.

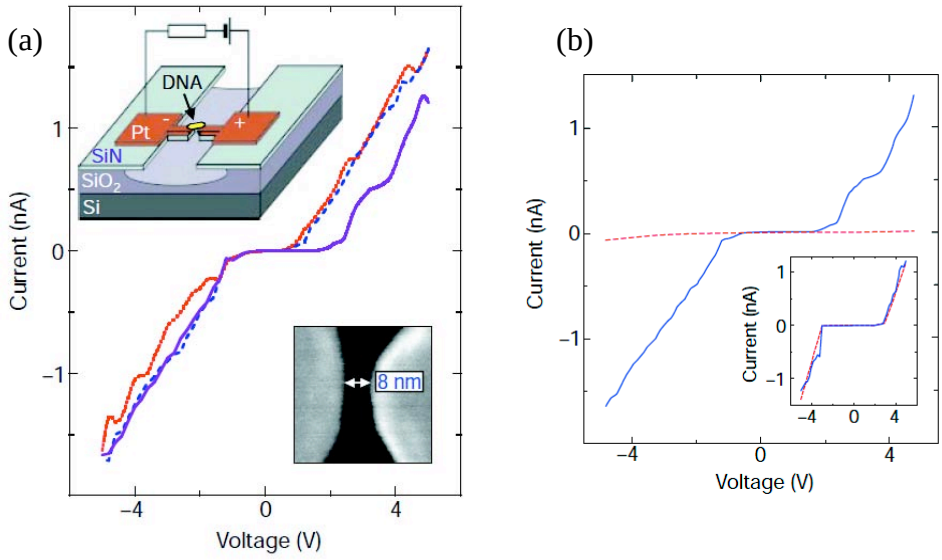

Figure 1.2-7
(a) *I-V* characteristics of a DNA molecule immobilized between Pt electrodes under atmospheric condition at room temperature. (b) *I-V* characterics that show that transport is indeed measured on DNA. The solid curve is measured after trapping a DNA molecule as in (a). The dashed curve is measured after incubation of the same sample for 1 hour in a solution with DNAse I enzyme. (From D. Porath, A. Bezryadin, S. de Vries, C. Dekker, *Nature* 403, 635 (2000).)

In addition, Storm et al. performed the expanded study in 2001 [28]. They measured the electrical characteristics both of individual DNA molecules and small DNA bundles (up to tens of molecules) that were connected to metallic electrodes. (Figure 1.2-8) The well-defined electrodes with nanogap ranging from 40 - 500 nm were employed. The electrodes were fabricated by electron-beam lithography and subsequent liftoff process. Pt or Au was used for electrode material, and the thickness was about 15 nm on top of a 3-nm-thick titanium sticking layer.

Results indicated no evidence of any electronic conductivity for DNA molecules with various length and base pair sequences. In case the DNA molecules with mixed-sequence was immobilized between Au electrodes spaced by 300 nm, the resistance was measured to be more than 10 TΩ that was lower limitation of the measurement device.

Moreover, in case Poly(dG)-Poly(dC) DNA molecules (100 ng/μl in buffer solution of 20 mM HEPES and 5 mM $MgCl_2$) were immobilized between platinum electrode spaced by 100 nm on SiO_2 substrate, the bundled DNA molecules were observed by AFM. However, the resistance was the same as mixed-sequence DNA, and no conduction was found again. Finally,

Poly(dG)-Poly(dC) DNA molecules were immobilized between platinum electrodes separated by 200 nm on mica substrate. Nonetheless, The result was the same as other results. As conclusion, DNA molecules were insulating at length scales longer than 40 nm.

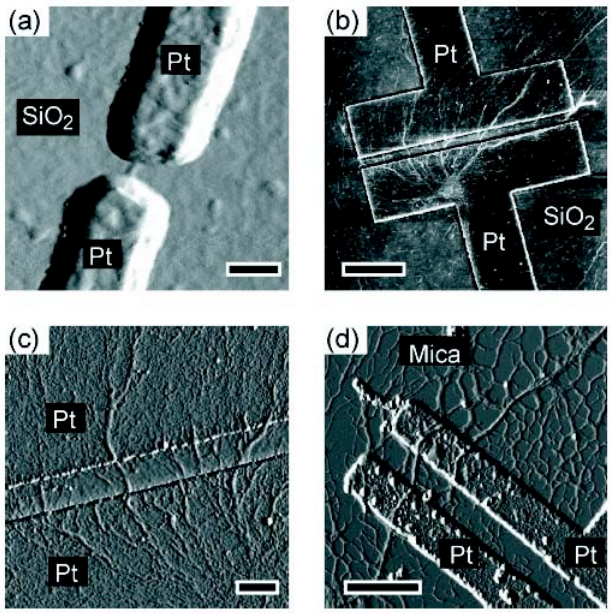

Figure 1.2-8
AFM images of DNA assembled in various devices. For all these devices, we observe an absence of conduction. (a) Mixedsequence DNA between platinum electrodes spaced by 40 nm. Scale bar: 50nm. (b) Height image of Poly(dG)-Poly(dC) DNA bundles on platinum electrodes. The distance between electrodes is 200 nm, and the scale bar is 1 mm. (c) High magnification image of the device shown in (b). Several DNA bundles clearly extend over the two electrodes. Scale bar: 200 nm. (d) Poly(dG)-Poly(dC) DNA bundles on platinum electrodes fabricated on a mica substrate. Scale bar: 500 nm. (From A.J. Storm, J. van Noort, S. de Vries, C. Dekker, *Appl. Phys. Lett.* 79, 3881 (2001).)

Kasumov et al. reported the surprising electrical characteristics of DNA in 2001 [29]. They measured the proximity-induced superconductivity of lambda DNA molecules below 1 K. (Figure 1.2-9) Lambda DNA was immobilized between rhenium-carbon electrodes (2 nm thickness) on mica substrate. The *I-V* characteristics showed the ohmic behavior at temperature ranging from room temperature down to 1 K. As the random base sequence was present in lambda DNA, it is natural to consider the molecular energy band is fluctuated along base sequence. This unique result may arise from the electrical connection between DNA molecules and rhenium-carbon electrodes, but other measurements tracking this result are not reported yet.

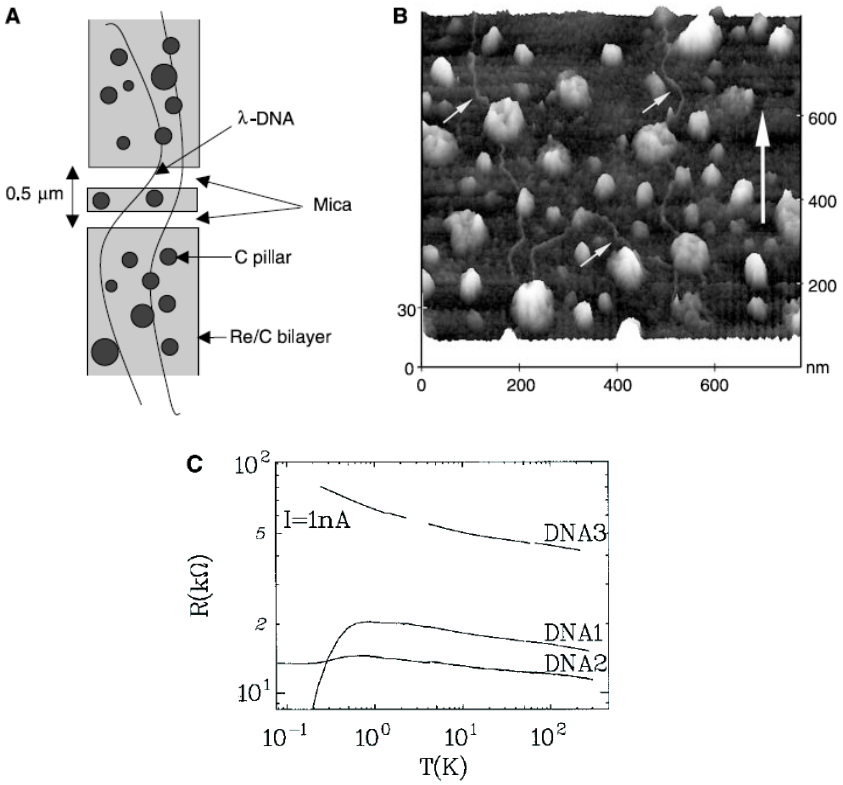

Figure 1.2-9
(**A**) Schematic drawing of the measured sample. (**B**) AFM image showing DNA molecules combed on the Re/C bilayer. The large vertical arrow indicates the direction of the solution flow. The small arrows point toward the combed molecules. (**C**) DC resistance as a function of temperature on a large temperature scale, showing the power law behavior down to 1 K. (From the report by A.Y. Kasumov, M. Kociak, S. Gueron, B. Reulet, V.T. Volkov, D.V. Klinov, H. Bouchiat, *Science* 291, 280 (2001).)

In 2000, the electrical conductivity of DNA networks was measured by the different measurement technique by AFM by Cai et al. [30]. (Figure 1.2-10) The synthesized DNA solution (250 ng/μl) containing Poly(dG)-Poly(dC) or Poly(dA)-Poly(dT) was deposited on the mica substrate and incubated for a minute. The residual solution was blown off by air blow. Then it was found that DNA network structure was formed on a mica substrate. In case of Poly(dA)-Poly(dT) DNA, various DNA strands were crossed over together and the height of bundle was 1.7 nm. On the other hand, in case of Poly(dG)-Poly(dC), a uniform reticulated structure with the height of 2.1 nm was observed. For the electrical measurements, two kinds of electrodes were used. As one-half of electrodes, Au layer was fabricated on the DNA network structure.

The conductive probe that was coated with Au layer was used as the other side of electrodes. After the tip was contacted with DNA network, *I-V* characteristics were measured by

applying bias voltage (±5 V) between Au layer and conductive tip. The sample was pretreated under vacuum (10^{-6} Torr) for 5 - 12 hours. The suitable position for the measurement was found by noncontact mode AFM. The loading force of the conductive tip was controlled to be 20 – 40 nN.

Typical *I-V* measurements of Poly(dG)-Poly(dC) showed two kind of characteristics at the different position of the conductive tip. One was linear ohmic, and the other was p-type rectifying character. (Figure 1.2-10 (c), (d)) On the other hand, the linear *I-V* characteristics was measured as for Poly(dA)-Poly(dT). The relationship between calculated resistance under the range of bias voltage of ±0.2 V and DNA length indicated that resistance was exponentially increased with increasing the length of DNA. As a base sequence dependency, the better conductance of Poly(dG)-Poly(dC) was found compared to Poly(dA)-Poly(dT).

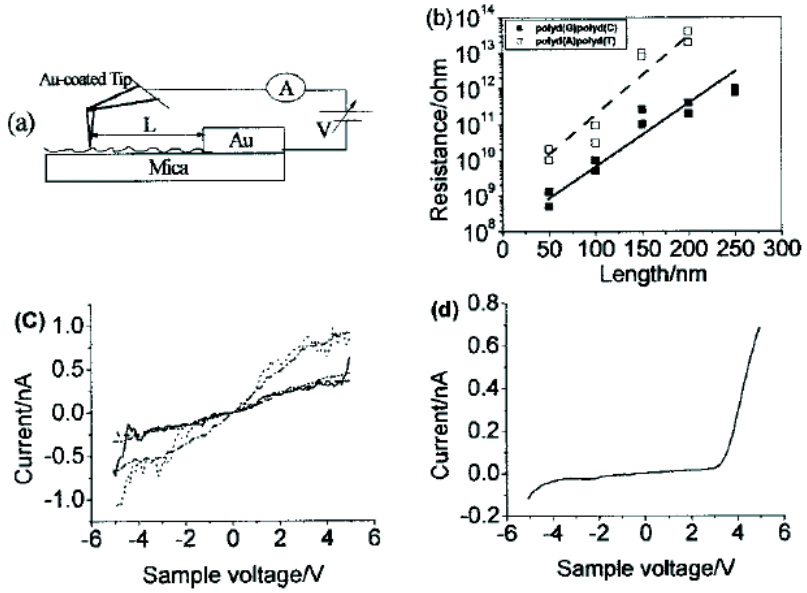

Figure 1.2-10
(a) Schematic illustration of the. (b) Relationship between resistance and DNA length. The exponential fitting plots of data are also shown. (c) Typical *I-V* curves of Poly(dG)-Poly(dC), the linear Ohmic behaviors on *L* = 100 nm at the repeat measurement of five samples. (d) Rectifying curves of Poly(dG)-Poly(dC) at *L* = 100 nm. (From the report by L. Cai, H. Tabata, T. Kawai, *Appl. Phys. Lett.* 77, 3105 (2000).)

P. J. de Pablo et al. reported the electrical measurement of lambda DNA by the similar AFM method in 2000 [31]. (Figure 1.2-11) Lambda DNA solution contains TE buffer (10 mM Tris, 1 mM EDTA, pH 8.0) and 2.5 mM $MgCl_2$ was dropped on the freshly cleaved mica

substrate. After the incubation time for 20 - 120 sec, mica was rinsed twice with distilled water and dried [32]. The Au layer was fabricated onto the lambda DNA molecules by a thin-wire shadow masking technique [33]. The temperature of the sample surface was measured and it was confirmed not to exceed 310 K during the whole evaporation process. The silicon nitride cantilevers coated with 20 nm titanium and 60 nm Au layers successively were used as conductive cantilevers. The minimum horizontal distance between Au layer and conductive tip as limited to be 70 nm in order not to measure the spurious current.

The *I-V* characteristics of different measurement showed insulative behavior under the range of 0 – 10 V. The estimated minimum resistivity was $\rho \approx 10^4\ \Omega\cdot$cm. Moreover, for the purpose of improving the sensitivity of electrical measurements, longer DNA molecules about 15μm were immobilized between electrodes spaced by about 3 μm. The number of molecules was estimated to be more than 1000. Although bias voltage of up to 12 V was applied between electrodes, the current measured was below the noise level of 1 pA. The minimum resistivity was calculated to be $\rho \approx 10^6\ \Omega\cdot$cm.

These results were inconsistent with the result by Fink et al. [26] and it was suspected that the LEEPS microscopy might cause the electron-induced hydrocarbon cracking. For the verification of this assumption, the effect of a low energy electron beam irradiation was also studied. The metallic like conductivity that showed liner *I-V* characteristic was actually

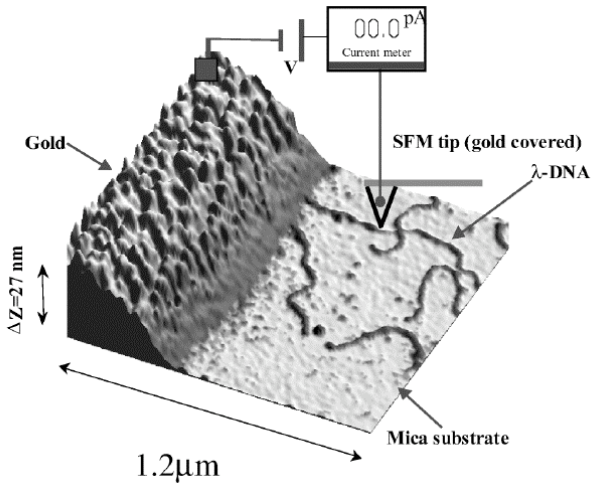

Figure 1.2-11
Three-dimensional SFM image of the channel border, showing two DNA molecules in contact with the left gold electrode. It is also presented the scheme of the electrical circuit used to measure the DNA resistivity. (From the report by P.J. de Pablo, F. Moreno-Herrero, J. Colchero, J, Gomez Herrero, P. Herrero, A.M. Baro, P. Ordejon, J.M. Soler, E. Artacho, Phys. Rev. Lett. 85, 4992 (2002).)

measured, and the formation of contamination layer over DNA was observed by SFM.

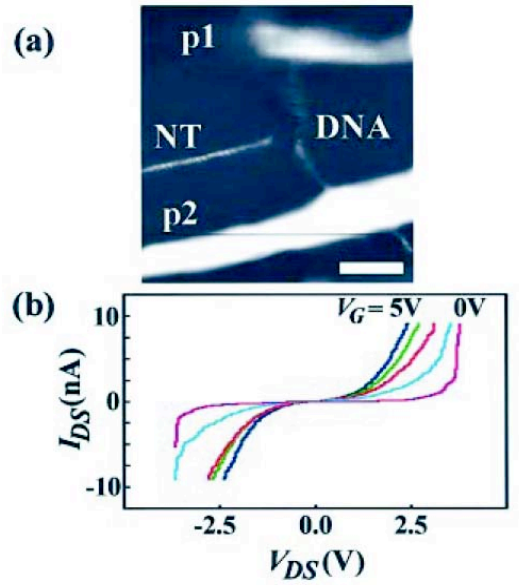

Figure 1.2-12
(a) AFM images (scale bar, 10 nm) of a three-terminal single DNA molecule device at source–drain distance (d_{DS}); 25 nm are shown. NT, P1, P2 indicate SWCNT (gate), first CNT probe (source), and second one (drain), respectively. (b) I_{DS}–V_{DS} curves for various gate voltages (V_G)=0, 1, 2, 3, 4, and 5 V is shown. (From the report by H. Watanabe, C. Manabe, T. Shigematsu, K. Shimotani, M. Shimizu, *Appl. Phys. Lett.* 79, 1 (2001).)

As a derived electrical measurement method by AFM, Watanabe et al. reported the electrical properties of single salmon sperm DNA by triple-probe AFM. [34] (Figure 1.2-12) DNA solution (300 mM NaCl, 10 mM Na citrate and 5 mM EDTA are included) was deposited on the SiO_2 / Si (100) substrate; the surface was rinsed by water after the immobilization of DNA and dried by nitrogen gas flow.

The nanotweezers that was composed of two MWCNTs at the apex of glass needle was fabricated. Controlling the vibration frequency of nanotweezers at the range of 100 – 800 kHz enabled them to control the steady position of CNTs without attaching to each other or the substrate. Additionally, conductive CNT-AFM probe (MWCNT was attached at the tip apex of AFM probe) was used in order to perform both of high spatial resolution imaging and electrical measurements. The two CNTs of nanotweezers were positioned on the single DNA molecule with less than 1 – 2 nm accuracy. These CNTs were used as source and drain electrode, respectively. Another SWCNT was also deposited on the substrate that DNA molecules were immobilized. The SWCNT was moved by CNT-AFM onto the DNA molecules between source

and drain electrode. After it was confirmed that the SWCNT was placed at the desired position, CNT-AFM was contacted to the SWCNT, and specific bias voltage as gate voltage was applied.

The electrical measurement with these three terminal electrodes was performed under dry nitrogen atomosphere at room temperature. The *I-V* characteristics at the distance of source and drain (d_{DS}) ~ 25 nm, nonlinear *I-V* curve was obtained. The voltage gap at lower bias voltage in this *I-V* curve was decreased with increasing the gate voltage from 0 to 5 V, and the conductance increased more than three orders. This result indicated that the electrical property of DNA was conductive and possibility of switching device with its gate biased.

Yoo et al. reported the direct electrical transport properties both of Poly(dA)-Poly(dT) and Poly(dG)-Poly(dC) by nanogap Au / Ti electrodes separated by 20 nm [35]. (Figure 1.2-13) This was similar measurement method reported by Porath et al. DNA molecules were immobilized between electrodes by the electrostatic trapping method [36]. They fabricated more than 20 samples and measured the electrical property under both of ambient and vacuum condition.

Most measurements under both conditions showed almost identical results, and therefore the effect of water on the conductance could be neglected. After all electrical measurements, samples were treated with DNAse enzyme that decomposes DNA molecules, and it was confirmed that the electrical transport properties were disappeared. The strong temperature dependence of the conductance at $V = 0$ was measured as for both of base sequences.

The *I-V* curves measured at various temperatures of Poly(dA)-Poly(dT) showed the linear shape at room temperature and nonlinear shape at lower temperature. The temperature dependence was measured until 50 K. A small polaron-hopping model could account for this temperature dependence. As for Poly(dG)-Poly(dC), behavior at various temperature was similar to that of Poly(dA)-Poly(dT), but the resistance (13.3 MΩ) was much smaller than that of Poly(dA)-Poly(dT) (100 MΩ). The temperature dependence was measured until 4.2 K.

Moreover, the gate-voltage effect on the *I-V* characteristic at room temperature was also studied. As for Poly(dA)-Poly(dT), the current was suppressed under the negative gate voltage was applied and slightly enhanced under positive gate voltage. On the other hand, as for Poly(dG)-Poly(dC), oppose characteristics were measured. The current was enhanced and depressed under negative and positive gate voltage, respectively. Therefore, it was concluded that Poly(dA)-Poly(dT) exhibited n-type semiconducting behavior, while Poly(dG)-Poly(dC) did p-type behavior.

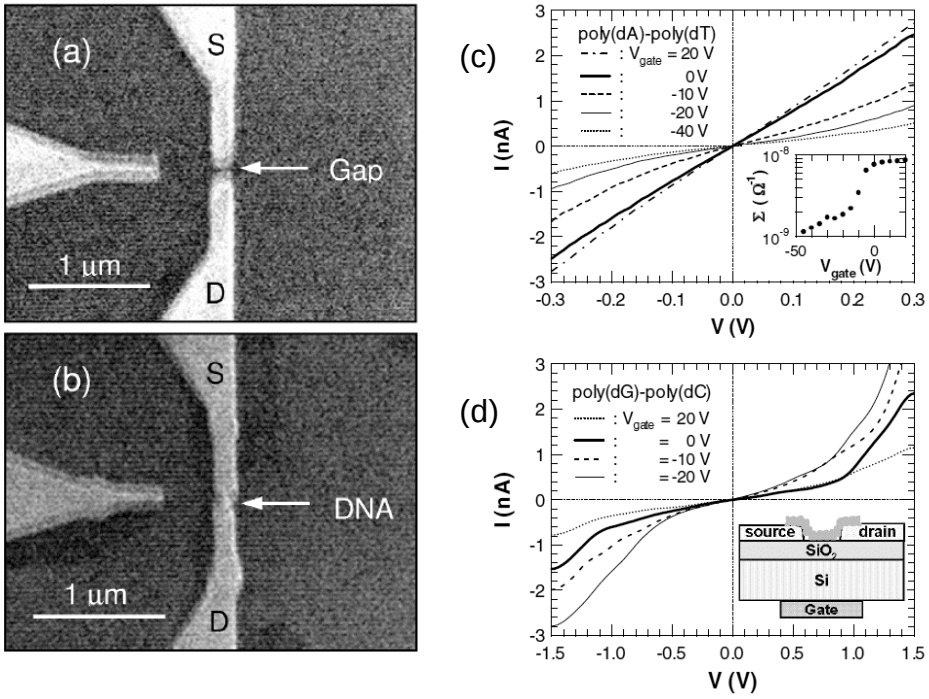

Figure 1.2-13
(a) SEM Image of the nanogap electrode separated by 20 nm. (b) SEM image of a Poly(dG)-Poly(dC) DNA molecule trapped between two electrodes. (c), (d) The *I-V* curves measured at room temperature for various values of the gate voltage for Poly(dA)-Poly(dT) (c) and Poly(dG)-Poly(dC) (d). In the inset of (c), the conductance at $V = 0$ is plotted as a function of gate voltage for Poly(dA)-Poly(dT). The inset of (d) is the schematic diagram of electrode arrangement for gate dependent transport experiments. (From the report by K.-H. Yoo, D.H. Ha, J.-O. Lee, J.W. Park, J. Kim, J.J. Kim, H.-Y. Lee, T. kawai, H.Y. Choi, *Phys. Rev. Lett.* 87, 198102 (2001).)

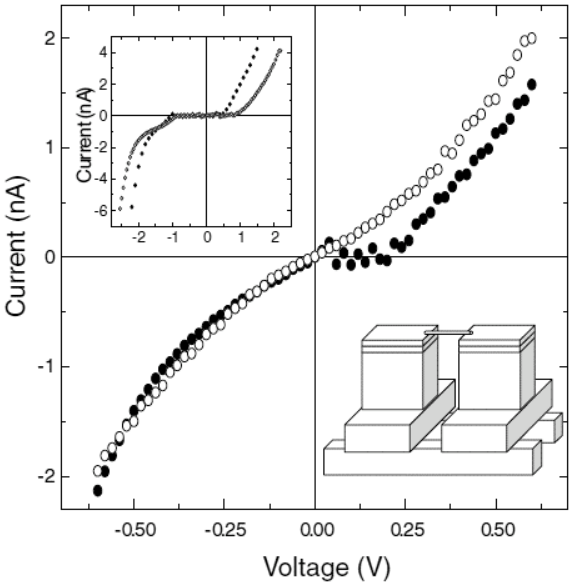

Figure 1.2-14
I-V characteristics measured in vacuum at room temperature on *M*-DNA (○) and *B*-DNA (●) molecules. Lower inset shows a schematic experimental layout. (From the report by A. Ratkin, P. Aich, C. Papadopoulos, Y. Kobzar, A.S. Vedeneev, J.S. Lee, J.M. Xu, *Phys. Rev. Lett.* 86, 3670 (2001).)

Ratkin et al. reported the electrical properties both of bundled lambda DNA (B-DNA) and M-DNA by micron scale gap electrodes [37]. (Figure 1.2-14) M-DNA used in the experiments contains a Zn metal ion replacing the imino proton of every base pair. It was also argued that the preliminary experiments by lithographically patterned Au electrodes on an insulating substrate might cause the difficulty in quantifying the possible contribution of the buffer solution on the measured electrical properties. Therefore, the new fabrication method of electrodes was developed in order to address this problem.

The fabrication procedure was as follows. Initially, thin metallic layers (Cr - Au or W – Pt - Au) of less than 1 μm in thickness were sputtered onto a thick dielectric substrate. The samples were then cracked by force mechanically, brought back together again, and later glued to a rigid support frame while applying external pressure. It was possible to control the interelectrode spacing down to about 1 μm. The presence of such a gap between the electrodes ensured that no traces of solution but those adsorbed on the DNA surface remained within the interelectrode space. The gap size between electrodes was measured to be 1 – 30 μm by optical microscope. DNA was prepared in 20 mM $NaBO_3$ buffer, pH 9.0 (or 20 mM Tris, pH 7.5) with 10 mM NaCl and 0.1 mM Zn^{2+} or 2 mM EDTA as appropriate.

DNA bundles with about 100 molecules were immobilized between electrodes and electrical measurements are performed under vacuum condition (10^{-3} Torr).

I-V characteristics of B-DNA showed a semiconductor like plateau about 200 meV, whereas such plateau was not measured as for M-DNA. These results suggested that the qualitative difference in *I-V* characteristics of M- and B-DNA at low bias could only be attributed to a difference in their conduction mechanisms. In case of B-DNA, taking the common assumption, the difference between the Fermi level of the Au electrode and the edge of molecular band of DNA suppresses tunneling through the DNA-electrode interface. Therefore, the plateau region was measured in the *I-V* curves. On the other hand, Inserting metal ions resulted in the formation of a *d* band aligned with the electrode Fermi level. As a result, injection of electrons (or holes) exhibited no voltage threshold and, consequently, no plateau appeared in the *I-V* dependence.

In 2002, Otsuka et al. [38] and Lee et al. [39] reported the effects of environmental condition on the electrical properties of DNA molecules.

Otsuka et al. reported the effect of humidity on the electrical conductivity of DNA thin film. The synthesized Poly(dG)-Poly(dC) solution was deposited on the nanogap electrodes separated by 100 nm, and fabricated the thin film after dried up the water. The *I-V* measurements were performed in a homemade desiccator under the condition that the relative humidity was changed. DNA films of Poly(dG)-Poly(dC) were found to be extremely affected by humidity; the resistance decreased exponentially with increasing relative humidity. Furthermore, AC measurement indicated the increase in the value of capacitance and the semicircles and spurs in the Coal-Coal plot.

Therefore, ionic conduction was found to dominate the conductivity of DNA film under the atmospheric condition. Moreover, the contact resistance affected the conductivity of DNA film. Results of this study showed that, in the case of measuring the DNA conductivity accurately with an external electrode, it was necessary to note the important factors: humidity and contact resistance between electrodes and samples. The detailed results are noted in the section 3.1. Similar results were reported after this result. Jo et al. reported the effect of humidity on lambda DNA immobilized between Au electrodes separated by 150 nm. [40] Kleine et al. reported the effect of humidity on lambda DNA immobilized between platinum electrodes separated by 20 – 3000 nm [41]. Both of these results indicated the insulative characteristics under dried condition.

Lee et al. reported the effect of oxygen on the electrical conductivity of DNA thin film. (Figure 1.2-15) Both of and Poly(dA)-Poly(dT) were used, and the DNA thin films were fabricated by the same method as Otsuka et al. *I-V* characteristics of these films were measured under different conditions: 1, in the atmospheric condition with 35 % relative humidity. 2, in the controlled condition that contain oxygen and nitrogen of 1 : 4 ratio with less than 0.1 % relative humidity. 3, in the vacuum condition (10^{-3} Torr).

The resistances of Poly(dG)-Poly(dC) film that were calculated at 1 V under various conditions changed from about 0.8 GΩ to 7 GΩ to 100 GΩ in that order. Similar results was obtained for Poly(dA)-Poly(dT) film, the resistance was smaller by a factor of 10 than that of Poly(dG)-Poly(dC) film. Then, the *I-V* measurement was performed under the pure oxygen purged condition, and it was found that the conductance of Poly(dG)-Poly(dC) film was increased by a factor of 100. On the other hand, the conductance of Poly(dA)-Poly(dT) decreased by a factor of 10.

These results showed both of oxygen doping and dedoping occurred on the Poly(dG)-Poly(dC) film and Poly(dA)-Poly(dT) film, respectively. These results might also

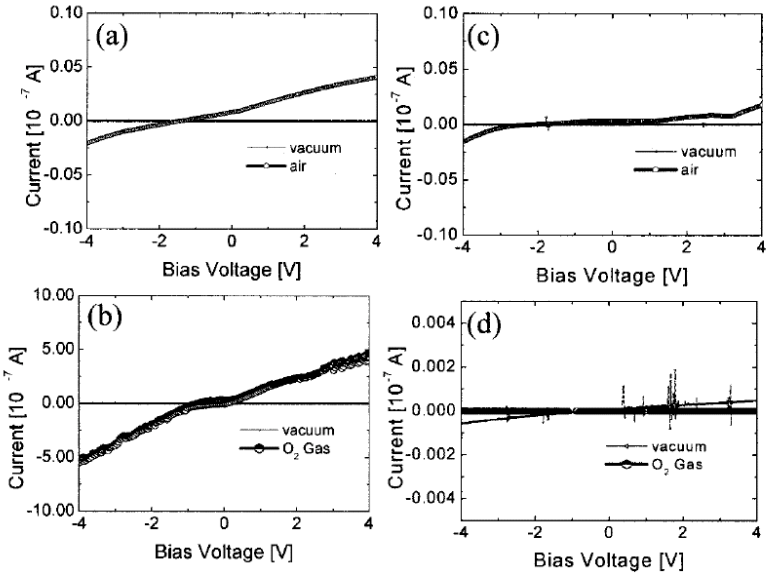

Figure 1.2-15
The *I-V* characteristics of a Poly(dG)-Poly(dC) [(a) and (b)] and Poly(dA)-Poly(dT) [(c) and (d)] DNA films. The I–V curves in an air showed in (a) and (c), whose difference shows the typical fluctuations of our data. The data in an oxygen ambient exhibited (b) and (d). The distance between the electrodes was about 100 nm. The I–V characteristics were measured several times, and the measured *I-V* curves were found to be quite reproducible. (From the report by H.-Y. Lee, H. Tanaka, Y. Otsuka, K.-H. Yoo, J.-O. Lee, T. Kawai, *Appl. Phys. Lett.* 80, 1670 (2002))

support early findings by Yoo et al. that Poly(dG)-Poly(dC) was a p-type, and Poly(dA)-Poly(dT) was n-type semiconductor.

Hwang et al. measured the electrical transport through 60 base pairs of Poly(dG)-Poly(dC) in 2002 [42]. (Figure 1.2-16) DNA solution was prepared by heating at the temperature of 97 ℃ for 5 min and natural cooling down to room temperature. After the DNA preparation was identified by several techniques such as UV spectroscopy, mass spectroscopy and gel electrophoresis, DNA solution was diluted with deionized water to the concentration of 25 μM. A 1 μl of solution was deposited on the center of the electrodes, water was evaporated and the device was finally dried by nitrogen gas. Electrodes were fabricated by e-beam lithography and liftoff process. Au / Ti layer (10 nm / 5 nm thickness) was thermally evaporated on the 200-nm-thick SiO2. The gap between electrodes was 20 nm.

The electrical measurements were performed under atmospheric condition and room temperature. *I-V* characteristics showed the clear staircases and maxima were observed in the *dI*/*dV* – *V*. Measurements were repeated more than 20 times over the time scale of several days, and the completely reproducible results were obtained. *I-V* measurements were also performed under vacuum condition, and no change was found. It was suggested that the *I-V* curve was originated from the electrical transport through 60 base Poly(dG)-Poly(dC) and the size of

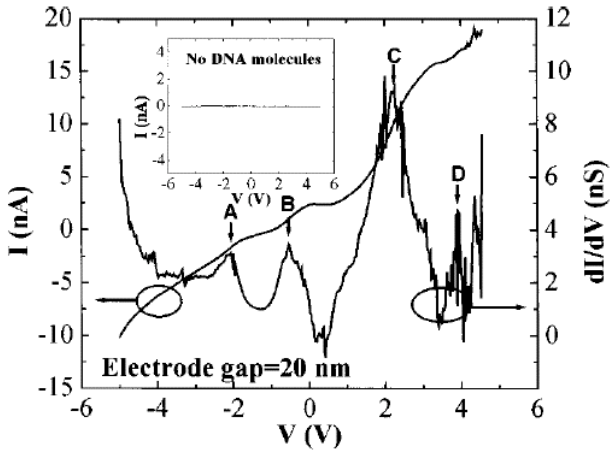

Figure 1.2-16
I-V and the *dI/dV–V* characteristics measured from the electrodes with the gap of 20 nm after dropping the diluted DNA solution. There are clear staircases in the *I-V* and maxima are observed in the *dI/dV–V*. The inset shows the *I-V* measured between the 20 nm gap electrodes after dropping the DI water. (From the report by J.S. Hwang, K.J. Kong, D. Ahn, G.S. Lee, D.J. Ahn, S.W.Hwang, Appl. Phys. Lett. 81, 1134 (2002).)

staircase was consistent with the energy gap calculated by one-band tight-binding model.

Zhang et al. reported the insulating behavior of lambda DNA immobilized micron scale electrodes [43]. (Figure 1.2-17) The point in this experiment was that the interface between DNA and Au electrodes were modified with Au – S chemical bonds. Lambda DNA contained single stranded 12-base 5' overhangs (sticky ends) at both sides of double strand. The sticky ends were modified with three deoxynucleoside triphosphates (dATP, dGTP, S^4-dTTP) by the standard reaction using Klenow fragment of DNA Polymerase. (Figure 1.2-17 (a)) As the thiol-modified dTTP (S^4-dTTP) could react with Au surface, the modified lambda DNA was chemically connected to the electrodes. Au electrodes were fabricated on a quartz substrate in parallel strips by standard photolithography. The electrodes were separated by 4 or 8 μm, and the width was 4 μm. DNA solution was deposited on the chip. After 20 min of incubation, a

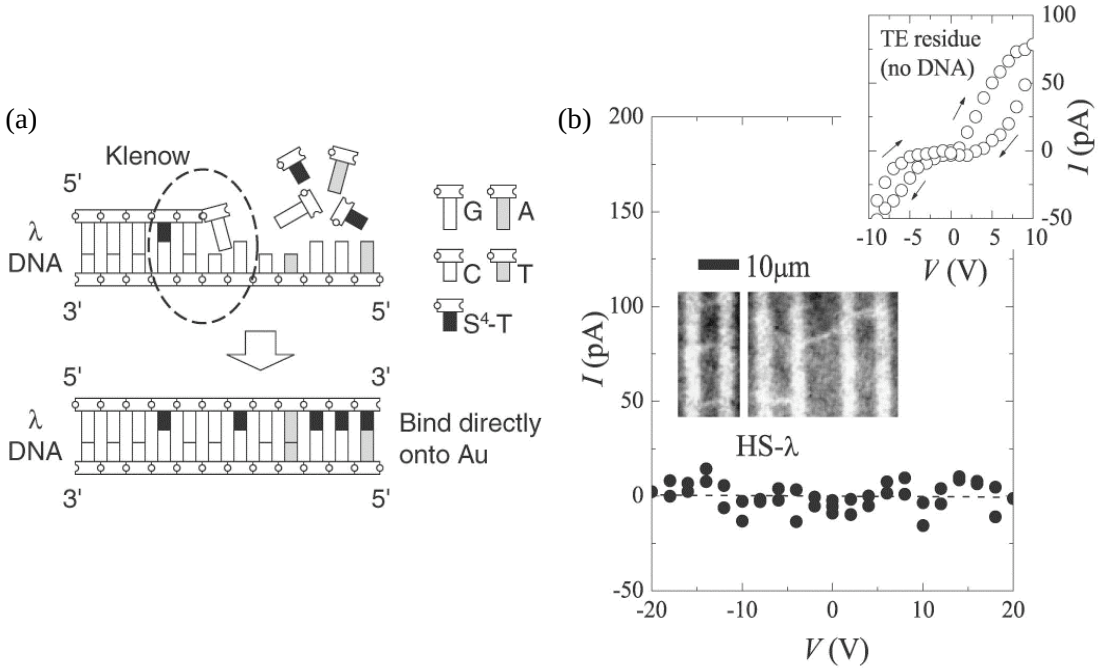

Figure 1.2-17
(a) The schematic of the incorporation of deoxynucleoside triphosphates into lambda DNA sticky ends using the Klenow fragment. (b) *I-V* characteristics for a sample of lambda DNA bridging two parallel Au electrodes separated by 4 μm. The DNA was rinsed with NH_4Ac before the measurement to remove the buffer salt residue. The dashed line is a linear fit to the data. The inset shows the *I-V* curve for a test chip containing TE buffer solution (without DNA). The chip was dried in vacuum but not subject to NH_4Ac rinsing. The observed conductance is entirely from trace TE salt residue. Both measurements were done in vacuum at 295 K. (From the report by Y. Zhang, R.H. Austin, J. Kraeft, E.C. Cox, N.P. Ong, *Phys. Rev. Lett.* 89, 198102 (2002).)

clean covers slip was put on the chip and a flow of the buffer solution was applied perpendicular to the electrodes. It was confirmed that modified DNA molecules were bridged between electrodes by fluorescence optical microscope.

Electrical measurements were performed in vacuum ($<10^{-7}$ Torr) and at room temperature. The semiconductor like history-dependent conductance was repeatedly measured. However, *I-V* characteristic of the sample prepared with only 1×TE buffer also showed the typical curve. Moreover, it was found that the treatment of DNA immobilized sample with solution (both of 10 mM $MgSO_4$ / 40 mM Tris-HCl (pH 8) and NH_4Ac) to remove buffer and salts diminished the electrical properties. After the treatment, no current was detected at up to 20 V although DNA molecules were connected to electrodes. This result was different from the results by Ratkin et al. [37] and it was suggested that the high conductance might arise from residual salts trapped between the DNA strands.

Hartzell et al. reported the effect of the structure of double stranded structure on the electrical properties in 2003 [44]. (Figure 1.2-18) Linear lambda DNA used possesses two short overhang regions 12 base long at both sides was complementary to the single strands of 12 bases long. The single strands were labeled with C3 S – S disulfide groups at their 3' ends. These single strand sequences were complementary to the 12 unpaired bases of each overhang region, and were hybridized to these regions, effectively providing a complete, double stranded molecule with a gap in each strand. (Figure 1.2-18 (a)) The hybridized DNA was connected to the Au electrodes through Au – S bonding as the similar method by Braun et al. [23].

Although each DNA could hybridize through 12 base overhang region, gaps (nicks) existed between 5' ends of the single strands and the 3' ends of lambda DNA. Then, the authors compared the *I-V* characteristics of nicked lambda DNA to identical lambda DNA samples with the nicks repaired by ligation technique.

Electrodes fabricated by standard lithography techniques were used. Au / Cr layer (30 nm / 8 nm thickness) was thermally evaporated on the 450-nm-thick SiO2. The electrodes were separated by 8 μm, and the width was 50 μm. DNA strands were immobilized between electrodes by electric field [45]. The alignment was followed by a rinse with de-ionized water to remove both unbound DNA and buffer solution. The sample was then dried under a flow of nitrogen gas.

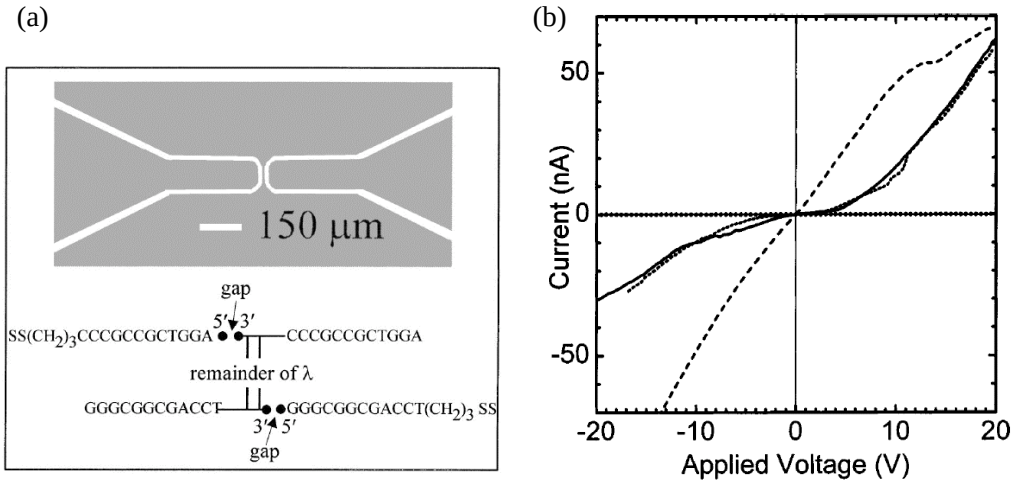

Figure 1.2-18
(a) Above: the Au electrode geometry. Below: sketch of the disulfide-labeled lambda DNA molecules used in this work. The nicked DNA features a gap between the 3' and 5' nucleotides, where indicated. In the repaired DNA, the gaps were repaired using T4 DNA ligase. (b) *I-V* characteristics measured at room temperature on disulfide-labeled l-DNA molecules. Dashes: repaired DNA; dots: nicked DNA, swept from negative to positive potential; solid line: nicked DNA, swept from positive potential to negative potential. (From the report by B. Hartzell, B. McCord, D. Asare, H. Chen, J.J. Heremans, V. Soghomonian, *Appl. Phys. Lett.* 82, 4800 (2003).)

I-V measurements were performed under ambient condition and at room temperature. It was noted that the slight dependence of humidity was noticed, but was neglected in this work. For the nicked DNA, the *I-V* characteristic was pronouncedly nonlinear, showed a conductivity gap up to ±3 V, beyond which sizable current flow occurs. On the other hand, the repaired DNA showed a significantly more ohmic behavior, with no observable conductivity gap when the same potential sweeps were applied. The low field at less than ±3 V dc conductivity of the nicked DNA was reduced by a factor ~ 20 compared to the repaired DNA. Whether the voltage threshold was due to the presence of an energy barrier, due to interband tunneling or due to a Coulomb blockade effect was uncertain at this point, but these results would indicate that the complete double helical structure plays an important role in electronic transport.

Zhou et al. reported the electrical conductivity of lambda DNA network by different electrode geometry [46]. (Figure 1.2-19) Former results of electrical measurements were performed by the bottom-contacted geometry type electrodes or conductive AFM. In the bottom-contacted geometry type electrodes, DNA molecules were immobilized between

electrodes after electrodes were fabricated. In this report, they developed the new fabrication process of nanogap electrode upon the DNA molecules (lead-on-top geometry). The electrical contacts were made by evaporating metal on DNA molecules through a nanoscale stencil mask etched in a freestanding silicon nitride membrane. The pattern in stencil mask was separated by 500 nm – 1 μm. The advantage of this electrode was avoiding problems in conventional fabrication scheme: the solvents used in electron beam lithography would destroy DNA molecules.

DNA solution (500 μg/ml lambda DNA, 10 mM Tris buffer, 1 mM EDTA) was diluted by a ratio varying from 10 to 100 with a solution of 11 mM $MgCl_2$ and 10 mM Tris. Magnesium ions in the solution were used to enhance the attraction of DNA molecules to the mica surface. A 10 μl of 10-fold diluted solution was deposited on the cleaved mica substrate. After incubation time of 2 – 3 min, the sample was rinced with sterilized water and spun dry. The contacts for these samples were fabricated from AuPd and designed to be 12 μm wide, separated by a gap of 1 μm. About hundreds of molecules were estimated to span the gap without a break.

The electrical measurements were performed under both of atmospheric and vacuum condition (10^{-5} – 10^{-6} Torr). The resistances under atmospheric and vacuum condition were 5 TΩ and 13 TΩ, respectively. When the sample was returned to air, the conductivity recovers after several hours. As control experiments similar electrical measurements were performed as for bare mica substrate. The resistances under atmospheric and vacuum condition were 3.5 TΩ and 50 TΩ (exceeding the limit of measurement setup), respectively. The atmospheric resistance was similar between DNA immobilized sample and bare mica substrate. However, the resistance of DNA sample was much lower than that of mica substrate.

Therefore, it was concluded that the measured conduction in air was predominantly due to water adsorbed on the hydrophilic molecule and mica substrate. On the other hand, a small residual conductivity was measured under vacuum that may be intrinsic to small bundles of DNA molecules.

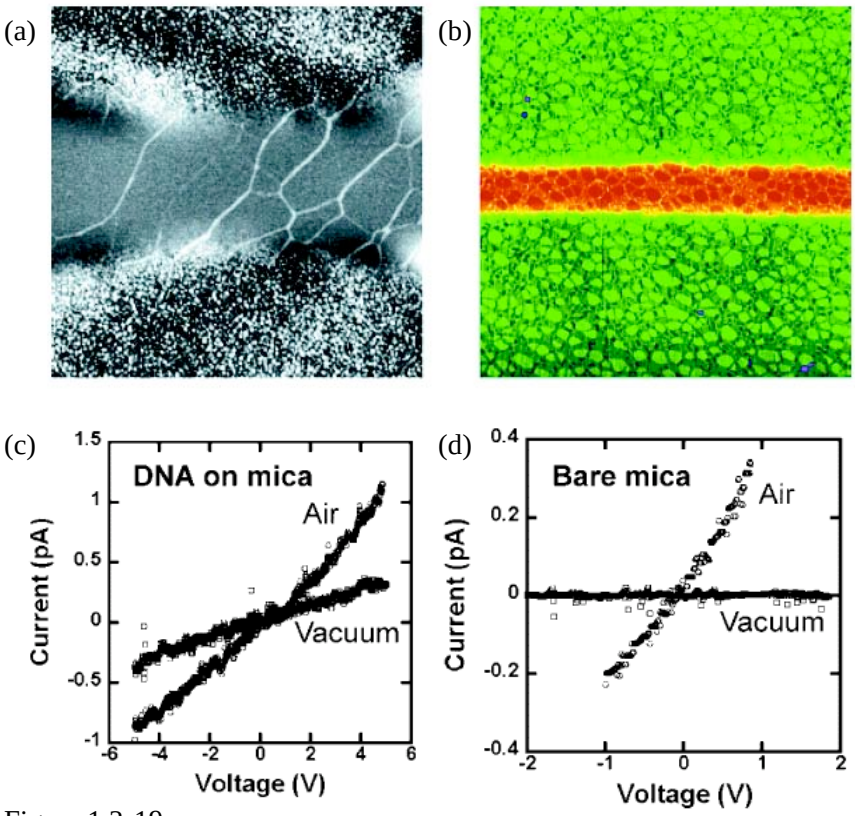

Figure 1.2-19
(a) AFM height image of several small DNA ropes contacted by gold leads separated by 1 mm. The scan width is 2.5 μm. (b) AFM height image of a dense DNA network contacted by 15-nm-thick, 12-mm-wide AuPd leads separated by 1 mm. The scan size is 8 mm. (c) *I-V* characteristics of a dense DNA network ((b)) in air and vacuum. (d) *I-V* characteristics in air and vacuum of a bare mica sample with electrodes identical to those of the circuit in (c). (From Y.X. Zhou, A.T. Johnson, J. Hone, W.F. Smith, *Nano Lett.* 3, 1371 (2003).)

Kasumov et al. again reported the electrical properties of lambda DNA from the viewpoint of structural deformation on the insulative substrate in 2004 [47]. (Figure 1.2-20) Thin Pt electrodes with thickness of 3 nm were fabricated on the mica substrate. Polymer film with thickness of 0.5 nm was fabricated on the surface both of Pt electrodes and mica by sputtering by glow discharge of pentylamine vapor. A drop of 10 – 15 μl of DNA solution was deposited on the surface treated with polymer film. The DNA solution contains 1 – 3 μg/ml of DNA, 10 – 30 mM of ammonium acetate and 7 – 9 mM of magnesium chloride. The samples were incubated for 5 – 10 min. The mica was then washed with water, blotted with filter paper, and dried with argon. The height distribution of DNA molecules on the surface by AFM indicated that DNA molecules on the substrates treated by pentylamine was 2.4 nm that is very close to the native thickness, while the average thickness of DNAs on the clean substrate the

thickness was 1.1 nm. This result was interpreted that the deposition of the polymer film decreases hydrophilicity of mica and thus its interaction with DNA molecules.

The electrical measurements were performed by both of spreading resistance mode (SRM) AFM and DC method between nanogap electrodes separated by 200 – 500 nm. Results by SRM indicated the conductive properties for 2-nm-height DNA molecules, but not for small-height DNA molecules. Moreover, the temperature-controlled measurements indicated that the resistances at room temperature and 4 K are 5 kΩ and 95 kΩ, respectively. The charge transport was measured at temperature below 1 K, and it also indicated the parasitic ionic conduction was excluded. These results were the confirmation that it was possible to prepare conductive DNA molecules by taking care of the surface chemistry not to deform the double stranded structure.

For more detailed reviews of electrical property of DNA, please see references cited [48 – 51].

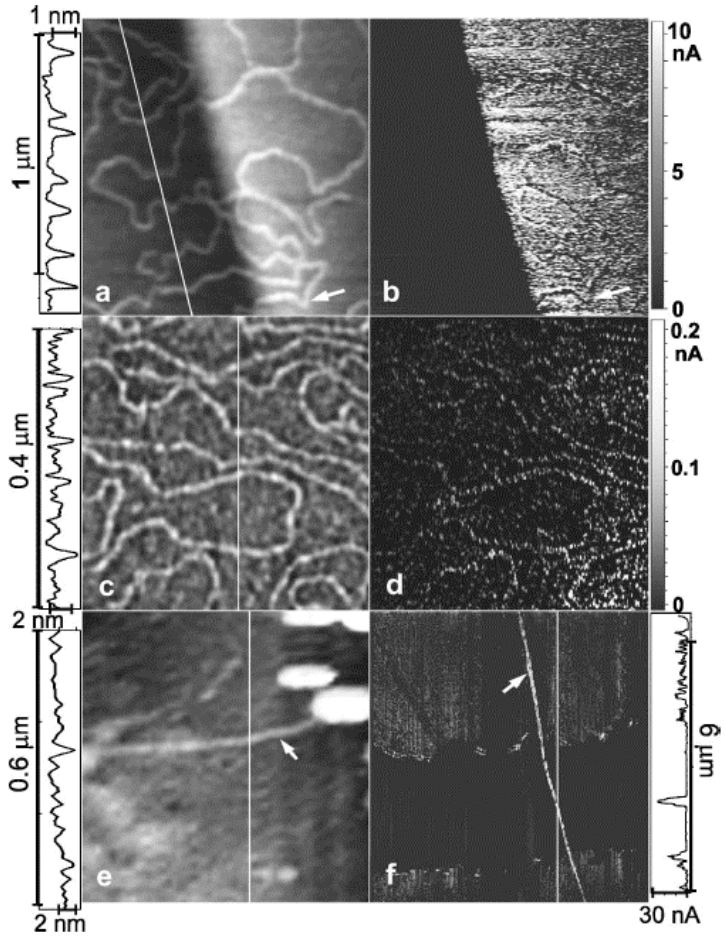

Figure 1.2-20
AFM (left) and SRM (right) images of DNA molecules: (a) AFM image of DNA molecules on the clean substrate without penthylamine; (b) SRM image of the same molecules (right bright part of (a) and (b) images is Pt); (c) AFM picture of DNA molecules on the substrate treated by penthylamine; (d) SRM image of the same molecules, Pt electrode is outside of the image; (e) AFM image of a DNA combed across the slit between Re/C electrodes on mica; (f) SRM image of a rope of DNA molecules combed between Pt electrodes on mica. On the left- and right-hand sides of the image there are profiles of DNA molecules and current scales of SRM (voltage was up to 0.23 V) images, respectively. Note that when (b) is plotted on the same current scale as (d), the DNA molecules on the mica still appear as black as the mica substrate. (Taken from the report by A. Yu. Kasumov, D.V. Klinov, P.-E. Roche, S. Gueron, H. Bouchiat, *Appl. Phys. Lett.* 84, 1007 (2004))

1.3. Purpose of Study

As noted in the previous section, reported experimental results vary such as insulator, semiconductor, ohmic conductor and superconductor. These results would indicate that the electrical measurement of DNA molecules in a solid state with “electrode – DNA – electrode” configuration is very difficult to obtain consensus. This is because various factors were involved in the experiments. Moreover, as for the style of report, most results were usually reported only in the letter-format. Therefore, details in the experimental section in such as sample preparation method and electrical measurement protocols tend to be shortened, and such situations make detailed analysis difficult.

Nevertheless, the comparison between former results would indicate some important factors that affect the electrical property of DNA molecules as follows.

1, Electrical contacts between DNA molecules and electrodes.

2, Structure of DNA molecules.

3, Environment around DNA molecules.

Controlling the electrical contacts is quite important because in case the electrical property of DNA molecule is studied, ohmic contact should be formed at the interface between electrode and DNA. If the contact resistance between electrode and DNA is much higher than that of DNA molecules, it is difficult to study the charge transport phenomenon along DNA molecules because the current is limited by contact resistance that arise from the potential difference between the Fermi level of metal electrode and molecular orbital of DNA.

Furthermore, the structure of DNA molecules between electrodes also affects their electrical properties. As it is assumed that the charge transport would be occurred through the π-stacked base molecules, the structural change such as bending or nicking would cause the localized potential barrier that results in increasing the resistance. The base sequence also affects electrical properties. The HOMO - LUMO gap of four base molecules are different each other, and guanine is easy to oxidize compared to other base molecules. The results of charge transfer study also indicated the effective charge transfer occurred in guanine-rich sequences. Therefore, the resistance of Poly(dG)-Poly(dC) seems lower than other base sequences such as Poly(dA)-Poly(dT) or lambda DNA (random sequences).

Lastly, environmental control would be essentially needed. As shown in the previous results about the effect of humidity, the electrical measurement should be performed under vacuum or dried condition. This is because ionic conduction is easy to occur under atmospheric

condition through the adsorbed water layer around DNA molecules.

The counter ions also affect the stability of structure. As the melting temperature of DNA in a solution is known to increase in the presence of counter ions, they would be needed to stabilize the structure in the sample preparation.

These three factors noted above do not solely exist, but affect each other. In case the water molecules around DNA are decreased under dried condition, the structural change from B-form to A-form might occur and the electrical properties might be changed. In case DNA molecules are connected to electrodes, structure would be changed.

Therefore, as shown in figure 1.3-1, all factors should be considered to measure the precise electrical property of DNA molecules.

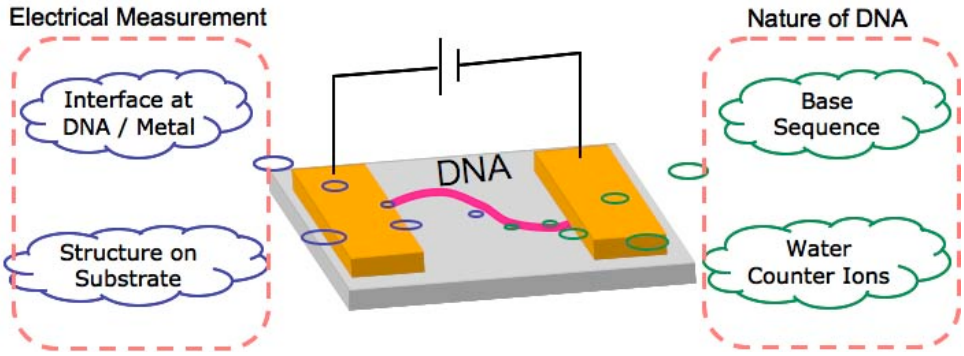

Figure 1.3-1
Important factors that would affect the electrical properties of DNA.

References

[1] J. Watson, F, Crick, *Nature* **171**, 737 (1953).
[2] D.D. Eley, D.I. Spivey, *Trans. Faraday. Soc.* **58**, 411 (1962).
[3] E. Helgren, A. Omerzu, G. Grũner, D. Mihailovich, R. Podgornik, H. Grimm, *e-print cond-mat*/0111299 (2002).
[4] Kuzyk, "Dielectrophoresis of nanoscale dsDNA and its electrical conductivity" University of JYVÄSKYLÄ, *Dissertation* 2005.
[5] R. A. Marcus and N. Sutin, *BioChim. BioPhys. Acta* **811**, 265 (1985).
[6] C.J. Murphy, M.R. Arkin, Y. Jenkins, N.D. Ghatlia, S.H. Bossmann, N.J. Turro, J.K. Barton, *Science* **262**, 1025 (1993).
[7] A.M. Brun, A. Harriman, *J. Am. Chem. Soc.* **114**, 3656 (1992).
[8] S. Priyadarshy, S.M. Risser, D.N. Beratan, *J. Phys. Chem*. **100**, 17678 (1996).
[9] F.D. Lewis, T. Wu, Y. Zhang, R.L. Letsinger, S.R. Greenfield, M.R. Wasielewski, *Science **277***, 673 (1997).
[10] K. Fukui, K. Tanaka, *Angew. Chem. Int. Ed.* **37**, 158 (1998).
[11] S.O. Kelley, J.K. Barton, *Science* **283**, 375 (1999).
[12] P.T. Henderson, D. Jones, G. Hampikian, Y. Kan, G.B. Schuster, *Proc. Natl. Acad. Sci. USA* **96**, 8353 (1999).
[13] J.K. Barton, C.V. Kumar, N.J. Turro, *J. Am. Chem. Soc*. **108**, 6391 (1986).
[14] M.D. Purugganan, C.V. Kumar, N.J. Turro, J.K. Barton, *Science* **241**, 1645 (1988).
[15] R.E. Holmlin, P.J. Dandliker, J.K. Barton, *Angew. Chem. Int. Ed. Engl.* **36**, 2714 (1997).
[16] C.A.M Seidel, A. Schulz, M.H.M. Sauer, *J. Phys. Chem*. **100**, 5541 (1996).
[17] H. Fernando, G.A. Papadantonakis, N.S. Kim, P.R. LeBreton, *Proc. Natl. Acad. Sci. USA* **95**, 5550 (1998).
[18] A.A. Voityuk, J. Jortner, M. Bixon, N. Rösch, *Chem. Phys. Lett.* **324**, 430 (2000).
[19] E. Meggers, D. Kusch, M. Spichty, U. Wille, B. Giese, *Angew. Chem. Int. Ed. Engl.* **37**, 460 (1998).
[20] B. Giese, M. Spichty, S. Wessely, *Pure Appl. Chem*. **73**, 449 (2001).
[21] B. Giese *Curr. Opin. Chem. Biol*. **6**, 612 (2002).
[22] M. Bixon, J. Jortner, *J. Am. Chem. Soc.* **123**, 12556 (2001).
[23] E. Braun, Y. Eichen, U. Sivan, G. Ben-Yoseph, *Nature* **391**, 775 (1998).
[24] Y. Okahata, T. Kobayashi, H. Nakyama, K. Tanaka, *Supramolecular Science* **5**, 317 (1998).
[25] H. Nakayama, H. Ohno, Y. Okahata, *Chem. Comm.* **2300** (2001).
[26] H.W. Fink, C. Schönenberger, *Nature* **398**, 407 (1999).
[27] D. Porath, A. Bezryadin, S. de Vries, C. Dekker, *Nature* **403**, 635 (2000).
[28] A.J. Storm, J. van Noort, S. de Vries, C. Dekker, *Appl. Phys. Lett.* **79**, 3881 (2001).
[29] A.Y. Kasumov, M. Kociak, S. Gueron, B. Reulet, V.T. Volkov, D.V. Klinov, H. Bouchiat, *Science* **291**, 280 (2001).
[30] L. Cai, H. Tabata, T. Kawai, *Appl. Phys. Lett.* **77**, 3105 (2000).
[31] P.J. de Pablo, F. Moreno-Herrero, J. Colchero, J, Gomez Herrero, P. Herrero, A.M. Baro, P. Ordejon, J.M. Soler, E. Artacho, *Phys. Rev. Lett.* **85**, 4992 (2002).
[32] M.J. Allen, E.M. Bradbury, R. Balhorn, *Nucl. Acids. Res.* **25**, 2221 (1997).
[33] P.J. de Pablo, M.T. Martinez, J. Colchero, J. Gomes-Herrero, W.K. Maser, A.M. Baro, *Adv. Mater.* **12**, 573 (2000).
[34] H. Watanabe, C. Manabe, T. Shigematsu, K. Shimotani, M. Shimizu, *Appl. Phys. Lett.* **79**, 1 (2001).
[35] K.-H. Yoo, D.H. Ha, J.-O. Lee, J.W. Park, J. Kim, J.J. Kim, H.-Y. Lee, T. kawai, H.Y. Choi, *Phys. Rev. Lett.* **87**, 198102 (2001).
[36] Bezryadin, C. Dekker, G. Schmid, *Appl. Phys. Lett.* **71**, 1273 (1997).
[37] Ratkin, P. Aich, C. Papadopoulos, Y. Kobzar, A.S. Vedeneev, J.S. Lee, J.M. Xu, *Phys. Rev. Lett.* **86**, 3670 (2001).
[38] Y. Otsuka, H.-Y. Lee, J.-H. Gu, J.-O. Lee, K.-H. Yoo, H. Tanaka, H. Tabata, T. Kawai, *Jpn. J. Appl. Phys*. **41**, 891 (2002).
[39] H.-Y. Lee, H. Tanaka, Y. Otsuka, K.-H. Yoo, J.-O. Lee, T. Kawai, *Appl. Phys. Lett.* **80**, 1670 (2002).

[40] Y.-S. Jo, Y. Lee, Y. Roh, *J. Kor. Phys. Soc.* **43**, 909 (2003).
[41] H. Kleine, R. Wilke, Ch. Pelargus, K. Rott, A. Puhler, G. Reiss, R. Ros, D. Anselmetti, *J. Biotech*. **112**, 91 (2004).
[42] J.S. Hwang, K.J. Kong, D. Ahn, G.S. Lee, D.J. Ahn, S.W.Hwang, *Appl. Phys. Lett.* **81**, 1134 (2002).
[43] Y. Zhang, R.H. Austin, J. Kraeft, E.C. Cox, N.P. Ong, *Phys. Rev. Lett.* **89**, 198102 (2002).
[44] Hartzell, B. McCord, D. Asare, H. Chen, J.J. Heremans, V. Soghomonian, *Appl. Phys. Lett.* **82**, 4800 (2003).
[45] M. Washizu and O. Kurosawa, *IEEE Trans. Ind. Appl.* **26**, 1165 (1990).
[46] Y.X. Zhou, A.T. Johnson, J. Hone, W.F. Smith, *Nano Lett.* **3**, 1371 (2003).
[47] Yu. Kasumov, D.V. Klinov, P.-E. Roche, S. Gueron, H. Bouchiat, *Appl. Phys. Lett.* **84**, 1007 (2004).
[48] Porath, G. Cuniberti, R.D. Felice, *Top. Curr. Chem.* **237**, 183 (2004).
[49] M.D. Ventra, M. Zwolak, "DNA Electronics" *Encyclopedia of Nanoscience and Nanotechnology* Volume 2, pp. 475-493(19).
[50] V. Bhella, R.P. Bajpai, L.M. Bharadwaj, *EMBO reports* **4**, 442 (2003).
[51] R.G. Endres, D.L. Cox and R.R.P. Singh, *Rev. Mod. Phys.* **76**, 195 (2004).

Chapter2

Development of Electrical Measurement Techniques in Nanoscale

2.1. Introduction

In case we measure electrical properties of molecules such as DNA molecules, it is very important to discuss the method to fabricate electrical contact to molecules. This is because the structure of molecules would show strong correlation with their electrical property.

Figure 2.1-1 shows the schematic illustrations of typical electrical measurement methods. Figure 2.1-1 (a) shows the electrical measurement of molecules by the so-called “Bottom -contacted geometry type electrode”. In this method, molecules are immobilized between electrodes that are fabricated by conventional photolithography and/or electron beam lithography. As just dropping molecular solutions usually performs the immobilization of molecules, it is very simple way to fabricate samples. Furthermore, electrodes that are separated in nanoscale each other can be fabricated by electron-beam lithography and a double-angle evaporation technique onto insulative substrate. Therefore, various kinds of measurements of molecules are reported so far.

Figure 2.1-1 (b) shows the electrical measurement of molecules by the so-called “Top-contacted geometry type electrode”. Unlike with bottom-contacted one, molecules are covered with electrodes that are fabricated after the immobilization of molecules on the substrate. The clear distinction between (a) and (b) is the structural change of molecules at the edge of electrodes. In case we measure the electrical properties of long and soft molecules such as DNA molecules especially, the structural change would cause the localization of conductive path along molecules. Therefore, the method shown in (b) seems appropriate for DNA study. However, it is impossible to employ conventional methods such as photo- and electron beam lithography for electrode fabrication, because both of the irradiation of light (electron beam) and the organic solvents in the lift-off process would cause damages to DNA molecules that are immobilized on the substrate beforehand.

Figure 2.1-1 (c) shows the electrical measurement of molecules by the so-called “conductive probe AFM”. The tip coated with conductive materials such as Au, Pt and W is usually employed. During the scanning of surface, the electrical measurements can be performed. The most distinctive function of this method is the possibility of local electrical measurements because it is possible to study the distribution of conductance in nanoscale. Like with top-contacted geometry type electrode, this method seems appropriate DNA study. However, as noted below, it is difficult to employ conventional technique due to structural deformation of molecules and instability of tip positioning.

Comparing these different methods enables us to understand that both of merits and demerits are included in all methods. That is, it is important to have an effort to retain structure of soft DNA molecules between electrodes, but conventional methods seem difficult to employ.

In order to solve these problems and measure electrical conductivity of DNA molecules, new measurement techniques are developed in my study. One is the method of simultaneous measurements both of nanostructures and local electrical characteristics by conductive probe AFM. The other is the method to fabricate top-contacted geometry type nanogap electrodes without conventional techniques that include wet process. In this chapter, the development of these measurement techniques are shown and discussed.

First, the new AFM method, called point-contact current-imaging AFM (PCI-AFM) which combines tapping mode (for mapping topographic image) and point-contact operation (for measuring *I-V* characteristics) will be discussed. This PCI-AFM technique can simultaneously map high-resolution topographic image and measure spatially resolved *I-V* characteristics of materials (placed on an insulative substrate and connected to Au electrode) on the nanoscale. The high performance of the PCI-AFM system was evaluated in experiments on single-walled carbon nanotubes (SWCNTs).

Next, the new method to fabricate top-contacted geometry type electrode, called angle-controlled thermal deposition method is discussed. This method enables us to fabricate nanogap electrodes on molecules that are immobilized on the substrate without wet process. The advantageous of this method is evaluated in experiments on porphyrin nanorods.

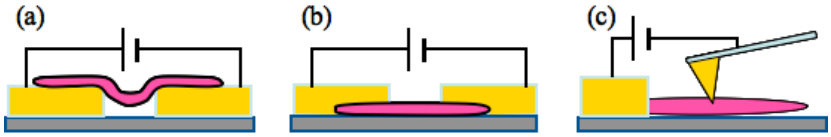

Figure 2.1-1
Schematic illustrations of electrical measurement methods. (a) Bottom contacted geometry type electrode. (b) Top-contacted geometry type electrode. (c) Conductive probe AFM method.

2.2. Point-contact Current Imaging Atomic Force Microscopy

Introduction

The electronic properties of various materials in nanoscale have recently been studied with a view to realize nanoscale devices. Typical materials are, for example, carbon nanotubes (CNTs) [1-3] and deoxyribonucleic acids (DNAs) [4,5] and nano organic crystals. [6] To realize nanoscale devices, these materials should be placed on insulative substrates and connected to conductive electrodes.

To characterize the electrical properties of such systems of nanoscale devices, AFM is more useful than STM because it can be applied to both conductor and insulator. In particular, contact-mode AFM (CM-AFM) [9] using a conductive cantilever can produce images that indicate the spatially resolved conductance of a π-conjugated molecule isolated in an insulating self-assembled monolayer.

In previous CM-AFM measurement, the samples kept their structure during the contact-mode scan because the molecules were densely packed on the substrate. However, problems arise with CM-AFM when it is used for measuring the conductivity of soft and/or nanoscale materials, which are easily deformed and damaged when the tip under a heavy load (about 10 nN) in order to produce electrical contact [10].

On the other hand, tapping mode AFM (TM-AFM) doesn't suffer the same difficulties with this kind of sample. That is, the damage to the tip and the samples is greatly reduced in comparison with CM-AFM because the tip taps sample surface intermittently. Thus, TM-AFM can perform high-resolution topographic image on the nanoscale; however, it cannot form electrical contact because it has a weak loading force and a short contact time with the sample.

For these reasons, *I-V* characteristics of nanoscale materials have been measured by point contact AFM (PC-AFM) [11–13], which are able to avoid lateral motion during *I-V* measurement. This method, however, faces the additional problems that the correspondence between the material structure and the electronic properties cannot be assessed by experiment because of error in tip positioning (i.e., tip drift).

In response to the above circumstances, we have developed a new method for measuring *I-V* characteristics on the nanoscale, namely, point-contact current-imaging atomic force microscopy (PCI-AFM). By combining tapping mode (for topographic image) and point-contact mode (for measuring *I-V* characteristics), this method can simultaneously provide

high-resolution topographic image and spatially resolved *I-V* characteristics. It is thus possible to measure the structure and electrical properties of a material, simultaneously. Furthermore, the problems concerning CM-AFM, TM-AFM, and PC-AFM noted above have been solved in the case of PCI-AFM. The instrumental set-up of the PCI-AFM system and the demonstration to measure the conductance of single walled carbon nanotubes (SWCNTs) connected to a Au electrode on a mica surface is shown as follows.

Development of PCI-AFM

System setup

The PCI-AFM measurement was conducted by a scanning-probe microscope (JSPM-4200, JEOL) equipped with two function generators (WF1946, NF). The setting of function genereters is shown in Figure 2.2-1.

Figure 2.2-2 (a) shows a schematic illustration of the PCI-AFM method. Topographic image is measured in tapping-mode scan (noted as “I”) and *I-V* characteristics are measured in point-contact mode during (noted as “II”) the interruption of the tapping-mode scan. Based on the spatially resolved *I-V* measurements, a current image can be formed at a chosen bias voltage. This means that the topographic image and the current image can be obtained simultaneously.

Figure 2.2-2 (b) shows the timing chart of the signals used in the PCI-AFM measurement. Feedback is controlled by a TTL signal. When the signal is high (period I), the feedback is active and the cantilever is oscillated at a resonant frequency of 150 kHz for the tapping-mode scan. In this period, the z-servo voltage is stored in the memory of the computer to form a topographic image.

When the tip meets the preset positions for *I-V* measurements, the lateral scan is set to stop and the feedback control signal decreases. This high-to-low transition provides the trigger signal for the measurement of *I-V* characteristics during period II. In this period, the feedback system is deactivated, the cantilever excitation is stopped, and the tip-sample separation is set so that the tip and the sample contact under a particular loading force. Stopping the excitation enables the tip to contact the sample statically. Then, the applied bias voltage is ramped up and the *I-V* characteristics are stored in the memory of computer.

Finally, the tip-sample separation is re-set to the former value, the feedback system is

reactivated, and tapping mode scan is restarted. These alternate operations are continued, and both the topographical data and the *I-V* data are obtained at 128 points lengthwise and crosswise (total: 16,384 points).

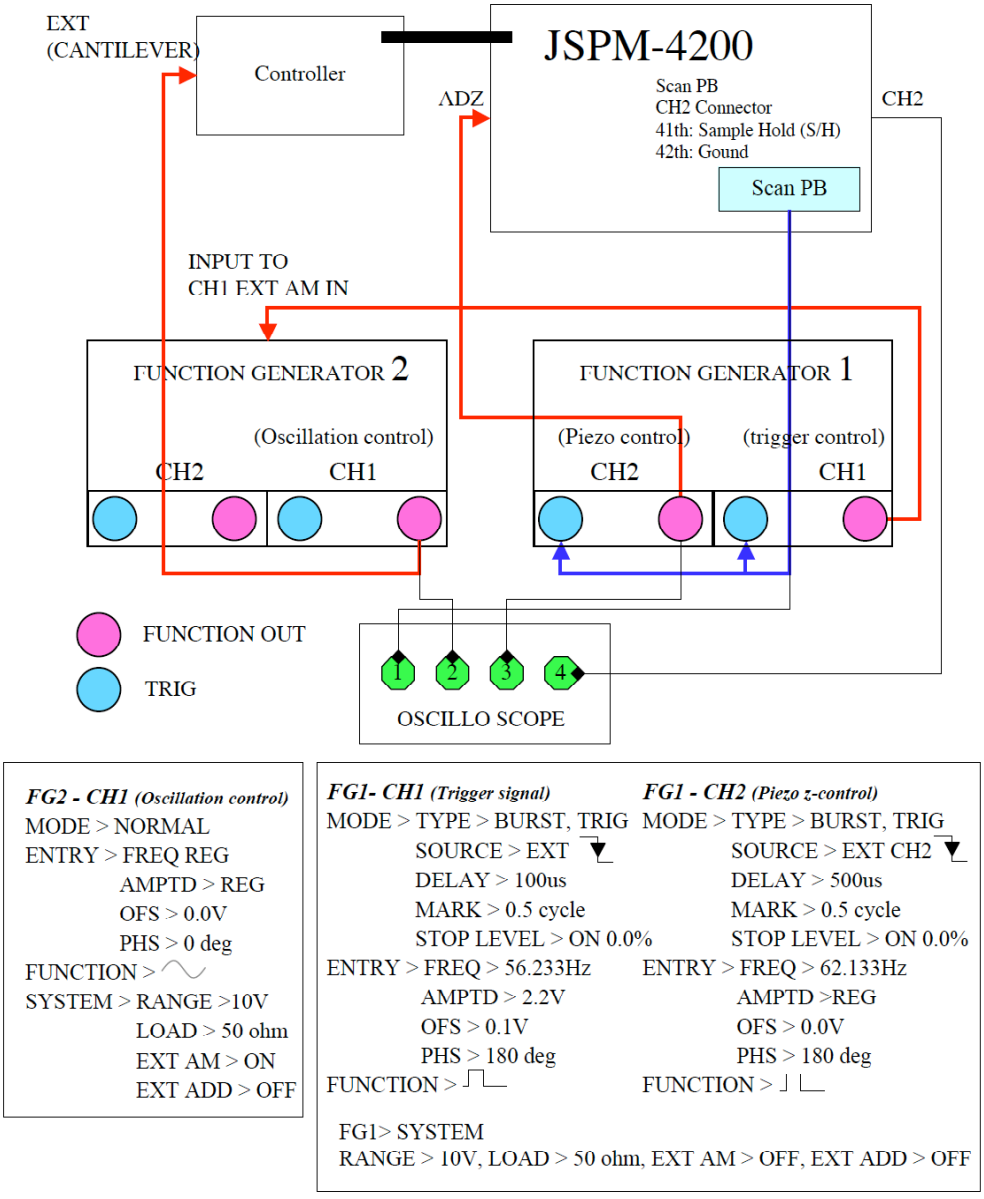

Figure 2.2-1
Electrical schematic diagram of PCI-AFM.

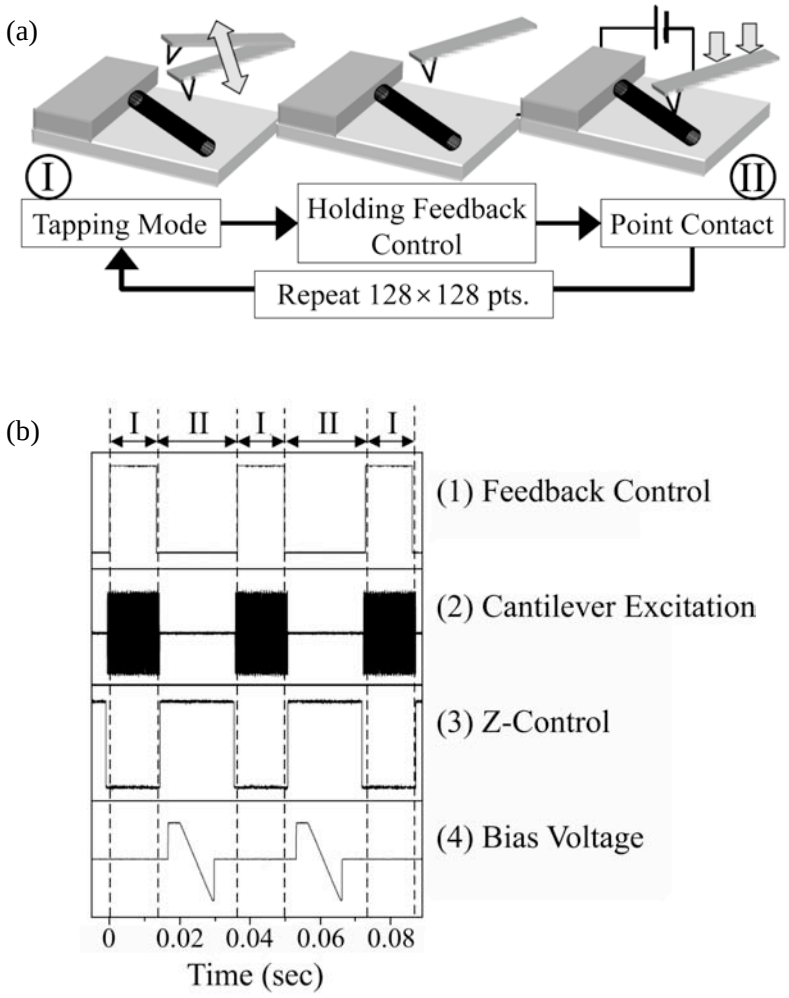

Figure 2.2-2
(a) Schematic illustration of the principle of PCI-AFM, which is operated by repetitive sequences: (1) Tapping-mode scan is employed for obtaining a topographic image, (2) Cantilever oscillation is stopped and feedback-loop is held to set tip position, (3) The tip approaches the sample for making electrical contact by additional input to the piezo scanner, and then *I-V* characteristics are measured. (b) Signals for the PCI-AFM operation. (1) Feedback control, (2) cantilever excitation, (3) Z-control, and (4) bias voltage for *I-V* measurement.

Analysis of tip oscillation

To analyze the tip behavior during PCI-AFM operation, the time-course of the cantilever displacements and the force curve are measured. The cantilever displacement is determined by measuring the deflection of a laser beam reflected off the back of the cantilever. The deflection is detected by a position-sensitive photodiode. The difference in the intensity of the upper half (A) segment of the photodiode and that of the lower half (B) is proportional to z-bending of the cantilever (V_{A-B}).

Figure 2.2-3 (a) shows signal V_{A-B} during the PCI-AFM operation. The cantilever oscillation during tapping mode remains for about 10 ms in period II after the stop of excitation. The measurement of *I-V* characteristics starts after the oscillation is quenching [as indicated in Fig. 2.2-2 (a)]. The inset shows the difference between the center oscillations of signal V_{A-B} in period I and the displacement of that in period II. The measured value of 0.011 V corresponds to the loading force during point contact. This force was estimated from a force curve obtained in the experiment described below.

Figure 2.2-3 (b) shows the force curve including the dynamic behavior of cantilever oscillation. When the tip is far from the sample surface, the cantilever oscillates freely. As the distance between the tip and sample decreases, the oscillation amplitude is suppressed by the tip-sample interaction, so the oscillation is quenched completely by the tip-sample adhesion when *d* is 35 nm. As the tip further approaches the sample, the cantilever displacement changes from negative to positive when the force changes from attractive to repulsive. In tapping mode, the feedback is set at about 70% of the amplitude of free oscillation (as indicated by point A). On the other hand, during the point-contact operation, the cantilever displacement observed in Fig. 2.2-2 (a) is 3.2 nm (indicated by point B) and the calculated loading force is 14 nN.

It is noted that the set point in tapping-mode operation is far from $d = 0$ (indicated by point O). Line C defines the position of the sample surface and line D indicates the lower turning point of the oscillating cantilever. Line D is 35 nm shifted from line C, suggesting that the tip does not touch the sample surface during tapping-mode operation. This result agrees with the former investigation reported by Pablo et al. [42] and implies that the operating conditions in tapping mode are not suitable for conductivity measurement.

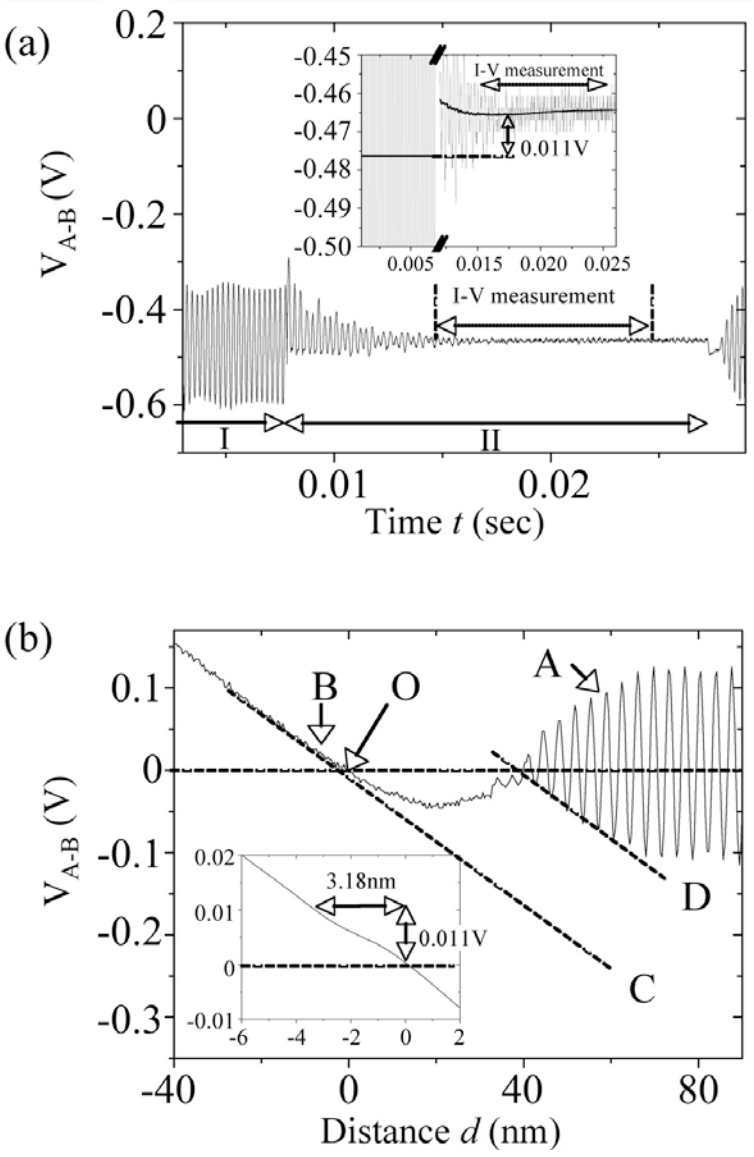

Figure 2.2-3
(a) Time-course of cantilever deflection during PCI-AFM operation. The inset shows the deflection for *I-V* measurement on a magnified scale.
(b) Force curve including the dynamic behavior in tapping mode. A and B show the set points for tapping mode and point contact. C and D indicate the positions of the sample surface and the turning point of cantilever oscillation.

Experimental Results ~Electrical conductivity along bundled SWCNTs~

In this section, we focus on spatially resolved conductivity measurement for bundled single-walled carbon nanotubes (b-SWCNTs) connected to a Au electrode on a mica surface. CNTs have attracted much attention due to their intriguing electrical properties, which make them prime candidates for nanoscale applications. For example, CNTs have been used as field effect transistors, single-electron transistors, rectifiers, and multi-terminal devices. [1-3, 14, 15] In these applications, the electrical and electric properties of CNT-CNT or CNT-metal interfaces strongly affect their device properties. For this reason, it is necessary to obtain the correspondence between local structure and electrical properties on the nanoscale in order to identify the properties of CNT-CNT/metal interfaces.

Materials and methods

Conductive cantilevers

The cantilever used have a platinum-coated tip (MikroMasch, NSCS-12/Pt) for current detection, and their force constant is 4.5 N/m and resonant frequency is about 150 kHz. The nominal tip radius was less than 40 nm.

PCI-AFM measurement

The PCI-AFM measurements were performed in a nitrogen-gas atmosphere in order to avoid electrochemical reactions at the tip and sample surfaces due to presence of oxygen and water.

Sample preparation

SWCNTs (Aldrich Corp.) with nominal diameters of 1.2 to 1.5 nm were suspended in N,N-dimethylformamide (10 mg/ml) [16] and the supernatant of the suspension was deposited on the cleaved mica surface. After an adsorption time of 1 min, surplus solution was removed by air blowing, and then the sample was dried. Au layer was deposited on half of the area of the sample surface to form electrical contacts with SWCNTs.

Results and Disucussion

Figure 2.2-4 shows a topographic image of b-SWCNTs and a Au layer (electrode) obtained by tapping-mode AFM. The cross-sectional profiles (**a** to **d**) show that the heights in the bundle are in the range of 6.3 to 8.3 nm. In the region of B to D, an additional SWCNT seems to be bundled because the height of this region is higher than that of region A by 1.5 or 2

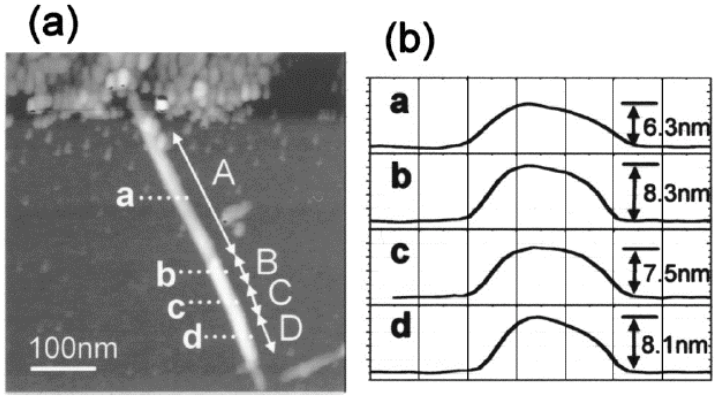

Figure 2.2-4
(a) Topographic image taken by tapping-mode AFM. One end of a bundled SWCNTs is covered with a gold electrode (top of figure). (b) Line profiles correspond to lines indicated in the image. The differences in height indicate that an additional SWCNT is adsorbed on the bundle in the region from B to D.

nm, which corresponds to the diameter of a single SWCNT. The additional SWCNT is clearly observed and distinguished from the other part by the gray scale difference in this image.

The effect of loading force on the electrical contact at the tip/SWCNT interface measured by PCI-AFM is shown in Figure 2.2-5. The topography and current images were obtained simultaneously. The current images are formed by the current values extracted from the *I-V* data at 1.0 V. Since the PCI-AFM method is able to choose set points separately for tapping-mode and point-contact measurements, the topographic images in Figure 2.2-5 (a) and (b) were taken with identical set points where the oscillation amplitude of the cantilever was reduced to 60% of free oscillation, respectively. On the other hand, the current images were obtained by point-contact measurements with a loading force of 11 nN in the attractive region and 10 nN in the repulsive region. The loading force was obtained by multiplying force constant of cantilever by z-displacement.

In comparison of current images with topography for the b-SWCNTs, differences in the width and brightness depending on loading force were observed. This difference is assumed to

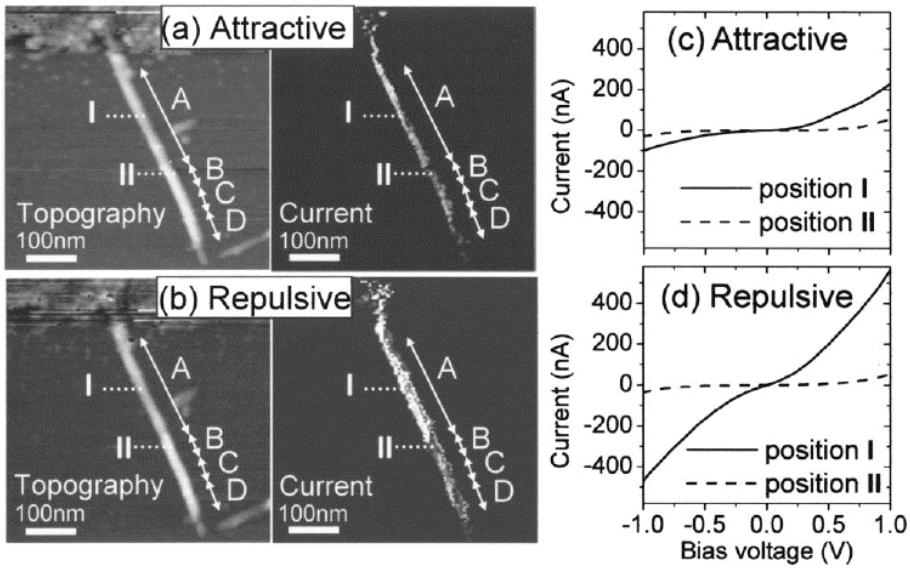

Figure 2.2-5
Topographic images (left panel) and current images (right panel) obtained by PCI-AFM. Gray scale of Current images shows the current values at 1.0 V bias voltage. These images were obtained with (a) attractive (adhesion) loading force of 11 nN and (b) repulsive loading force of 10 nN. (c), (d) *I-V* characteristics obtained by PCI-AFM. Solid and dotted lines correspond to positions **I** and **II** indicated in Fig. 3(a) and (b), respectively.

come from the different convolutions of the effective tip shape required to achieve electrical contact between the tip and the bundle. In the case of attractive loading force, the tip interacts mainly with the contamination layer covering the tip and sample, and only the tip apex can form the electrical contact. As a result, the tip size contributing the electrical contact is smaller than that working in the topography measurements, and the electrical contact is assumed to be insufficient. On the contrary, measurements with repulsive force make it possible to achieve electrical contact even at the side part of the tip. For this reason, the effective tip size for electrical contact becomes larger than that used in the topography.

Furthermore, the current image shows the difference in gray-scale distribution for the b-SWCNTs depending on loading force. When attractive loading force is applied, the additional SWCNT (parts B, C, and D) is observed with the same brightness as the other part as shown in Figure 2.2-5 (a). In contrast, the current image with repulsive loading force shows that the additional SWCNT gives weak brightness in comparison with the other part. These results are consistent with the investigation reported by Pablo et al. [10] They suggested that stable electrical contact of SWCNTs requires sufficient loading force to penetrate a contamination layer overlaying the samples. Our results indicate the effect of loading force on contact

resistance through images of the conductance.

To clarify the origin of loading force dependence, *I-V* characteristics were examined. When the loading force is attractive (Figure 2.2-5 (c)), the current at position **I** is a few times larger than at position **II** on the additional SWCNT. On the other hand, when the tip is pushed until the loading force becomes repulsive (Fig. 2.2-5 (d)), the current at **I** becomes much larger than that at **II**. In this measurement, it is noteworthy that the *I-V* curves at position **II** show agreement between the attractive and repulsive loading forces. Namely, loading force has considerable influence on *I-V* curves at position **I**, but the change at position **II** is almost negligible on the additional SWCNT. These results suggest that the contact resistance between SWCNTs is much higher than the tip-sample contact resistance.

A schematic illustration of the point-contact measurement for b-SWCNTs and an additional SWCNT is given in Figure 2.2-6 (a). Here, R_1 is contact resistance between a Au electrode and b-SWCNTs, R_2 is resistance of b-SWCNTs, and R_3 is contact resistance between b-SWCNTs and the additional SWCNT. R_4 is contact resistance between SWCNTs and the tip, and it is assumed to be constant regardless of tip position and changes only with the variation in loading force. Figure 2.2-6 (b) shows the variation in total resistance R along SWCNTs. The abscissa is the distance from the Au electrode to the tip. Although R in region A shows scattered values ranging from 2×10^6 to 2×10^7 owing to defects and contamination, the averaged R value does not change in this region. Therefore, R_2 can be neglected in the analysis of contact resistance, and the total resistance is given by $R_{add} = R_1 + R_3 + R_4$ on the additional SWCNT and $R = R_1 + R_4$ on the other part. The value of R_3 can be obtained from the difference between R_{add} and R. Conversely, $R_1 + R_4$ cannot be separated into individual components because R_1 and R_4 are identical in R_{add} and R.

The values of contact resistance are plotted as a function of bias voltage as shown in Figure (c) and (d). These values were obtained from measurements with (c) attractive and (d) repulsive loading forces. In both measurements, the R_3 value is one or two orders higher than $R_1 + R_4$. In the case of attractive loading force, the $R_1 + R_4$ value is several times higher that that obtained by repulsive loading force. Since R_1 is identical in both measurements, this result means R_4 (repulsive) < R_4 (attractive). In contrast, R_3 at high bias ($|V| > 0.5$V) shows similar values ranging from 1×10^7 to 1×10^8 ohms. This implies that the contact resistance between SWCNTs is not influenced by loading force at high bias voltage. However, at the low bias ($|V| <$ 0.3V), the R_3 with attractive loading force is one order higher than that with repulsive force. This suggests that the origin of contact resistance between SWCNTs has two or more factors

that behave in different ways to loading force. This assumption is supported by the fact that a shoulder is observed in the *I*-*V* curve of R_2 at $|V|$ =0.3V in Figure 2.2-6(d).

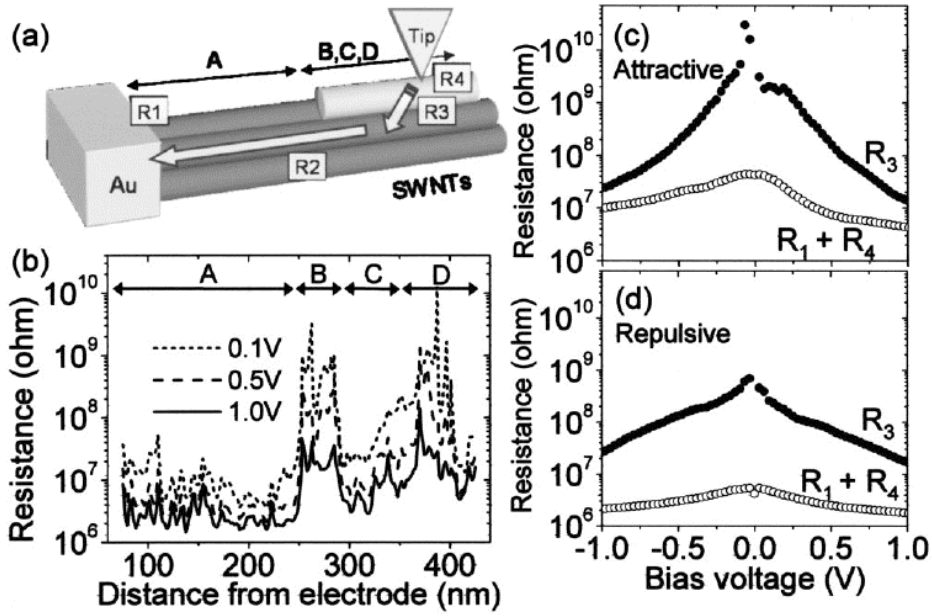

Figure 2.2-6
(a) Schematic illustration of bundled SWCNTs used in this study. (b) Relationship between total resistance *R* and the distancedistance between the tip from and gold electrode. Resistance data are plotted in logarithmic scale at bias of 0.1V, 0.5V and 1.0V. Arrows (A to D) correspond to the part of the bundled SWCNTs in Figure 3. (c), (d) Partial resistance R_1 $+R_2+$ R_4 and R_3 are plotted as a function of bias voltage with attractive and repulsive forces. R_3 corresponds to contact resistance between SWCNTs shown in (a).

Conclusion

Electrical resistance of bundled single-walled carbon nanotubes (b-SWCNTs) are measured by PCI-AFM. Simultaneous mapping of the topographic information and current level through SWCNTs enable us to investigate the relationship between structure and conductance. Variation in resistance of a b-SWCNTs indicates that the resistance between SWCNTs was higher than 10^7 ohms with strong voltage dependence.

As mentioned above, PCI-AFM provides a detailed picture of the electrical contact at the SWCNT-SWCNT interface. We demonstrated that PCI-AFM is a powerful tool for characterizing local properties of nanotube devices. In particular, PCI-AFM enables us to measure conductance along the vertical direction to the substrate surface. This advantage cannot be found in non-contact type microscopy such as electric force microscopy and Kelvin probe microscopy [17,18]. This ability will be important in future investigations of nanomechanoelectric devices [19].

2.3. Top-contacted geometry type nanogap electrodes

Introduction

The construction of electrical circuits with molecules has been proposed and studied with much enthusiasm due to the several advantages of this method. There are three primary factors to consider when designing this type of circuit. First, the electronic properties of molecules can be designed by employing well-established synthetic chemistry. Recent progress in chemistry has enabled us to obtain long molecules of about 40 nm [20]. Second, the size of each molecule is so small that it might be possible to fabricate extremely small functional electrical elements, and the fabrication costs would fall because molecules can be synthesized in large quantities at a time. Third, distinctive nanostructures can be fabricated by self-assembly with specific molecules [21].

Although the development of molecular devices looks promising, it is crucial to recognize that there are problems in connecting molecules to electrodes, mainly related to electrical contacts and structural deformation. Usually, molecules tend to form higher-order structures such as crystals and self-assembled monolayers, with the exception of matter comprising single molecules [22, 23]. Because there is a complex relationship between structural and electrical properties, it is essential to measure the electrical characteristics of molecules that are connected to electrodes while retaining the molecular structures.

Molecular electronic properties have usually been examined using electrodes with nanoscale gaps (nanogaps) as small as the molecular sizes, fabricated by electron beam (EB) lithography, photolithography or electromigration methods [24–27]. The molecules are fixed between electrodes by dropping the solution after the electrodes are fabricated (bottom-contacted geometry).

The problem with these methods is that the structure of molecules between electrodes is unclear. When molecules are fixed between electrodes, the structure of the molecules can become bent and/or deformed at the edge of the electrodes, as shown in Figure 2.3-1 (a) [28]. This deformation can cause electrical phenomena such as electron scattering or reflection at the locally deformed conductive path. Therefore, it is important to develop a new approach to retaining the molecular structure.

Figures 2.3-1 (b) and (c) show schematic illustrations of approaches to overcoming this problem. In both cases, the electrical characteristics of molecules can be measured without

structural deformation. Figure 2.3-1 (b) shows that the molecules are positioned on the coplanar electrodes with an insulating substrate. The coplanar electrode would be useful for achieving not only deformation-free electrical characterization but also spatially resolved characterization by scanning probe microscopy. This is due to an open structure, permitting a tip to approach the molecules without interfering with the electrodes. Although such an advantage exists with coplanar electrodes, a problem remains: during fabrication, it is difficult to obtain a surface flat enough to use in the study of molecular electrical properties. Moreover, fixation of molecules to coplanar electrodes might cause local aggregation or deformation due to the difference in surface energy between the insulating substrate and the electrode.

The top-contacted geometry electrode (TCE) features advantages over the bottom-contacted geometry electrode mentioned above. Figure 2.3-1 (c) shows that the molecules are positioned on the flat surface and they are top-contacted by electrodes. Because electrodes are fabricated on molecules that are fixed on the flat substrate beforehand, the structural deformation can be avoided thanks to the homogeneous surface energy. However, there are still problems for electrode fabrication with this method. One is that the irradiation of EB as well as lift-off processes may cause structural degradation and denaturing of molecules due to the EB and organic solvents.

In this part, we report a new fabrication method, the angle-controlled shadow-masking method, for nanogap TCE (nTCE) without using photo- or EB lithography techniques. We have successfully and reproducibly fabricated nTCEs separated by less than 100 nm. Previous results have demonstrated electrode fabrication by nanoscale stencil masks [29] in order to preserve the molecular structure; however, the reported gap length was about 1 μm [30].

Because the proposed method is very simple, it is possible to fabricate nanogap electrodes faster than by conventional methods and to obtain statistical results for use in reproducibility studies. Furthermore, we have obtained the electrical characteristics of molecular nanorods made of a porphyrin derivative by nTCE.

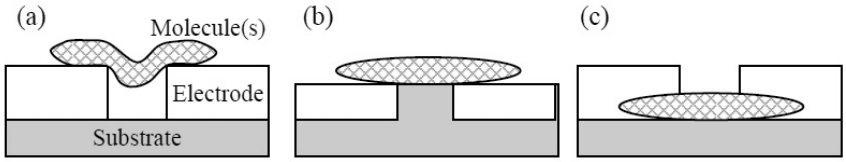

Figure 2.3-1
Schematic illustrations for measuring electrical properties of molecules. Molecules are connected to electrodes with (a) Bottom-contacted geometry and (c) top-contacted geometry. (b) Molecules are positioned onto a coplanar electrode.

Development of fabrication method

Figure 2.3-2 (a) illustrates the fabrication procedure of the angle-controlled shadow-masking method for nTCE. The procedure is as follows.

(1) Molecules are placed or patterned on the substrate (substrate A). The substrate should be flat to avoid the conformational change in the molecules.

(2) A small piece of silicon wafer (Si(100)), which was cleaved along its crystal axis, was mounted on substrate A. This is used for the mask. The silicon mask and substrate A were clipped together by alligator clip or fixed together by homemade gigue.

(3) The first Au electrode layer was fabricated by thermal evaporation method, after which the silicon mask was removed. With such an atomically sharp edge of the cleaved silicon substrate, it is possible to fabricate electrodes with very sharp edges. Figures 2.3-2 (b) and (c) show the topographic image and cross-section of the first-layer electrode obtained with an atomic force microscope (AFM, Digital Instruments, Nanoscope IIIa), respectively. Note that the electrode has a very sharp edge and there is no structural change such as thermal migration of metal particles occurring near the electrode.

(4) A metal mask was mounted onto substrate A, and Au electrodes (second layer) were fabricated by thermal evaporation method. The metal mask has a pattern of nine windows, each with a width of 5 μm, in this study. The direction of the evaporation angle was controlled to be oblique against the first layer to form a shadow.

This method is based on a previous report by Naitoh et al. [31] and Philipp et al. [32] Following fabrication of the second layer, gaps between the first and second layer formed due to the shadow of the first layer. The gap length G can be ideally estimated as

$$G = H(1/tan\theta_2 - 1/tan\theta_1),$$

Where H is the height of the first-layer electrode, and θ_1 and θ_2 are the angle of the edge of first-layer electrode and the oblique deposition angle of the second-layer electrode, respectively. This indicates that the gap length can be controlled by changing the thickness of the first-layer electrode and the oblique angle in the fabrication process of the second-layer electrode.

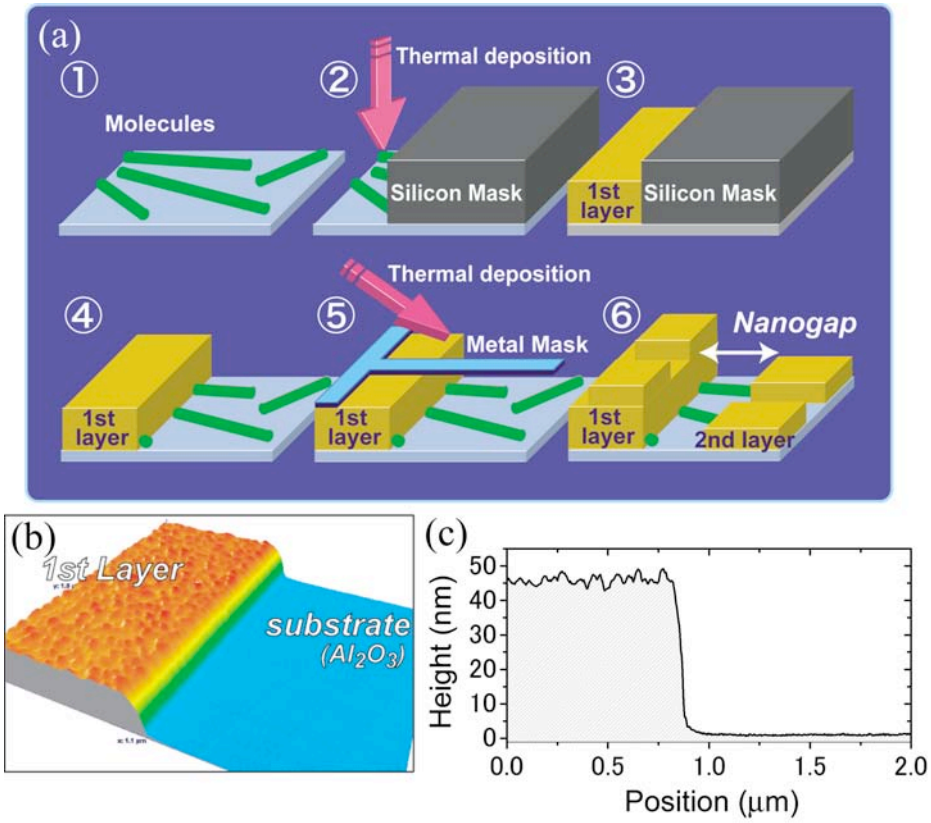

Figure 2.3-2
(a) Fabrication procedure of angle-controlled shadow-masking method. The width of the metal mask shown in the fifth image is actually much wider than shown in the illustration. (b) Topography of first-layer electrode obtained by AFM. (c) Cross-section of the first-layer electrode measured by AFM.

Fabrication of electrodes

Figures 2.3-3 (a) and (b) show a representative image of nTCE without molecules as observed by optical and scanning electron microscopy, respectively. The thicknesses of the first- and second-layer electrodes were 80 nm and 30 nm, respectively, as measured by a quartz thickness monitor. The oblique angle for second-layer deposition was set to 30 degrees.

Figure 2.3-3 (a) shows the first-layer electrode and nine patterned second-layer electrodes fabricated on a substrate. The nanogaps are formed inside the square marked in the image. The gap length between the first-layer electrode and the second-layer electrode was measured as 65 nm as shown in Fig. 2.3-3 (b), although the minimum length attained to date is 40 nm. The smallest reproducible gap length we have been able to produce for a fabricated nTCE is less

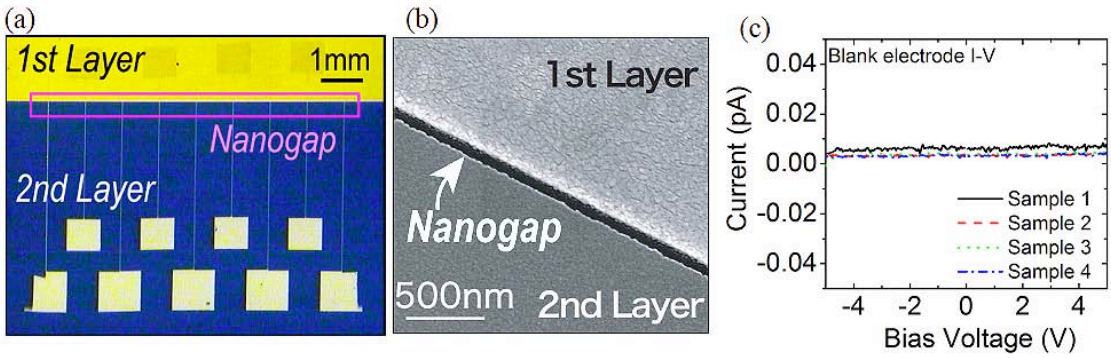

Figure 2.3-3
(a) Image of nanogap electrodes observed by optical microscope. The narrow white lines are the 5-μm-wide electrodes. (b) SEM image of nanogap between first- and second-layer electrodes. (c) *I-V* characteristics of four electrodes without molecules.

than 100 nm.

Figure 2.3-3 (c) shows *I-V* characteristics of four electrodes without molecules, and these measurements were performed under a vacuum condition (10^{-4} Torr). The resistance exceeded 10^{14} Ω, which is the apparatus' detection limit. This value is high enough for the electrical measurement of molecules, as shown later. It should also be noted that this electrode is stable under the application of a ± 5 V bias voltages.

The effect of fixation of silicon mask on the 1st layer Au electrode fabrication

Next, the difference of fixing silicon mask on the sample between two different methods is studied. Figure 2.3-4 shows the schematic illustration of the method to fix the silicon mask on the sample. (a) shows the fixation method by alligator clip. (b) shows the method by homemade gigue made by Al. Each left and right figure shows the front and side view, respectively. The alligator clip is made blade spring, and therefore the pressure is given uniformly all over the contact area between clip and silicon mask.

On the other hand, the homemade gigue is composed of tension plate, base and screw. The tension plate and the base are connected by screws, which are arranged to the both side of the tension plate. The silicon mask is fixed on the sample by tighten up screws. As the strongest pressure is given at both side of the plate, the pressure distribution along the silicon mask is rather different from that of by alligator clip.

That is, as the tensions are applied at the position that screws are tighten, and the width of

silicon mask is controlled to be wider than that of sample, both of tension plate and silicon mask would be bent as shown in figure 2.3-4 (c). If both of tension plate and silicon mask is bent and fixed on the sample, the space is formed between silicon mask and sample, and the degree of space would be changed with increase the distance from the screw. Then, after the first Au layer electrode is fabricated on it by thermal deposition, the form of the edge of the electrode would be changed due to the space between silicon mask and sample.

Supporting this assumption is obtained by measuring the distance between electrodes by SEM. Figure 2.3-5 shows because the edge of the first Au layer electrode is changed from steep edge to gentle one, and that the variation of nanogap electrode that are fabricated on the same substrate, simultaneously. The distance between electrodes is observed to change for adjacent pairs of electrode, each other. The minimum distance is observed at the center part of the sample substrate.

The important viewpoint in these results is that top-contacted geometry electrodes with different nanogap distance can be fabricated simultaneously due to the space between silicon mask and sample.

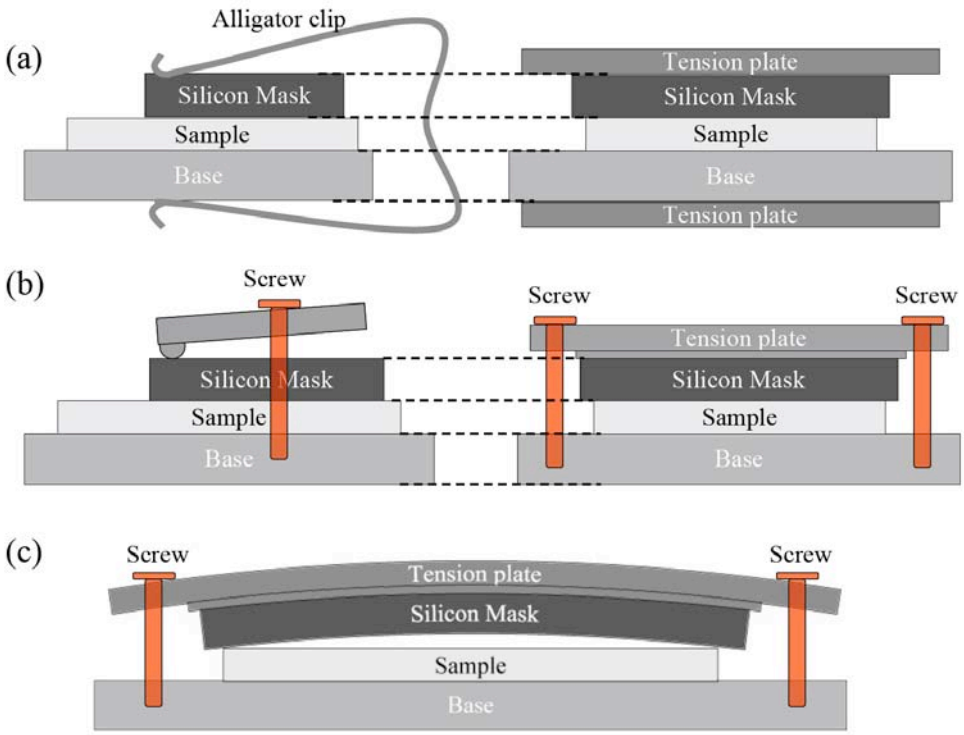

Figure 2.3-4
Schematic illustration of the method to fix the silicon mask on the sample.

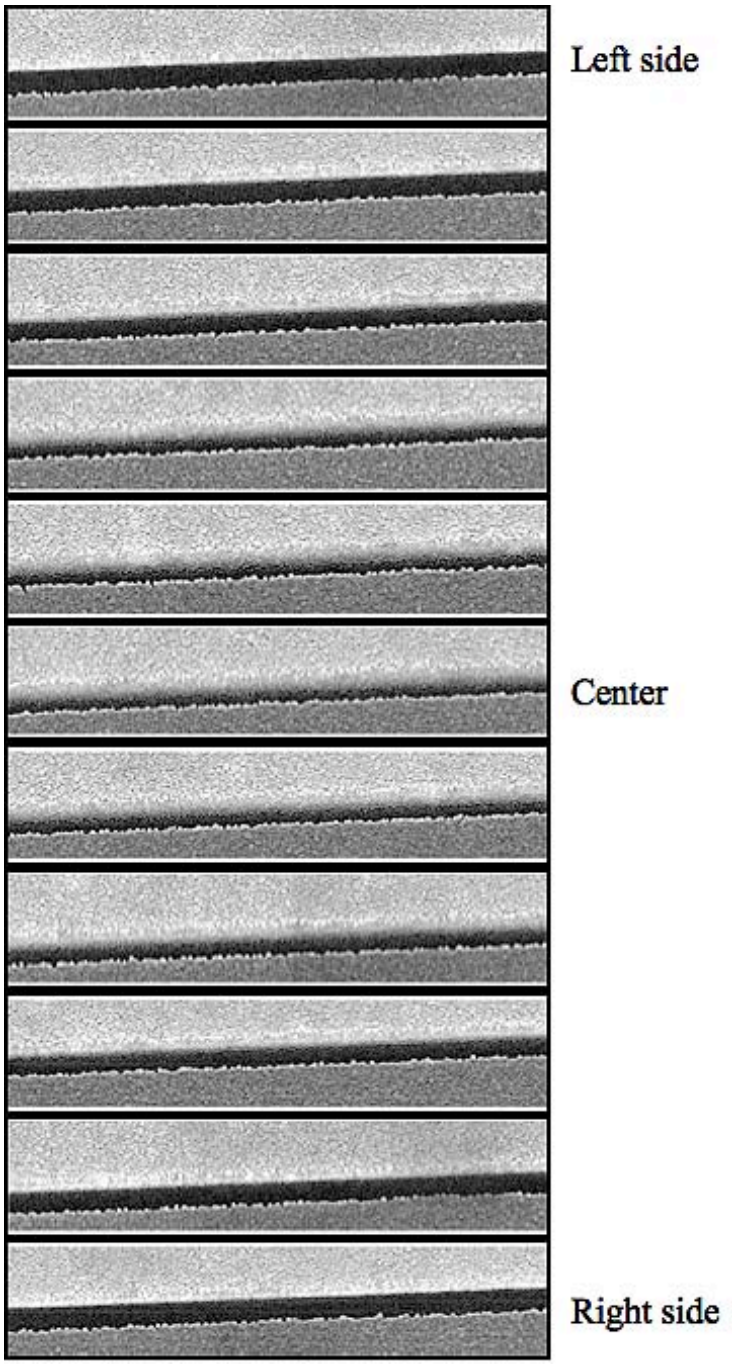

Figure 2.3-5
SEM images of nanogap electrodes fabricated by the developed shadow masking method. Each electrode is fabricated on the same substrate. The position of electrodes is also noted, and it is correspond to the position of aligned electrode as shown in figure 2.3-3 (a).

Experiment ~Electrical conductivity along porphyrin nanorods~

In this section, we focus on conductivity measurement porphyrin nanorod by top-contacted nanogap electrodes. The molecular nanorod made of porphyrin-derivative molecules (TPPS: 5,10,15,20 - tetraphenyl - 21H, 23H - porphyrine tetrasulfonic acid) shows the formation of J-aggregates inside. (Figure 2.3-6 (a))

Experimental findings reveal that the electrical conductivity of TPPS nanorods decreased under oxygen and nitrogen gas-purged conditions. Furthermore, comparing between these results to previously reported results would indicate the structural deformation arising from the type of electrical connection between electrodes and molecules affects electrical conductivity strongly.

Material and methods

Porphyrin Nanorods

Synthesized TPPS [33] was dissolved in MilliQ to a final concentration of 6.7×10^{-5} M (pH = 4.85), after which the TPPS solution was deposited onto the sapphire substrate and dried at 55℃ in a drying machine. The sapphire substrate was treated in a boiling acid solution beforehand to clean it and to introduce hydroxyl groups onto the surface [34].

Fabrication of Electrodes

We have employed both polished Si(100) with a 300-nm thick layer of SiO_2 (Electronics and Materials Corp., Japan) and annealed sapphire (Al_2O_3(0001)) (Shinkosha Corp., Japan) as substrates. Au (99.95%, Nilaco Corp., Japan) electrodes were fabricated by thermal evaporation in a homemade chamber under a vacuum pressure of 10^{-7} Torr. In this study, the deposition rates for Au were 1.5 Å/sec for the first-layer electrode and 3 Å/sec for the second-layer electrode. The silicon mask is fixed on the sample by the alligator clip.

Electrical Measurements

Electrical measurements were performed by a semiconductor characterization system (Keithley 4200) under different condition such as vacuum, N_2 gas purged and O_2 gas purged condition..

Spectrum Measurements

The absorbance spectrum was obtained with UV/visible spectrometer (Ultrospec 3300 pro, Amarsham Biosciences). The circular dichroism (CD) is measured with a CD spectrometer (J-820, JASCO)

Results and Discussion

Structure of Nanorods

Figure 2.3-6 (b) shows a topographic image of the prepared sample measured by AFM. It was found that the distinctive nanorod structure was formed after the evaporation of water solvent, and as shown in the inset, the mean height was 25.2 nm with a standard deviation of 4.5 nm. The length of each rod was measured to be a few micrometers. Previous results reported the formation of TPPS nanorods with a smaller diameter by a different fabrication method from ours [35].

In order to study the structure of TPPS nanorods, we measured the absorbance spectra of both the TPPS solution and the TPPS nanorods on the sapphire substrate, as shown in figure 2.3-6 (c). The TPPS solution exhibited absorbance peaks at 413 nm and 433 nm, which are attributed to the π-π^* transition of the TPPS molecule (solet band) in free-base form and the diacid monomer, respectively (Figure 2.3-6 (a)) [36]. On the other hand, TPPS nanorods showed maximum peaks at 491 nm and 705 nm, which are attributed to the B-band and the Q-band, respectively, of J-aggregates. The formation of J-aggregates indicates that molecules are stacked head-to-tail and aligned along one direction inside each nanorod [32, 37 – 39].

To measure the TPPS nanorods' electrical conductivity, we fabricated nTCE on TPPS nanorods and measured the *I-V* characteristics under vacuum (10^{-4} Torr) and gas-purged conditions. The thickness of the first-layer and the oblique angle for thermal deposition were 80 nm and 15 degrees, respectively. The gap length was estimated to be about 225 nm from the results of an electrode without molecules as shown in Figure 2.3-3 (b). We employed this estimation because it was difficult to measure the gap length by SEM due to charging of the sapphire substrate or by AFM due to the resolution limit of the finite tip apex for relatively large TPPS nanorods. About 30 nanorods were estimated to exist between electrodes from the AFM results mentioned above.

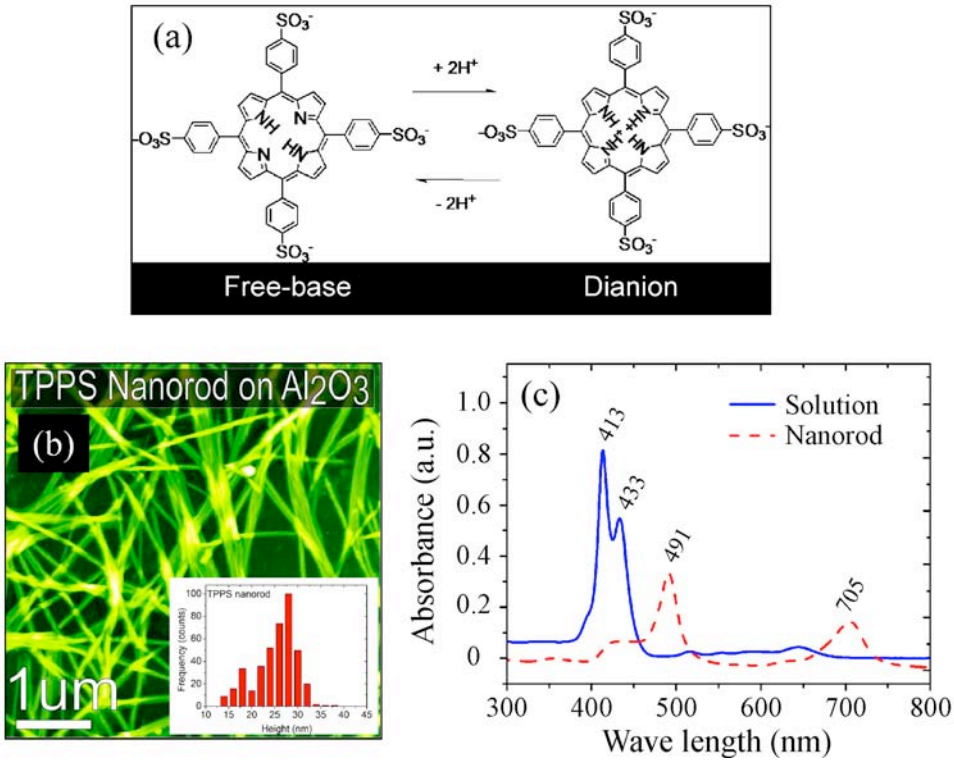

Figure 2.3-6
(a) Molecular structure of TPPS. Left and right structure correspond to the free-base form and dianion form, respectively. (b) TPPS nanorods on sapphire substrate observed by AFM. (c) UV-Vis absorbance spectrum of TPPS molecules in solution and as nanorods. The straight line corresponds to the solution and the dotted line to a nanorod.

Electrical measurements

Figure 2.3-7 (a) shows the averaged current-voltage (*I-V*) characteristics of seven samples under the vacuum condition. Linear *I-V* characteristics were measured, giving an estimated mean resistance of 8.1×10^{10} Ω. The standard error of the mean was calculated to be 6% of the mean resistance, a small value that indicates the homogeneous distribution of nanorods on the substrate and the fabrication of uniform electrodes. N_2 and O_2 were introduced into the evacuated chamber (10^{-4} Torr) until atmospheric pressure was attained. As a result, the current decreased following the introduction of both N_2 and O_2 gases, but the magnitudes of current changes were quite different between these gases. As Figure 2.3-7 (b) shows, the resistances under N_2 and O_2 gases were ten times and three orders of magnitude, respectively, higher than that under the vacuum condition.

Figures 2.3-7 (c) and (d) indicate the time course of the change in current at 4 V of applied bias voltage. Figure 2.3-7 (c) illustrates that the current fell sharply to below the apparatus' detection limit immediately after introducing O_2 gas; in contrast, N_2 introduction led to a more gradual decrease (Fig. 2.3-7 (d)). After evacuation of the chamber, the current increased with time to almost the same level as the initial state (Fig. 2.3-7 (b)).

These results suggest that a conductive path might form inside the TPPS nanorods under the vacuum condition. This means that because J-aggregates form inside the nanorods, it is possible for the carriers to pass through the π-stacked porphyrin molecules. On the other hand, under the gas-purged conditions, the conductivity decreased due to the introduced molecules. Figures 2.3-7 (c) and (d) clearly show that O_2 has a stronger effect on the current than N_2 does. Since the gas pressure was maintained at atmospheric pressure under both N_2 and O_2 gas conditions in this experiment, gas pressure can be ruled out as an influence on the differences in conductivity. Thus, the different changes in conductivity between O_2 gas and N_2 gas might be due to local oxidation of the nanorods or local structural change induced by the introduced O_2

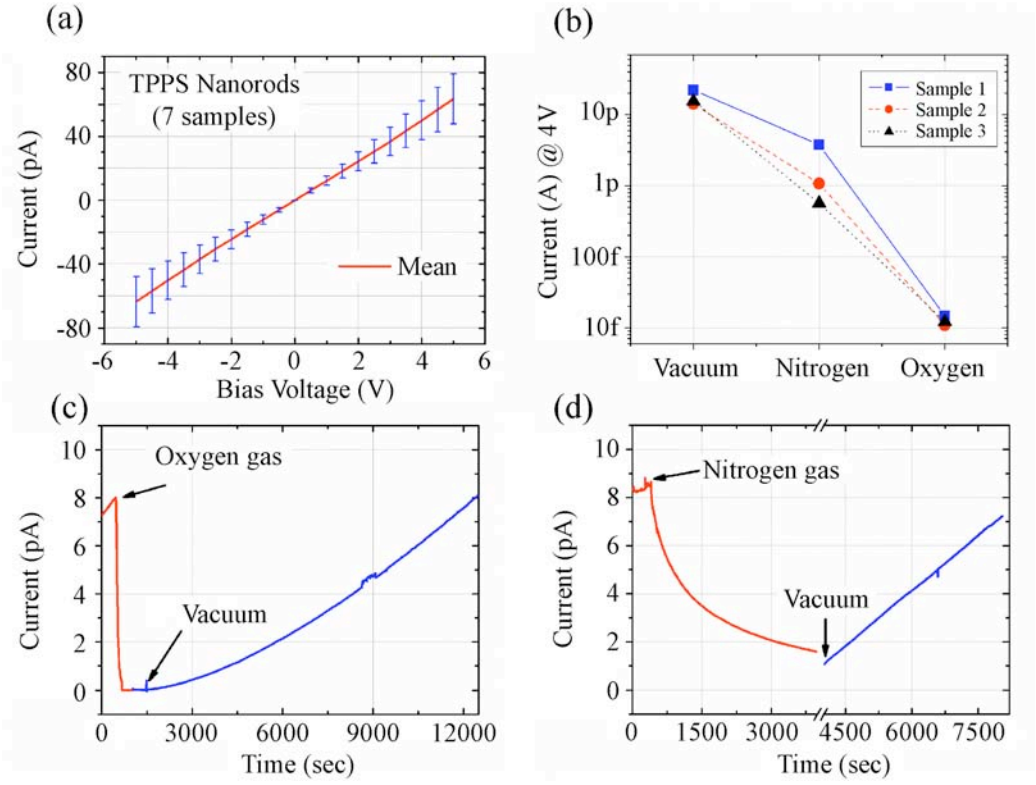

Figure 2.3-7
(a) Current-voltage characteristics of TPPS nanorods under the vacuum condition for seven samples. (b) Current change of TPPS nanorods under various conditions. (c) and (d) Current change in TPPS nanorod under oxygen and nitrogen gas conditions, respectively. The current was measured under 4 V of applied bias voltage.

gases. A detailed investigation into this mechanism is needed, but the change of local structure along nanorod is probable. Figure 2.3-8 shows the CD spectrum measured under various environmental conditions. As it is difficult to identify the differences in experimental results, the differential spectrum is shown in lower part. It is clearly observed that chirality changes between oxygen and vacuum condition, nitrogen and vacuum condition and oxygen and nitrogen condition, respectively.

This result indicates that the structure is changed under various conditions. The method to control the chirality in J-aggregates is studied previously [40]. As the nanorods used in this study are fabricated just by drying solution on the substrate, it is conceivable that the mixed chirality exist inside nanorods. Therefore, it is quite difficult to identify the origin of peaks in the differential spectrum, and the detailed study is needed as the next step. However, this result is the evidence that the change in local structure affect electrical transport properties.

It also should be noted that the previous study had suggested that TPPS nanorods with smaller diameters, obtained by a bottom-contacted geometry electrode [41], had insulating characteristics. The different results could be attributed to electro-scattering at locally deformed structures of the nanorod at the edge of the electrode or at the defect inside the smaller nanorods.

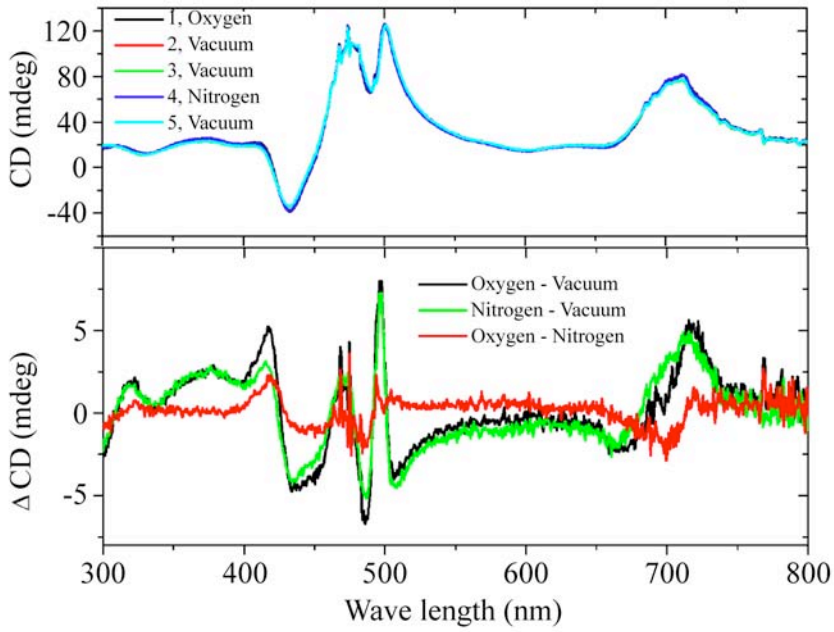

Figure 2.3-8
CD spectrum of TPPS nanorod under various environmental conditions. Upper and lower graph show experimental results and differential results between different environmental conditions, respectively.

Conclusion

We have developed the fabrication method of nanogap electrodes by the angle-controlled shadow-masking method without employing conventional lithography techniques, which involve a wet process. By using this method, it is possible to measure the electrical characteristics of nanostructured molecules and/or materials at the nanoscale without structural deformation resulting from a solvent and/or electron beam. We measured the electrical characteristics of TPPS nanorods, and the findings show that a conductive path is formed along TPPS nanorods and that conductivity is strongly affected by the environmental gas condition.

The point of these studies is to determine whether electrical measurement of TPPS nanorods, a nanostructured organic molecule, could actually be performed with nTCE. Obtained results indicate that if a wet process were to be used in the fabrication of nanogap electrodes, both of these molecules would be deformed and/or dissolved.

This method is applicable not only to organic materials but also to non-organic materials. Moreover, the method makes it possible to fabricate electrodes with different materials, facilitating study of the electrical alignment between electrodes and molecules, which is an interesting topic in the field of molecular electronics.

References

[1] V. Derycke, R. Martel, J. Appenzeller, Ph. Avouris, *Nano lett.* **1**, 453 (2001).
[2] A. Bachtold, P. Hadley, T. Nakanishi, C. Dekker, *Science* **294** (2001) 1317.
[3] J. Kong, C. Zhou, A. Morpurgo, H.T. Soh, C.F. Quate, C. Marcus, H. Dai, *Appl. Phys. A* **69**, 305 (1999).
[4] E. Braun, Y. Eichen, U. Sivan, G.B.Yoseph, *Nature* **391**, 775 (1998).
[5] C. Mao, W. Sun, Z. Shen, N.C. Seeman, *Nature* **397**, 144 (1999).
[6] T.W. Kelly, C.D. Friesble, *J. Vac. Sci. & Technol. B* **18**, 632 (2000).
[7] L. Zhang, T. Sakai, N. Sakuma, T. Ono, *Jpn. J. Appl. Phys.* **39**, 3728 (2000).
[8] H. Sakaguchi, A. Hirai, F. Iwata, A. Sasaki, T. Nagamura, E. Kawata, S. Nakabayashi, *Appl. Phys. Lett.* **79**, 3708 (2001).
[9] X.D. Cui, X. Zarate, J. Tomfohr, O.F. Sankey, A. Primak, A.L. Moore, T.A. Moore, D. Gust, G. Harris, S. M. Lindsay, *Nanotechnology* **13**, 5 (2002).
[10] P.J. de Pablo, M.T. Martınez, J. Colchero, J.G. Herrero, W.K. Maser, A.M. Benito, E. Munoz, A. M. Baro, *Adv. Mater.* **12**, 573 (2000).
[11] P.J. de Pablo, F.M. Herrero, J. Colchero, J.G. Herrero, P. Herrero, A.M. Baro, P. Ordejon, J.M. Soler, E. Artacho, *Phys. Rev. Lett.* **85**, 4992 (2000).
[12] P.J. de Pablo, C.G. Navarro, J. Colchero, P.A. Serena, J.G. Herrero, A.M. Baro, *Phys. Rev. Lett.* **88**, 036804 (2002).

[13] X.D. Cui, A. Primak, X. Zarate, J. Tomfohr, O.F. Sankey, A.L.Moore, T. A.Moore, D. Gust, G. Harris, S.M. Lindsay, *Science* **294**, 571 (2001).
[14] S.J. Tans, M.H. Devoret, H. Dai, A. Thess, R.E. Smalley, L.J. Geerligs, C. Dekker, *Nature* **386**, 474 (1997).
[15] M. Bockrath, D.H. Cobden, P.L. McEuen, N.G. Chopra, A. Zettl, A. Thess, R.E. Smalley, *Science* **275**, 1922 (1997)
[16] J. Liu, M.J. Casavant, M. Cox, D.A. Walters, P. Boul, W. Liu, A.J. Rimberg, K.A. Smith, D.T. Colbert, R.E. Smalley, *Chem. Phys. Lett.* **303**, 125 (1999).
[17] A. Bachtold, M.S. Fuhrer, S. Plyasunov, M. Forero, E.H. Anderson, A. Zettl, and P.L. McEuen, *Phys. Rev. Lett.* **84**, 6082 (2000).
[18] P. J. de Pablo, C.G. Navarro, A. Gli, J. Colchero, M.T. Martinez, A.M. Benito, W. K. Maser, J. G. Herrero, A. M. Baro, *Appl. Phys. Lett.* **79**, 2979 (2001).
[19] T. Rueckes, K. Kim, E. Joselevich, G.Y. Tseng, C.L. Cheung, and C.M. Lieber, *Science* **289**, 94 (2000).
[20] A. Tsuda, A. Osuka, *Science* **293**, 79 (2001).
[21] T. Yokoyama, S. Yokoyama, T. Kamikado, Y. Okuno, S. Mashiko, *Nature* **413,** 619 (2001).
[22] J.Park, A.N. Pasupathy, J.I. Goldsmith, C. Chang, Y. Yaish, J.R. Petta, M. Rinkoski, J.P. Sethna, H.D. Abruna, P.L. McEuen, D.C. Ralph, *Nature* **417,** 722 (2002).
[23] W. Liang, M.P. Shores, M. Bockrath, J.R. Long, H. Park, *Nature* **417**, 725 (2002)
[24] H. Park, A. Lim, A. Alivisatos, J. Park, P.L. McEuen, *Appl. Phys. Lett.* **75,** 301 (1999).
[25] S.J. Tans, A.R.M. Verschueren, C. Dekker, *Nature* **393,** 49 (1998).
[26] G. Maruccio, P. Visconti, V. Arima, S. D'Amico, A. Biasco, E. D'Amone, R. Cingolani, R. Rinaldi, S. Masiero, T. Giorgi, G Gottarelli, *Nano Lett.* **3,** 479 (2003).
[27] D. Porath, A. Bezryadin, S. Vries, C. Dekker, *Nature* **403,** 635 (2000).
[28] A. Bezryadin, A.R.M. Verschueren, S.J. Tans, C. Dekker, *Phys. Rev. Lett.* **80,** 4036 (1998).
[29] K. Ono, H. Shimada, S. Kobayashi, Y. Otsuka, *Jpn. J. Appl. Phys.* **35,** 2369 (1996).
[30] Y.X. Zhou, A.T. Johnson Jr, J. Hone, W.F. Smith, *Nano Lett.* **3,** 1371 (2003).
[31] Y. Naitoh, K. Tsukagoshi, K. Murata, W. Mizutani, *e-J. Surf. Sci. Nanotech.* **1**, 41 (2003).
[32] G. Philipp, T. Weimann, P. Hinze, M. Burghard, J. Weis, *Microelectron. Engrg.* **46,** 157 (1999).
[33] TPPS molecules are synthesized and purified by Tamai.
[34] Please see chapter 6.
[35] A.D. Schwab, D.E. Smith, C.S. Rich, E.R. Young, W.F. Smith, J.C. de Paula, *J. Phys. Chem. B,* **107,** 11339 (2003).
[36] J.M. Ribó, J. Crusats, J.A. Farrera, M.L. Valero, *J. Chem. Soc., Chem. Commun.*, **681**. (1994)
[37] O. Ohno, Y. Kaizu, H. Kobayashi, *J. Chem. Phys.* **99**, 4128 (1993).
[38] D.L. Akins, H.R. Zhu, C. Guo, *J. Phys. Chem.* **98**, 3612 (1994).
[39] D.L. Akins, H.R. Zhu, C. Guo, *J. Phys. Chem.* **100** 5420 (1996).
[40] J.M. Ribó, J. Crusats, F. Sagués, J. Claret, R. Rubires, *Science* **292**, 2063 (2001).
[41] A.D. Schwab, D.E. Smith, B. Bond-Watts, D.E. Johnston, J. Hone, J.C. de Paula, W.F. Smith, *Nano Lett.* **4**, 1261 (2004).
[42] J. Colchero, P. de Pablo, M. Luna, J.G. Herrero, A.M. Baro, *Ext. Abstr. 2nd Int. Workshop on Non-Contact Atomic Force Microscopy* "nc-AFM '99" (1999) p. 61.

Chapter3

Direct Electrical Measurements of DNA

In this chapter, results of the electrical measurements of DNA molecules are noted. The measurements were performed by both of the conventional and newly developed methods noted in the chapter 2. At first section, the results obtained by top-contacted geometry type electrode are shown. The results by PCI-AFM and bottom-contacted geometry type electrodes are shown in these orders later.

3.1. Bottom-contacted geometry type nanogap electrodes

Introduction

DNA plays important roles, such as protein synthesis, in many activities of life on earth. It possesses all of the information required to maintain the homeostasis of life. Furthermore, DNA has a unique double-stranded structure and the characteristic that it can self-recognize its bases. Recently, not only from a biological viewpoint but also from a physical one, the electrical conductivity of DNA has been studied closely with the aim of producing nanoscale devices such as molecular wire in several ways [1-8]. Many studies have thus been accomplished in order to determine whether DNA is conductive or not [9-11]. Various models explaining both of the charge transfer and charge transport of DNA have also been proposed [12-17]. Several factors are thought to contribute to the charge transport of DNA, that is, electric (hole) conduction along the base pair sequences, ionic conduction related to counter ions and protons, and loss of conduction due to dipole orientation in the water layer around the DNA [17]. DNA molecules are composed of three parts: phosphates, sugars, and bases. In aqueous solution, phosphates face towards water; therefore, the structure of the double strand is stabilized. Any change in the DNA's environment, particularly in humidity, might affect the characteristics of the DNA. In order to study the effect of humidity in more detail, we fabricated DNA film on nanogap electrodes and measured their electrical conductivity under various humidity conditions.

Experimental Results

Material and Methods

Sample fabrication

A drop of DNA solution (0.3 μl; Amersham Pharmacia Biotech co.) containing 1.25 μg/μl poly(dG)-poly(dC) was placed at the center of a comb-shaped nanogap electrode. The DNA used in these experiments was synthesized to form homopolymers consisting of 50 bases as starting materials and synthesized DNA strands are held together by hydrogen bonds between the bases in the solution. This solution also contains about less than 10 mM NaCl as counter ions for stabilizing the DNA structure. After being incubated for about 10 minutes, the samples were dried at room temperature. The macrostructure of the DNA film was observed under an optical microscope. The lengths of the poly(dG)-poly(dC) was also determined by electrophoresis. the length of poly(dG)-poly(dC) was widely distributed from 1 kbp to over 35 kbp.

Nanogap Electrodes

The comb-shaped nanogap electrode is fabricated by the combination of photolithography and a double-angle evaporation technique onto insulative SiO2/Si substrate. The set of electrode is composed of ten electrodes with a pitch of 100 nm.

Electrical Measurements

Direct *I*-*V* measurements were carried out under relative humidity from 30 % to 95 % and in vacuum (Keithley 213 Quad Voltage Source, Keithley 236 Source Measurement Unit). Relative humidity was controlled in a laboratory-made airtight container.

In order to elucidate the conduction mechanism, AC measurements were carried out under various relative humidity. (Solartron SI 1260 Impedance / Gain-Phase Analyzer) As external electrodes, Au wires were connected to the nanogap electrodes by silver paste.

Results and Discussion

Formation of DNA film

Figure 3.1-1 (a) and (b) shows the SEM image of nanogap electrodes and the morphology of DNA film measured by optical microscopy. The DNA film of Poly(dG)-poly(dC), shows a dendrite structure. The amount of DNA between electrodes separated with a distance of 100nm is estimated to be about $5\sim7\times10^{-2}$ ng. We measured X-ray diffraction and RHEED, but there was no specific peak observed. Hence, the structure of DNA film is thought to be in the amorphous state. As each DNA molecule exists randomly between electrodes, the electrical conductivity of DNA film indicates that there is no anisotropic characteristic. One of the

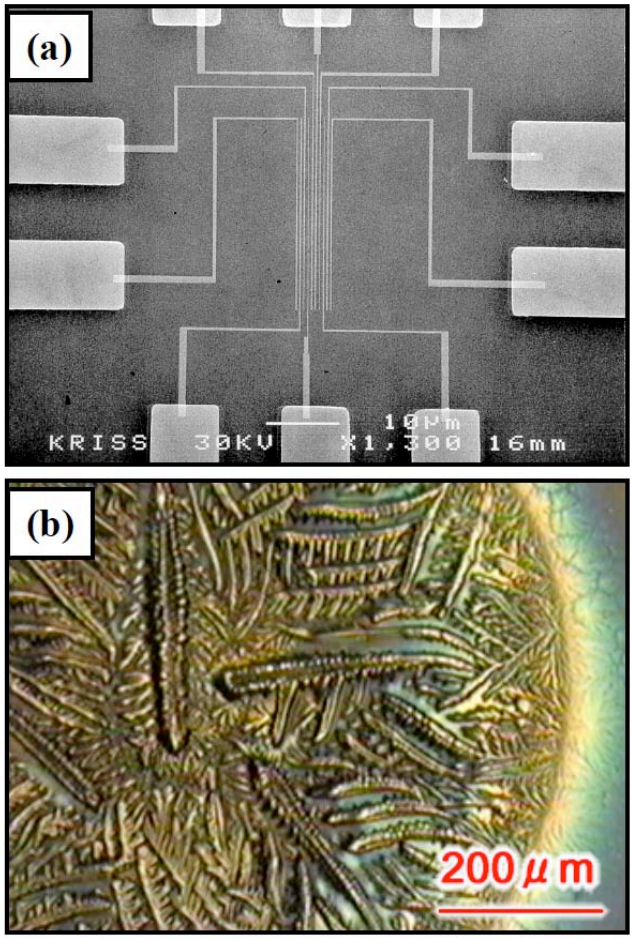

Figure 3.1-1
(a) SEM image of comb-shaped nanogap electrodes. Each electrodes are separated 100 nm, respectively. (b) Morphology of dried DNA films. poly(dG)-poly(dC) DNA formed dendrite structure. Concentration of DNAs is 1.25 μg/μl.

possible explanations for the formation of dendrite structure is due to the concentration of NaCl in the solution.

Current-voltage measurement of DNA film

The *I-V* measurements were performed under both vacuum and atmospheric conditions (typical relative humidity was approximately 28 %). Figure 3.1-2 shows the typical results of *I-V* measurements of poly(dG)-poly(dC). Under the atmospheric condition, the resistance was estimated to be 1.7×10^{10} Ω, whereas under the vacuum condition, the resistance was estimated to be 3.9×10^{12} Ω. After measuring under the vacuum condition, the resistance was measured under the atmospheric condition for the second time, and was almost the same as that under the first atmospheric condition (result not shown here). This suggests that the dramatic change of resistance is strongly depend on the atmospheric condition and shows reversible character.

In order to study the effect of humidity on DNA film conductivity, *I-V* measurements were performed under controlled relative humidity. The temperature was maintained at 18 ℃. As the relative humidity increases, conductivity increases rapidly. As shown in Figure 3.1-3, the resistance decreases exponentially with increasing relative humidity. In particular, it decreases

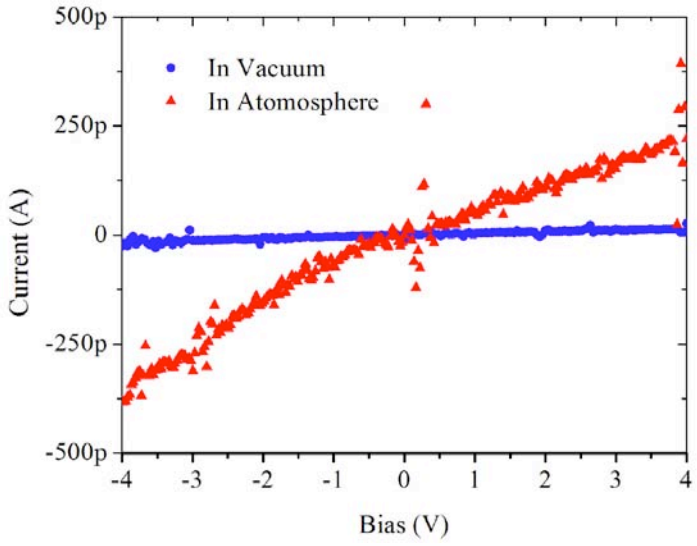

Figure 3.1-2
Typical I-V curves of DNA film (poly(dG)-poly(dC)). Squares and triangles indicate the I-V curve measured in vacuum and the atmospheric condition at the relative humidity of 28%, respectively.

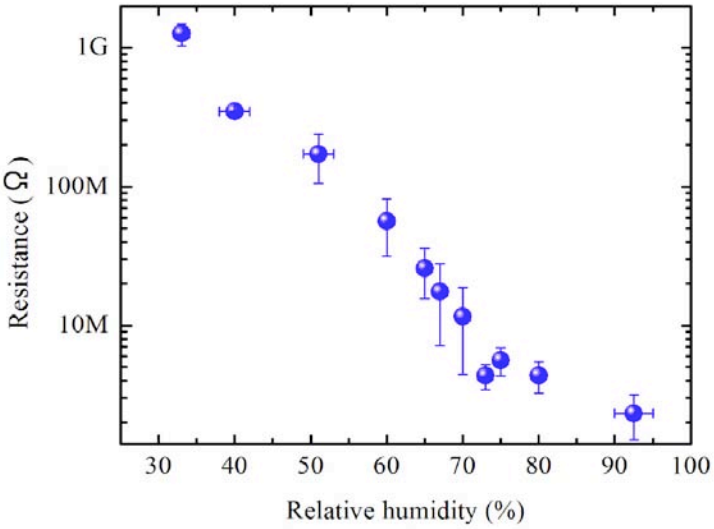

Figure 3.1-3
Relationship between relative humidity and resistance of DNA film. Resistances are estimated from the I-V measurements at the voltage of –2 V under each relative humidity condition.

rapidly by about one order of magnitude at a relative humidity of 65 ~ 70 %. Overall, the resistance decreases dramatically from $\approx 10^9$ Ω at 30 % relative humidity to $\approx 10^6$ Ω at 90 % relative humidity. It is understood that the amount of water molecules adsorbed by the DNA affects the decrease in resistance.

This transition is explained as follows. DNA is composed of three parts: phosphoric acids, sugars, and bases. Because of the hydrophilic phosphoric acid around the base pairs of DNA, water molecules are easily adsorbed and form hydrogen bonds between the phosphoric acid and the water molecule. Infrared spectroscopy has revealed that five or six water molecules are coordinated to the oxygen atom of single phosphoric acid at 65 % relative humidity. Furthermore, as the relative humidity is over 65 %, additional water molecules will hydrate to the amino groups, imino groups and keto groups of the bases. At the relative humidity of 80 %, the number of water molecules adsorbed is about 20 [18]. When the next water molecule comes, it is physically adsorbed through hydrogen bonding to the neighboring water molecule. This process is consistent with that illustrated in Fig. 3.1-3.

The electric conducting mechanism in a physically adsorbed layer of water molecules on the DNA surface may be similar to that of aqueous solution. Without rotation of the water molecules, a hydrogen bond and a covalent bond between the hydrogen atom and an oxygen atom of a neighboring water molecule can easily and quickly exchange. Continuous exchange of protons through the physically adsorbed water layer occurs in this way [19]. Although sodium ions act as counter ions for stabilizing the DNA, protons move several times faster than

sodium ions in aqueous solution (mobility of a proton is 36.3×10^{-4} $cm^2\cdot s^{-1}\cdot V^{-1}$ and that of sodium ion is 5.19×10^{-4} $cm^2\cdot s^{-1}\cdot V^{-1}$). [20] Therefore, at higher relative humidity, the proton conductivity dominates the ionic conduction.

Alternating current measurement of DNA film

Considering the results of AC measurements, Fig. 3.1-4(a) shows the Cole-Cole plot of the DNA film at 83 % relative humidity. Although this is an incomplete semicircle, a complete semicircle will be estimated at a much higher frequency than 1 MHz. At relative humidity lower than 80 % and in vacuum, no semicircles were measured in the Cole-Cole plot. Some studies have been reported on interpreting the deviation from the ideal semicircular behavior observed in Cole-Cole plots [21]. In the previous literature [22], impedance spectroscopy of SnO_2 shows that a low-frequency spur has been observed in the Cole-Cole plots at higher relative humidity and it is concluded to be due to the migration of ions towards the electrode sample contact region. In our case, the Cole-Cole plot is similar to that of this previous literature; the spur is thought to appear at frequencies lower than 100 Hz. Therefore, our results indicate that the conduction mechanism is ionic conduction under high humidity. We have adopted the equivalent circuit for fitting the experimental data. The equivalent circuit is composed of three

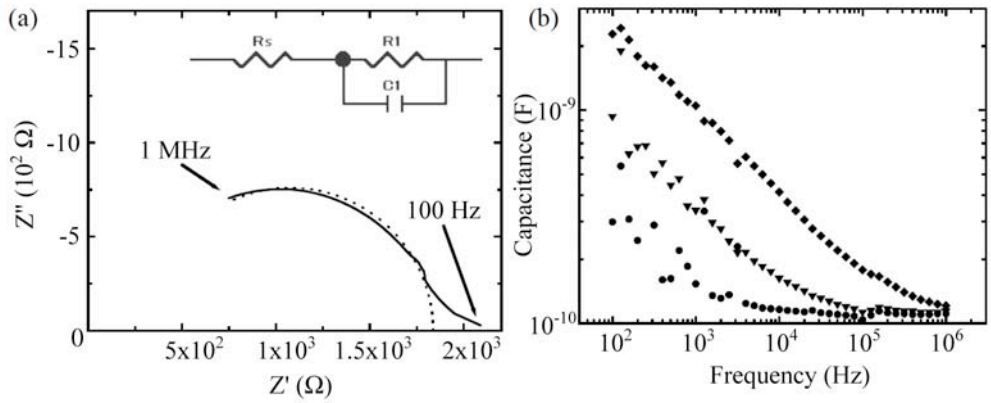

Figure 3.1-4
(a) Cole-Cole plot of DNA at 83% relative humidity. Solid line and dotted line indicate the measured result and the fitted curve, respectively. The equivalent circuit adopted for fitting is shown in the inset. R_S, R1 and C1 are calculated to be $3.2\times10^2\,\Omega$, $1.5\times10^3\,\Omega$ and 1.6×10^{-10} F, respectively. ◆ (83%), ▼ (70%) and ● (50%). (b) AC measurement of capacitance vs. frequency of applied electric field (25 mV) under various relative humidity.

parts, as shown in the inset in Fig. 3-4(a). R1 and C1 represent the contributions to resistance and capacitance, respectively, arising from the DNA boundaries and electron depletion regions. R_S is a resistance added in series to the parallel capacitance resistance combinations. R_S, R1 and C1 are calculated to be $3.2\times10^2\,\Omega$, $1.5\times10^3\,\Omega$ and 1.6×10^{-10} F, respectively.

We compared the degree of capacitance, one of the important factors in the electrical conduction. As shown in Fig. 3.1-4 (b), capacitance increases with increasing relative humidity. At the relative humidity of 50 %, the capacitance is constant at frequencies higher than 10^4 Hz. With increasing relative humidity, the saturation is shifted to the higher range, up to 10^6 Hz. Finally, at the relative humidity of 83 %, no constant area is observed. This increase in the values of capacitance indicates the proton transfer through the physically adsorbed layer of water, enhanced with increasing humidity [22]. On the other hand, in the case of 40 ~ 80 % relative humidity, the phases of AC measurements of DNA film are θ = -70° ~ -90° and Debye-type dielectric dispersion is observed. These findings suggest that the DNA film is partially dissolved and DNA molecules, which have the dipole moment, can relax up to the frequency of 10^4 Hz. The AC measurements support that the conduction is strongly affected by humidity and the main conduction mechanism is ionic conduction.

Lastly, it must also be noted that the contact resistance between the electrode and DNA film affects the total conductivity of the DNA-electrode system. To distinguish between contact resistance and DNA resistance, resistance was measured by the conventional four-probe technique. The four-probe technique eliminates the contact resistance; therefore, we can determine the actual resistance of the sample itself. The temperature was 19 ℃ and the relative humidity was maintained at 85 %. The measured resistance was $1.5\times10^3\ \Omega$. As a comparison, in the two-probe measurement, the resistance under the same conditions was approximately $\approx 10^6\ \Omega$. These results suggest that the contact resistance is three orders of magnitude higher than that of DNA film. The issue of contact resistance between sample and electrodes is particularly important in mesoscopic science. Therefore, we need to establish a means of fixing DNA molecules to electrodes with ohmic contact in the next step.

Conclusion

The humidity dependence of DNA film conductivity using a nanogap electrode is studied. DNA films of poly(dG)-poly(dC) were found to be extremely affected by humidity; the resistance decreased exponentially with increasing relative humidity. Furthermore, AC measurement indicated the increase in the value of capacitance and the semicircles and spurs in the Coal-Coal plot. Therefore, ionic conduction was found to dominate the conductivity of DNA film under the atmospheric condition. Moreover, the contact resistance affects the conductivity of DNA film. The contact resistance is three orders of magnitude higher than the conductivity of DNA film. Results of this study show that, in the case of measuring the DNA conductivity accurately with an external electrode, it is necessary to note the important factors: humidity and contact resistance between electrodes and samples.

3.2. Point-contacted Current Imaging Atomic Force Microscopy

Introduction

Previous results obtained by the top-contacted geometry type electrodes in section 3.1 shows that the electrical conductivity of DNA thin film increases exponentially with increasing the relative humidity. This is because the water molecules are adsorbed on the DNA molecules, and the ions included in the solution move through the water layer around DNA. Meanwhile, the electrical conductivity is not measured under vacuum condition. (Resistance is much more than the background resistance of apparatus.) As it can be imagined that the structure of DNA is bend at the edge of electrode, the insulative behavior might originate from such structural bending.

The PCI-AFM, which is noted in the previous chapter 2.1, enables us to measure both of the structure and the *I-V* characteristics simultaneously in nanoscale. Moreover, the samples (molecules) are immobilized on the substrate and electrodes are connected to them by top-contacted geometry. Hence, the structural deformation anticipated in the measurement by bottom-contacted geometry type electrode noted in the previous section would be prevented, and the PCI-AFM seems suitable for the electrical measurements of DNA.

In this section, the results of electrical measurements of DNA network on a mica surface by PCI-AFM are noted thereafter. The effect of relative humidity is also discussed.

Experimental

Material and Methods

Sample preparation

The DNA sample used in our study consisted of synthetic nucleic acids comprising poly(dG)·poly(dC) (Amersham Pharmacia Biotech Co., Tokyo, Japan). DNA is diluted with 17.4 MΩ deionized water to concentrations of 500 μg/ml.

A 10 μl sample drop was dropped on the freshly cleaved mica and spread over an area approximately 10 mm diameter. Freshly cleaved muscovite green mica (Nilaco Co., Japan) was used as substrates. After 1 min of incubation at room temperature, the sample solution was

blown off with air.

Electrical measurments

An Au layer was deposited over half of the sample surface area to form electrical contacts with the DNA network. Cleaved silicon substrate is used as mask and it mounted on the sample. Silicon mask and sample are clipped together by alligator clip. The thickness of the Au electrode was nominally 20 nm.

The PCI-AFM measurement was conducted using AFM (JSPM-4200, JEOL) equipped with a two-function generator (WF1946, NF Corporation). The range of bias voltage is set to be -5 to +5 V. The cantilever used have a platinum-coated tips (MikroMasch, NSCS-12/Pt) for current detection, and their force constant is 4.5 N/m and resonant frequency is about 150 kHz. The nominal tip radius was less than 40 nm.

The atmospheric condition is changed by controlling the relative humidity. Initially, dry nitrogen gas was filled in the vacuum chamber of the AFM system (0 % of relative humidity), and the water steam was injected to it in an effort to control the humidity.

Results and Discussion

DNA network structure on the substrate

Figure 3.2-1 (a) shows the topography of DNA network structure on mica substrate. A different morphology at the upper part in the image indicates that Au layer is fabricated on the DNA network structure. As the thin Au layer (around 20 nm) is fabricated, it is possible to observe the network structure through Au layer. The height and width distribution of network structure are measured approximately 2 – 4 nm and 10 – 50 nm, respectively. As is reported previously, it is well known that the actual height of DNA on the substrate is quite smaller than the nominal diameter of DNA strand. Assuming the distribution of height to be 0.5 – 1.2 nm, the number of DNA strand in the network structure is estimated to be 2 – 8.

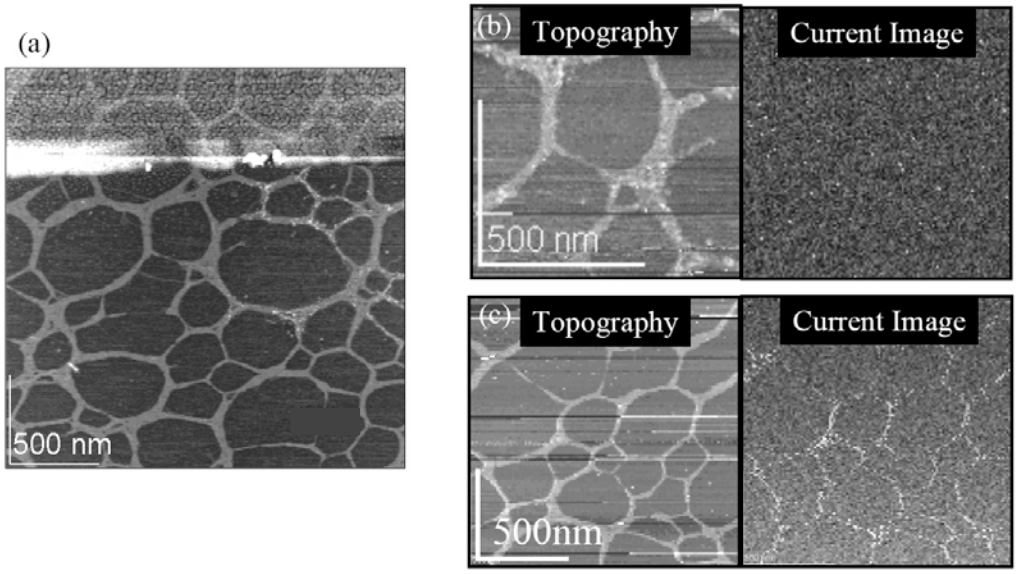

Figure 3.2-1
(a) Topographic image of DNA network on mica substrate. The gold electrode is shown in upper part of the image. (b) Topographic image (left) and current image (right) obtained by PCI-AFM. The relative humidity is 15 %. The current image shows the current level as 2.8 V is applied between gold electrode and tip. (c) Topographic image (left) and current image (right) obtained by PCI-AFM. The relative humidity is 60 %. The current image shows the current level as 4.4 V is applied between gold electrode and tip.

Electrical measurements

Electrical measurements are performed by PCI-AFM. Figure 3.2-1 (b) and (c) show the image obtained under 15 % and 60 % of the relative humidity, respectively. The closest distance between the Au layer and tip in figure 3.2-1 (b) and (c) is 100 nm and 300 nm, respectively. The loading force of the tip is set to be 20 nN. In order to assure the presence of metal coating of the tip during measurements, it is confirmed that ohmic contact is obtained after the tip is contacted with the Au layer. This confirmation is performed between each measurement by PCI-AFM.

Under the condition that the relative humidity is 15 %, topography shows the network structure as shown in figure 3.2-1 (a), but nothing is observed in the current image. Previous results of the electrical measurements of single-walled carbon nanotubes by PCI-AFM showed the current image along nanotubes that is exactly correspond to topography (chapter 2.2). Therefore, the current image for these measurements implies that the resistivity of DNA

network is as much as that of mica. The resistance is estimated to be more than 500 GΩ from the *I-V* characteristic.

On the other hand, different results are obtained under the condition that the relative humidity is kept to be 60 %. Note that the topography shows the similar network structure as dried condition (figure 3.2-1 (a)), and this indicates the network structure is stable even under higher humidity condition. The current image shows the brighter contrast at the position that DNA network structure exists. That is, the current level between DNA network and mica substrate is different. The current is measured to be 60 pA on the DNA network and 40 pA on mica substrate from the *I-V* characteristics at 5 V of bias voltage.

These results may indicate that it seems possible to conduct an electrical current through DNA molecules, but it doesn't actually. Although the differences in current are measured to be 20 pA at 5 V of bias voltage, it was impossible to ascertain the change in current with increasing the distance between Au layer and conductive tip. Namely, the absence of distance dependency between electrodes is obtained. Moreover, as the sweeping of bias voltage is limited to be 100 Hz in the PCI-AFM, it is impossible to measure the charge transport phenomenon originate from conductive carrier with lower mobility.

Previous results of the effect of humidity on the conductivity of DNA thick film indicated that the DC conductivity is strongly affected by the relative humidity [23]. (Chapter 3.1) The resistance decreased exponentially with increasing relative humidity. The time course of current also showed the decrease in current to the limit of measurement apparatus as the time of applying bias voltage increased. Furthermore, AC measurements indicated that the capacitance increased with increasing relative humidity. The origin of capacitance is the proton transfer through the physically adsorbed water layer around DNA molecules.

As the bias voltage with the sweeping time of 100 Hz is applied to electrode, counter ions adsorbed around DNA molecule or water molecules would be attracted toward electrode. Therefore, the differences in current would be originate from the charging at the electric double layer formed at the metal / DNA interface.

The electrical measurements of DNA network by PCI-AFM show no evidence of the charge transport along DNA molecules. The presumable origin of these results would be;

1, DNA is insulative. Hence, no current can be conducted.

2, The limitation of electrical measurements by PCI-AFM. It is impossible to detect the current by this method.

The reason for impossibility of PCI-AFM would be;

1, Limitation of the distance between the tip and Au electrode.

Due to the finite size of tip apex, it is difficult to shorten the distance between tip and electrode. Moreover, in case the electrode is contained in the area of PCI-AFM measurement, the electrode is destroyed due to the electro-migration of Au layer under the extremely higher electrical field. Therefore, the minimum distance is limited to be 100nm for the sake of risk-free measurements.

2, Limitation of the speed of bias voltage sweep.

As is already noted, as the sweeping of bias voltage is limited to be 100 Hz, it is impossible to measure the charge transport phenomenon originate from conductive carrier with lower mobility.

3, Electrical contacts between tip and DNA.

The conductive tip is used as one-side electrodes, and it is contacted with DNA for *I-V* measurements. The electrical contacts between tip and DNA is different from that between DNA and Au layer. The interface between Au layer and DNA would be cleaned because the Au is deposited on the DNA by thermal deposition (~10^{-4} Torr). On the other hand, as the tip is transferred to the chamber as it is bought (tip is not cleaned before use), it is acceptable that the surface of tip is covered with phisisorbed water layer and contamination. Hence, the interface between tip and DNA contains such layers that are not favorable to form the stable electrical contacts.

In order to clarify the origin of these results, the presumable origins noted above must be solved. As shown in chapter 3.3, the results by top-contacted geometry type electrodes are found to be the best way to solve these problems.

Conclusion

In conclusion, we measured the electrical conductivity of DNA network structure on mica substrate by PCI-AFM. It was impossible to obtain the evidence of charge transport along DNA network under 15 % of relative humidity. On the other hand, a distinctive current image is obtained under 60 % of relative humidity. The differences in current level would be originated from the charging at the interface between metal electrode and physisorbed water layer around DNA molecules. These results indicate that the PCI-AFM technique is not appropriate for electrical measurements of DNA, and possible problems included in this measurement method must be solved.

3.3. Top-contacted geometry type nanogap electrodes

Introduction

As noted in the section 3.1 and 3.2, different type of measurement technique is employed for the study of charge transport along DNA molecules. Despite of efforts, no evidence of intrinsic electrical properties of DNA is obtained. Electrical current through DNA molecules are measured under atmospheric condition or higher relative humidity condition due to the ionic current or the charging current through the water layer around DNA, but it was impossible to discuss the charge transport phenomenon under vacuum condition. The information derived in these experiments to achieve the electrical measurements of DNA in vacuum would be as below.

1, Prevent structural deformation of DNA molecules between electrodes.

2, Distance between electrodes should be smaller than 100 nm.

3, Stable electrical contacts between electrodes and DNA.

Therefore, we have developed the new fabrication method of nanogap electrode that satisfies requirements noted above. As noted in section 2.2, the top-contacted geometry type nanogap electrodes make it possible to fabricate electrodes that are separated less than 100 nm each other on the DNA molecules.

In this section, results of electrical measurement of DNA molecules immobilized on the APS coated SiO_2 substrate by the developed nanogap electrodes is noted. Moreover, the electrical property of G-wire in which the G-quadduplexes are formed inside is studied. G-quadduplexes are hydrogen-bonded arrays of guanine bases (G-quartets, Figure 3.3-1), and they are stacked together by π-π interactions. (Figure 3.3-6(a)) The study of G-wire originate from the structure analysis of G-rich sequences in telomeric DNA. This is because the telomeric ends of chromosomes are fundamental in protecting the cell from recombination and degradation [24]. The disruption of telomere maintenance leads to cell death. Hence, the structure of G-quartets of the telomeric DNA has been studied for therapeutic intervention in cancer [25-27].

The reason why the G-wire is used in this study is that it is expected that the conductivity will be enhanced compared to the natural double stranded DNA molecules, because G-wire is composed of four guanine bases that possess lowest ionization potential. Moreover, the enhanced electrical properties are expected, but the detailed study of electrical properties is not

reported previously.

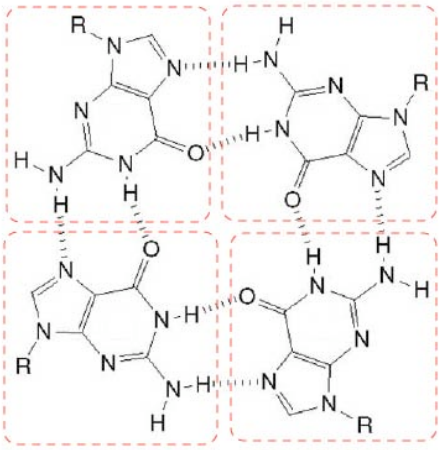

Figure 3.3-1 Schematic representation of G-quartets.

Experimental

Material and Methods

DNA solution

Different kinds of DNA molecules are used such as lambda DNA (Takara bio, Japan), Poly(dA)-Poly(dT) (Amersham Pharmacia Biotech Co. Tokyo, Japan) and Poly(dG-dC)-Poly(dG-dC) (Poly $(dG\text{-}dC)_2$, Amersham Pharmacia Biotech Co., Tokyo, Japan) in this study. Lambda DNA solution is used as bought. Synthesized DNA (Poly(dA)-Poly(dT), Poly$(dG\text{-}dC)_2$) powders as bought are first diluted with phosphate buffer in advance and incubated at 4 ℃ overnight.

Finally, both of the lambda DNA and synthesized DNA solution are diluted with phosphate buffer (0.1 M) and counter ion solution (1 M NaCl or $MgCl_2$) before use. The final concentration of DNA, phosphate buffer and counter ions are 0.37 O.D. (18.5 μg/ml), 87 mM, 100 mM, respectively. The mixed solution is incubated at 4 ℃ for overnight before use. The solution (40 μl) is dropped on the APS coated SiO_2 substrate. After 20 min of incubation, the surpass solution is removed by nitrogen gas flow. Immediately after it, the surface is rinsed with 80 μl of ultra pure water 2 times and dried by nitrogen gas flow.

G-wire solution

Single stranded DNA molecules with different sequences are synthesized by standard phosphoamidide method (Takara bio, Japan). Sequences are 1, "5'-gggg-TT-gggg-3'" (SEQ1) and 2, "5'-ggggTggggTgggg-3'" (SEQ2). Each DNA powder is dissolved in the solution prepared beforehand. The solution is prepared by mixing Tris-HCl (1M, pH 7.5), KCl (1 M), $MgCl_2$ (1 M) solution. The final concentration of DNA, Tris-HCl, KCl, $MgCl_2$ are 250 μg/ml, 50 mM, 50 mM and 10mM, respectively. The mixed solution is heated at 95 ℃ for 120 sec, and incubated at 37 ℃. After 48 hours of incubation, the solution is diluted with the solution (Tris-HCl : KCl : $MgCl_2$ = 50 mM : 50 mM : 10 mM) to be tenth of concentration (25 μg/ml). Then the solution (40 μl) is dropped on the APS coated SiO_2 substrate. After 5 min of incubation, the surface is rinsed with 500 μl of ultra pure water and dried by nitrogen gas flow. The hybridization methods are based on the reports by Marsh et al. and others [28-30].

Fabrication of samples

SiO_2/Si (100) substrate (electronics and material corp. Japan) is cleaned by UV-Ozone treatment (NL-UV253, Laser Techno, Japan) for 1 hour and it is reacted with aminopropyltrimethoxysilane (APS, Wako corp. Japan) immediately. The substrate is placed in the sealed container with small vial. 20ul of APS solution is put in the vial. The container is heated at 230 degree centigrade for 30 min. The substrate is picked up and washed with ethanol and ultra pure water for 3 min, successively. The surpass water is removed by dried nitrogen gas flow and the substrate is heated at 100 degree centigrade to remove water and promote the condensation of APS molecules. The SiO_2 substrate reacted with APS molecules (APS SiO_2) used for DNA immobilization as soon as possible. After the immobilization of DNA, Au (99.95%, Nilaco Corp., Japan) electrodes were fabricated by thermal evaporation in a homemade chamber under a vacuum pressure of 10^{-6} Torr.

Electrical Measurements

Electrical measurements were performed by a semiconductor characterization system (Keithley 4200) under vacuum (10^{-4} Torr) and dark condition. Temperature is changed by liquid nitrogen gas and temperature control system that is equipped inside vacuum chamber.

Spectrum Measurements

The circular dichroism (CD) is measured with a CD spectrometer (J-820, JASCO).

Results and Discussion

AFM observation of DNA immobilized surfaces

Figure 3.3-2 shows the AFM images of prepared samples. Figure (a) and (b) shows the image of SiO_2 after UV-Ozone treatment and APS SiO_2, respectively. The root square mean (RMS) of surface roughness for both image are 0.24 nm and 0.22 nm and significant difference is not measured. Figure (c) and (d) shows the image of APS SiO_2 treated with control solution. The control solution contains $MgCl_2$ and Phosphate buffer. The RMS of surface roughness is slightly increased to be 0.29 nm. Figure (e) and (f) shows the APS SiO_2 treated with lambda DNA solution. Figure (g) and (h) shows the APS SiO_2 treated with Poly(dA)-Poly(dT) solution. The RMS of surface roughness of (e) and (g) are increased to be 0.44 nm and 0.63 nm, respectively.

Comparing images of DNA immobilized samples to control samples, it is obvious that the surface morphology is changed and roughness is increased. The increases in surface roughness indicate that DNA molecules are immobilized on the surface. The degree of increase is different between lambda DNA and Poly(dA)-Poly(dT). As the synthesized Poly(dA)-Poly(dT) is composed of hybridized small pieces of fragment both of Poly(dA) and Poly(dT), Poly(dA)-Poly(dT) would forms not only double stranded structure, but also higher-order structure. Therefore, the differences in surface roughness between lambda DNA with perfect double stranded structure and Poly(dA)-Poly(dT) would originate from the structure of DNA molecules.

Figure (f) and (h) shows the magnified image of (e) and (g), respectively. It is impossible to identify the isolated DNA molecules on APS SiO_2. On the other hand, it is possible to observe the isolated DNA molecules on SiO_2 treated with UV-Ozone (not shown here). As APS treatment is widely used for DNA immobilization because of the strong electrostatic interaction between phosphate groups around DNA molecules and protonated amino groups of APS [31,32], these results would indicate that APS SiO_2 is covered with DNA molecules all over. The immobilization of DNA on APS treated glass surface is also noted in chapter 6. These results show that the strong electrostatic interaction exists between DNA and APS SiO_2 due to the protonated amino groups at the surface, and they are immobilized on the surface firmly.

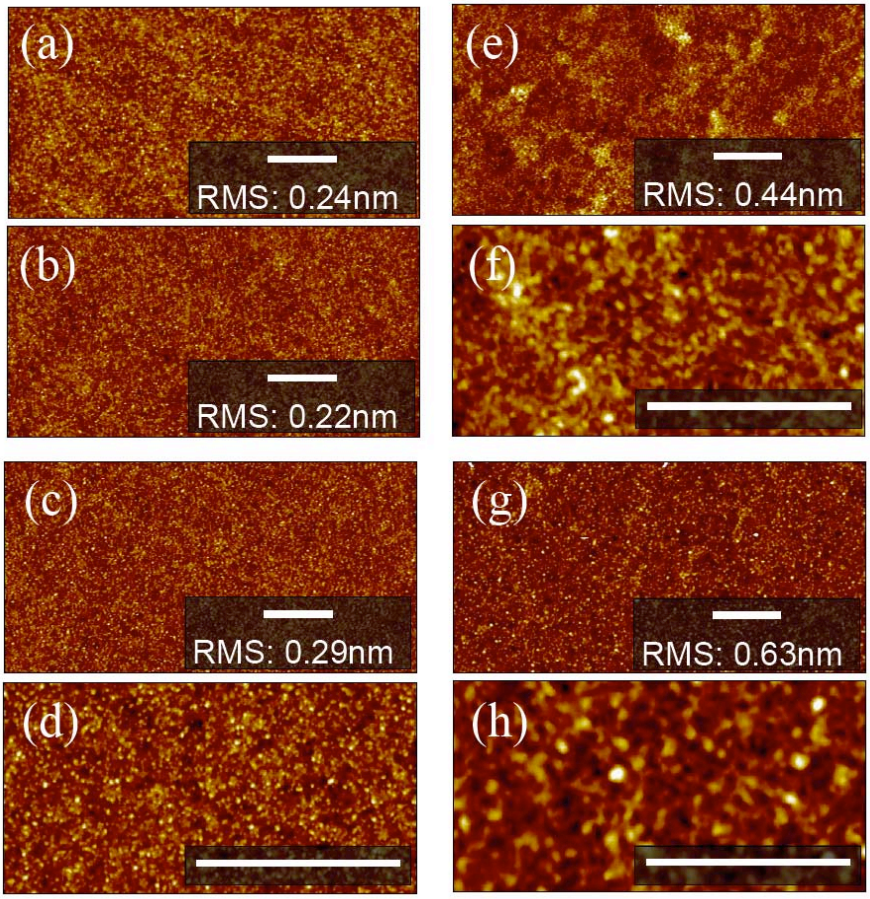

Figure 3.3-2
AFM image of prepared sample. Scale bars shown in every images are correspond to 500 nm. (a) SiO_2 after UV-Ozone treatment (b) APS SiO_2 (c), (d) Control solution with $MgCl_2$ and phosphate buffer on APS SiO_2 (e), (f) Lambda DNA solution on APS SiO_2 (g), (h) Poly(dA)-Poly(dT) solution on APS SiO_2.

As the postscript, the reason why the synthesized Poly(dG)-Poly(dC) is not used in this study is noted below. Figure 3.3-3 shows the structure of Poly(dG)-Poly(dC) on APS SiO_2. As shown in figure (a) and (b) observed by optical microscope, aggregation over 10 μm is observed. Figure (c) shows the AFM image. Then, the smaller aggregation is again observed. Isolated DNA strand is observed around the aggregation, and this might shows the aggregation is composed of these strands. As noted in the next paragraph and it has been found that the DNA strand with guanine rich sequence tend to form the higher order structure which is totally different from double stranded structure. Moreover, the result supporting this assumption is obtained from CD spectroscopy as shown in figure 3.3-15 (d). The presence of positive peak and negative peak around 260 nm and 240 nm of wavelength indicate the formation of quadduplex. The detail is noted in next topic.

This postscript indicates that it is difficult to use Poly(dG)-Poly(dC) because of the formation of big aggregation on the APS SiO_2, although Poly(dG)-Poly(dC) is attractive from the point of view that poly(dG) is composed with only G that is oxidized (hole-doped) easier compared to other base molecules, and hence the higher conductivity is expected [33-35].

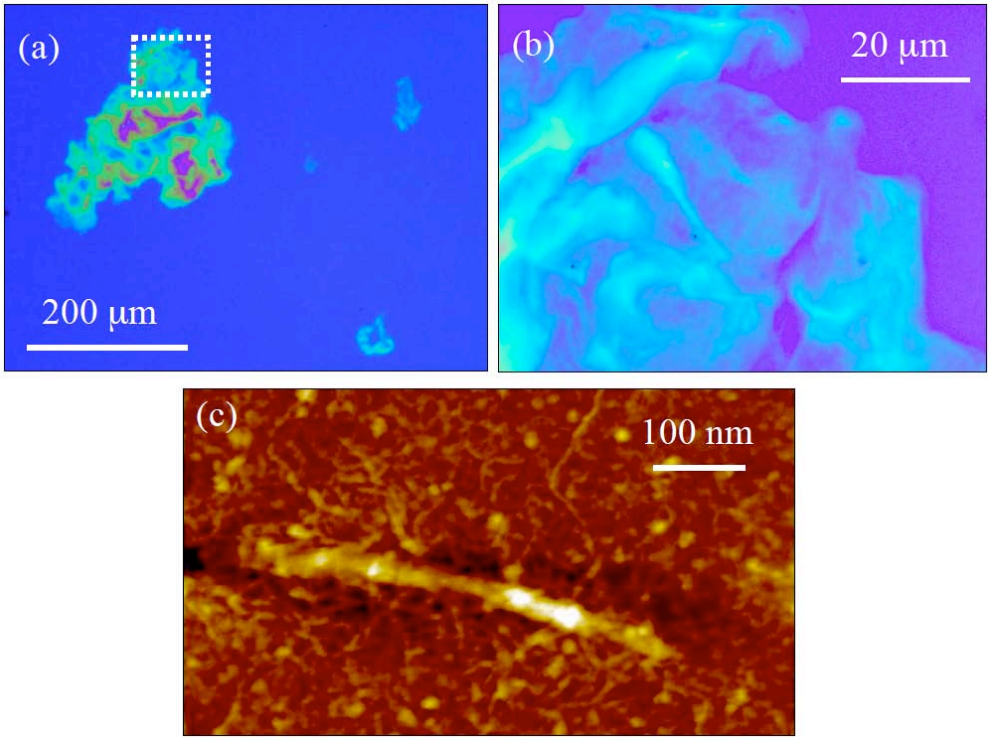

Figure 3.3-3
(a), (b) Optical images of aggregation of Poly(dG)-Poly(dC) on APS SiO_2. (b) the magnified image at the position framed by the square in (a).
(c) AFM image of Poly(dG)-Poly(dC) immobilized on APS SiO_2.

CD spectrum measurements of G-wire and AFM observations of G-wire immobilized surfaces

The prepared G-wire solution is put into the CD spectrum measurement in order to study the structure of G-wire. The G-quartet structures can be classified into 3 patterns; [36]

1, Tetramolecular parallel quadduplexes. (G4-DNA)

2, Unimolecular antiparallel quadduplexes. (G4'-DNA)

3, Bimolecular antiparallel quadduplexes. (G'2-DNA)

The schematic illustrations of these DNA are shown in figure 3.3-4. These structures are strongly affected by the factors as; [37]

1, Different ions (monovalent or divalent).

2, DNA and ion concentrations.

3, DNA length of the G-rich strand.

4, Watson-Click complementary DNA.

5, Sequence differences.

The structure of quadduplex can be assigned by CD measurements. It has been studied that the folded structure (G4'-DNA and G'2-DNA) possess a positive CD peak near 295 nm, whereas four stranded structure (G4-DNA) possess a positive peak near 265 nm and a negative peak near 240 nm [38-40].

Figure 3.3-5 shows the CD spectrum for both of SEQ1 and SEQ2, respectively. It is measured that the spectrum shows the positive peak around 264 nm and negative peak around 240 nm. Therefore, these results indicate that both of DNA (SEQ1 and SEQ2) are hybridized each other to form the tetramolecular parallel quadduplexes (G-wire). The structure of G-wire fabricated by the similar method as ours is suggested as figure 3-3-6 [28,41]. As four oxygens of guanine surround the cavity inside the G-quartet, K^+ ion is sandwitched in between two G-quartets (G8-K^+). This G8-K^+ octamers can stack to form G-quadduplex.

Figure 3.3-7 shows the AFM image of G-wire immobilized on two kinds of substrate. Figure (a), (b) and (c), (d) show the G-wire immobilized on the mica substrate and APS SiO_2, respectively. The distinctive wire structure is observed on the mica substrate, as it is projected from the CD spectrum. The height distribution is measured, and the average height is measured to be 2.2 nm (Figure 3.3-8). This is agreement with the value (2.8 nm) measured by the X-ray crystallography [42,43]. On the other hand, G-wires are densely immobilized on the APS SiO_2.

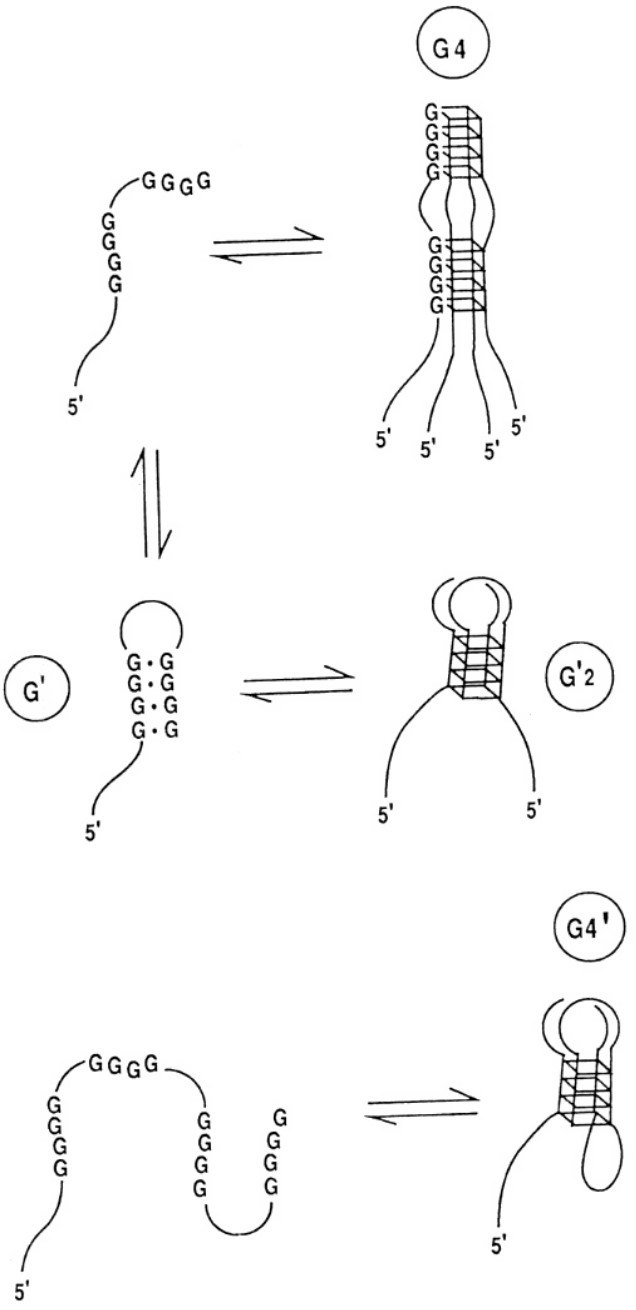

Figure 3.3-4
The schematic illustrations of different G-quartet structures.
(Taken from D. Sen, W. Gilbert, *Methods In Enzymology* 211, 191 (1992))

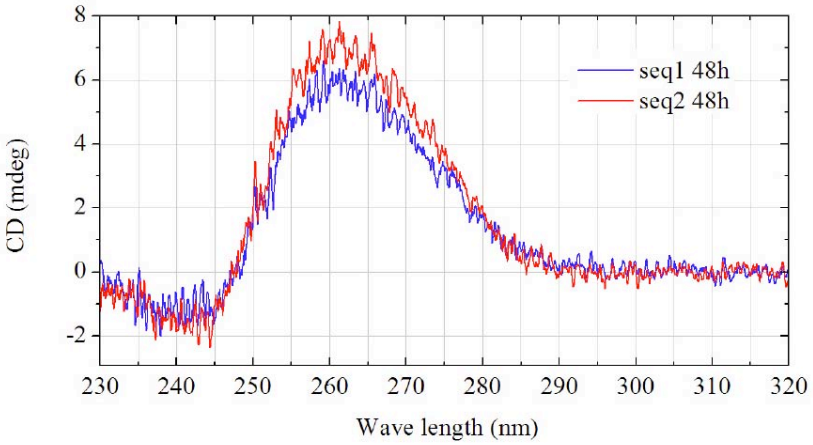

Figure 3.3-5
CD spectrum of G-wire solution.

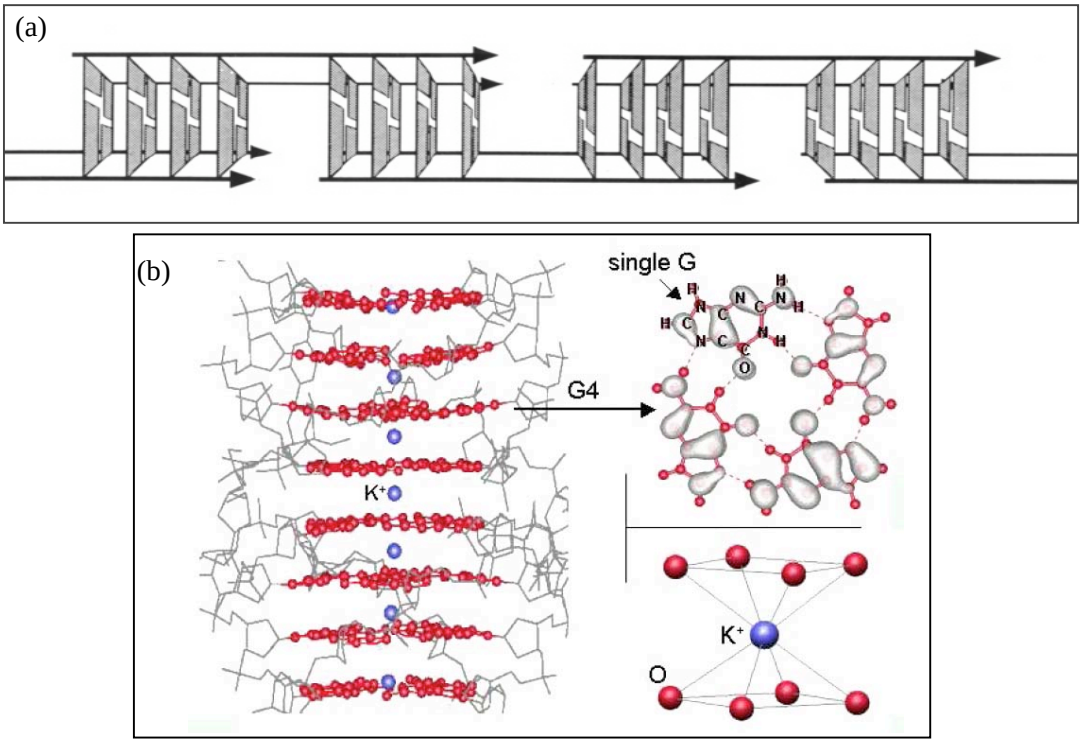

Figure 3.3-6
(a) Proposed structure of G-wire by Walsh et al. Synthesized DNA with guanine rich sequences are hybridized each other to form G4-DNA domains. The overlapping slipped G4-DNA structures are responsible for the formation of the G-wire. Inner cavity is filled with K^+ ion, hence the structure of G-wire is stabilized. (b) (left) Side view of G-wire derived from an experimental X-ray structure. Note that K^+ ion is coordinated with 8 oxygens inside cavity (lower right). (Taken from the result by T.C. Marsh, E. Henderson, *Biochemistry* 33, 10718 (1994) and A. Calzolari, R.D. Felice, E. Molinari, A. Garbesi, *cond-mat* 041012 (2004).)

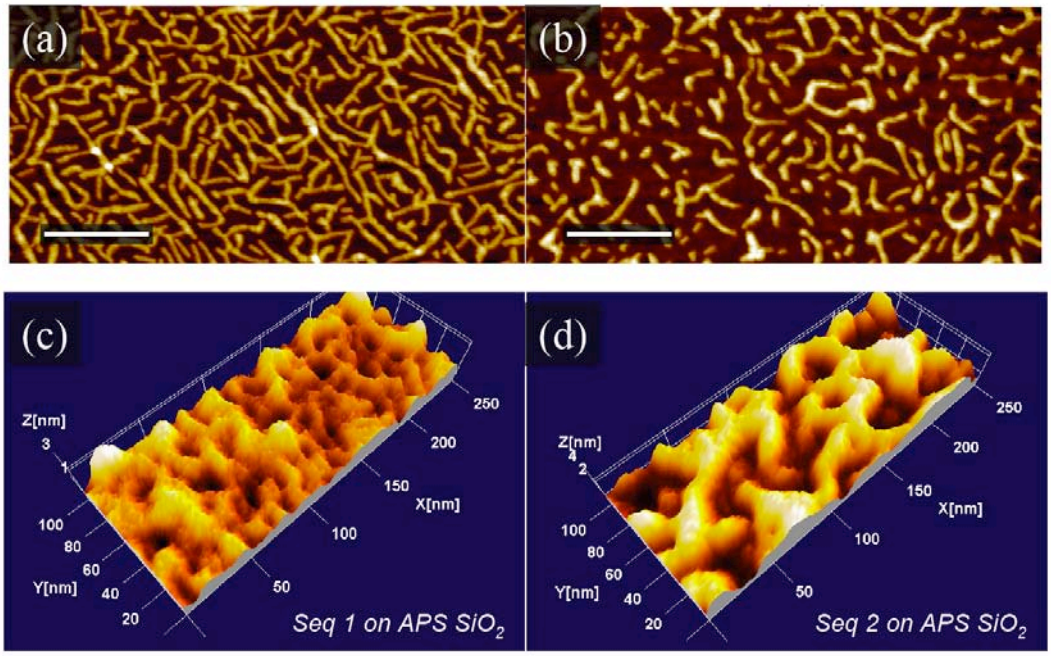

Figure 3.3-7
(a), (b) AFM image of G-wire immobilized on mica substrate. Scale bars in each images are correspond to 200 nm. (c), (d) 3D image of G-wire immobilized on APS SiO_2. The sequence of DNA used for (a), (c) is SEQ1 and for (b), (d) is SEQ2, respectively.

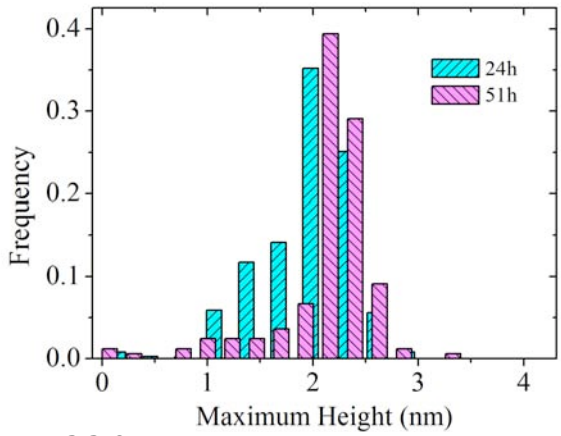

Figure 3.3-8
Height distribution of G-wire (SEQ1) on mica substrate

As is noted in the previous topic, the surface property is different between mica and APS SiO_2. The interactions between G-wire and substrate affect the number and morphology of immobilized G-wire strongly. Figure 3.3-9 shows the AFM image of G-wire (SEQ1) immobilized on the mica, SiO_2 treated with UV-Ozone and APS SiO_2, respectively. The similar result is obtained for the mica substrate. On the other hand, the amount of G-wire immobilized

on the surface decreased (increased) on the SiO_2 (APS SiO_2) substrate.

These results show that the strong electrostatic interaction exists between G-wire and APS SiO_2 due to the protonated amino groups at the surface [34,35]. Therefore, APS SiO_2 is covered with G-wire all over even after the rinse with water. The surface of SiO_2 treated with UV-Ozone, on the contrary, has the hydroxyl groups in the front (silanol groups), and they are dissociated under the pH of 7 because the isoelectric point of silanol group is 2;

$SiOH \rightarrow Si\text{-}O^- + H^+$

The dissociated part is negatively charged, and therefore there would be small interactions between G-wire because the surface of G-wire is composed of the phosphate groups that are negatively charged. Nonetheless, the immobilization of G-wire on this surface would occur in the presence of counter ions such as K^+ and Mg^{2+} that play a part to "glue" G-wires on the surface [45]. After the rinse of surface with water, immobilized G-wires would be washed away because both of the mobile counter ions that glue G-wire on the surface and small interaction between G-wire and surface.

Previous results also showed the effect of counter cation on the immobilization of DNA on mica substrate. The magnesium ion covers the mica surface that is the atomically flat layer composed of Si-O-Si bond. Therefore, it is possible to immobilize DNA on mica substrate to some extent even after the rinse with water.

In case the electrical measurements are performed, it is better to use the atomically flat surface such as mica in order to minimize the structural bending of DNA. However, the use of mica substrate contains the intrinsic technical problem. That is, it is quite difficult to obtain the atomically flat surface that is large enough to fabricate top-contacted geometry type electrode. As there are wrinkles and large steps on the mica substrate, they become the barrier that results in the breaking of the electrode. Therefore, we used the APS SiO_2 because there is no barrier for electrode fabrication. As the structure of SiO_2 is amorphous, the surface roughness tends to larger. So, we prepared the SiO_2 with mirror finished surfaced. The surface roughness is measured to be 0.2 nm as noted above.

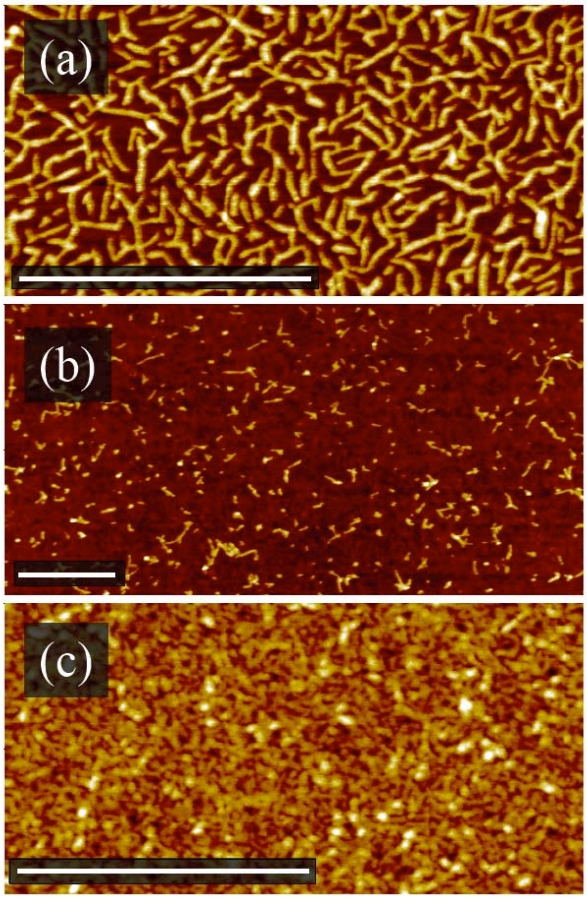

Figure 3.3-9
AFM image of G-wire immobilized on different substrate. (a), (b) and (c) indicate the image for mica, SiO_2 treated with UV-Ozone and APS SiO_2, respectively. Scale bars in each images are correspond to 500 nm. The sequence of DNA is SEQ1.

Electrical measurements

I-V characteristics and time course of current

Figure 3.3-10 shows the *I-V* characteristics of lambda DNA for different pairs of electrodes. Even under vacuum condition, symmetrical *I-V* characteristics are measured for various kinds of samples. This is noteworthy result because other results by different electrical detection methods such as bottom-contacted geometry type electrode and PCI-AFM noted in previous sections indicate that no detectable current is measured.

Figure 3.3-11 shows the time course of current of Poly(dG-dC)$_2$. The change in current is measured with increasing the time under 1 V of bias voltage is applied between electrodes. The continuous current is measured for different pairs of electrodes over 4 hours. This is again noteworthy result because the previous results of the same electrical measurement by top-contacted geometry type electrode under atmospheric condition indicate the sudden decrease in current with increasing the time due to the ionic current.

These results shown here would indicate that it is possible to conduct an electrical current through DNA, and the charge transport phenomenon by conductive carriers is measured. In order to clarify the difference of current level, the relationship between current (resistance) and gap size of electrode-pair is studied in the next section.

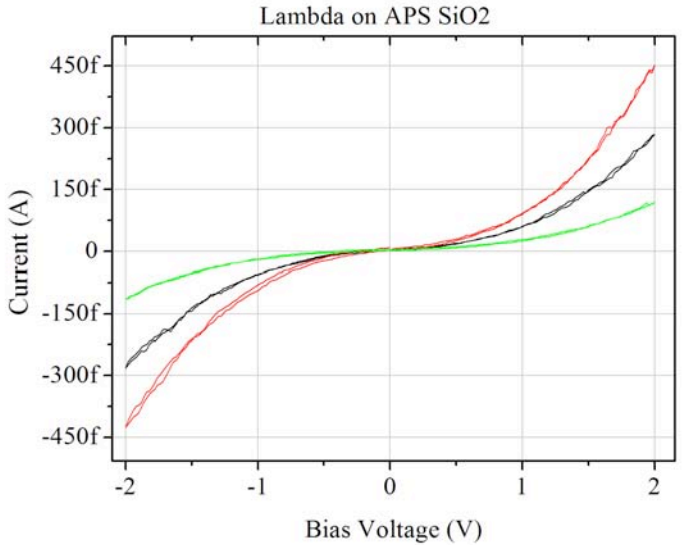

Figure 3.3-10
I-V characteristics of Lambda DNA for different pairs of electrodes.

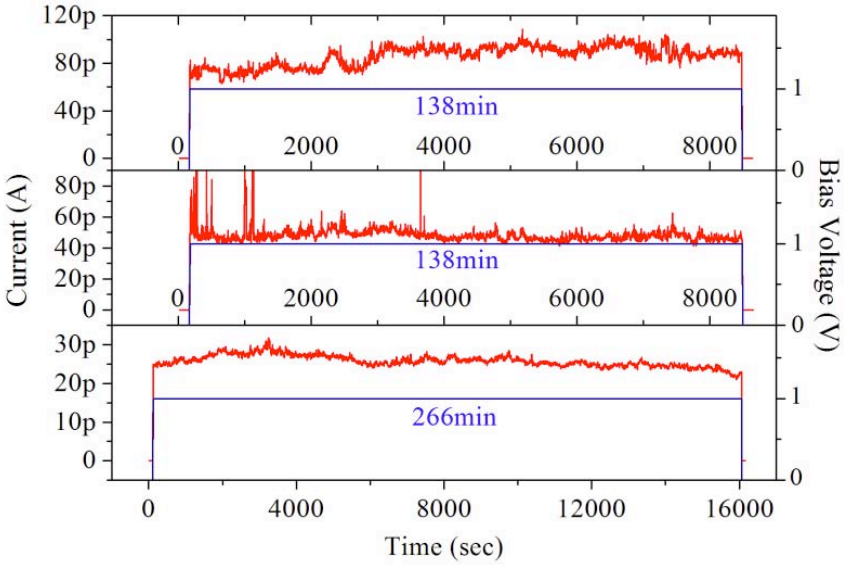

Figure 3.3-11
Time course of current of Poly(dG-dC)$_2$. The change in current is measured with increasing the time under 1 V of bias voltage is applied between electrodes.

Distance dependency on electrical conductivity

Then, as it is possible to fabricate electrodes with different size of nanogap on the same substrate (noted in the previous chapter), the gap-size-dependency on the electrical characteristic is studied. Figure 3.3-12 shows *I-V* characteristics of lambda DNA for different pairs of electrodes. The distance between electrodes is measured by SEM, is also noted in each chart. Symmetrical *I-V* characteristics are measured for every different nanogap electrodes again. Similar *I-V* characteristics are performed for different type of DNA.

Figure 3.3-13 show the correlation chart between resistance and distance between electrodes. In order to discuss the change of conductivity, the resistance is estimated by calculating *V/I*. The current level *I* under 1.0 V of applied bias voltage is used. Figure (a) shows the results for control measurements. The electrical measurements are performed for the APS SiO_2 treated with the control solution that is composed of counter ion and phosphate buffer. The difference between the control solution and DNA solution is only the existence of DNA molecules. The result indicates the ***linear*** correlation between the resistance and gap distance. Moreover, it is found that the limit of nanogap fabricated by this method is 40 nm. That is, the short circuit is formed between electrodes for the nanogap separated less than 40 nm.

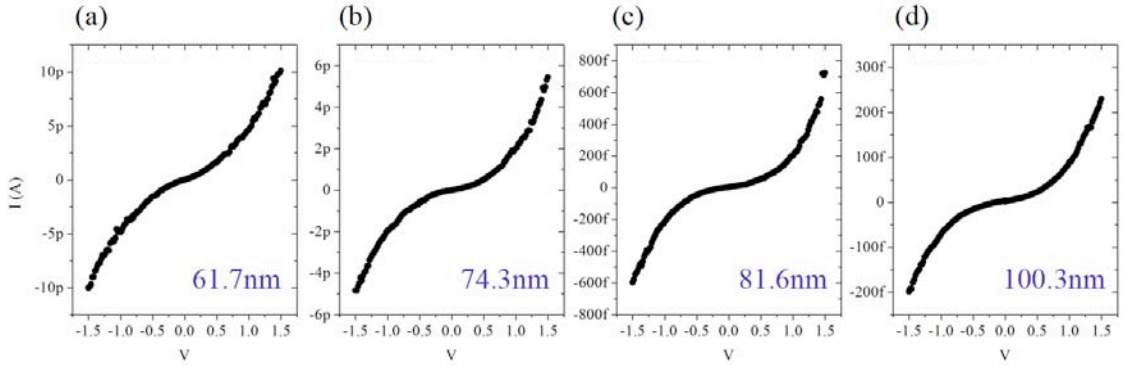

Figure 3.3-12
I-V characteristics of lambda DNA for different pairs of electrodes. The distance between electrodes is also noted in each charts that is measured by SEM.

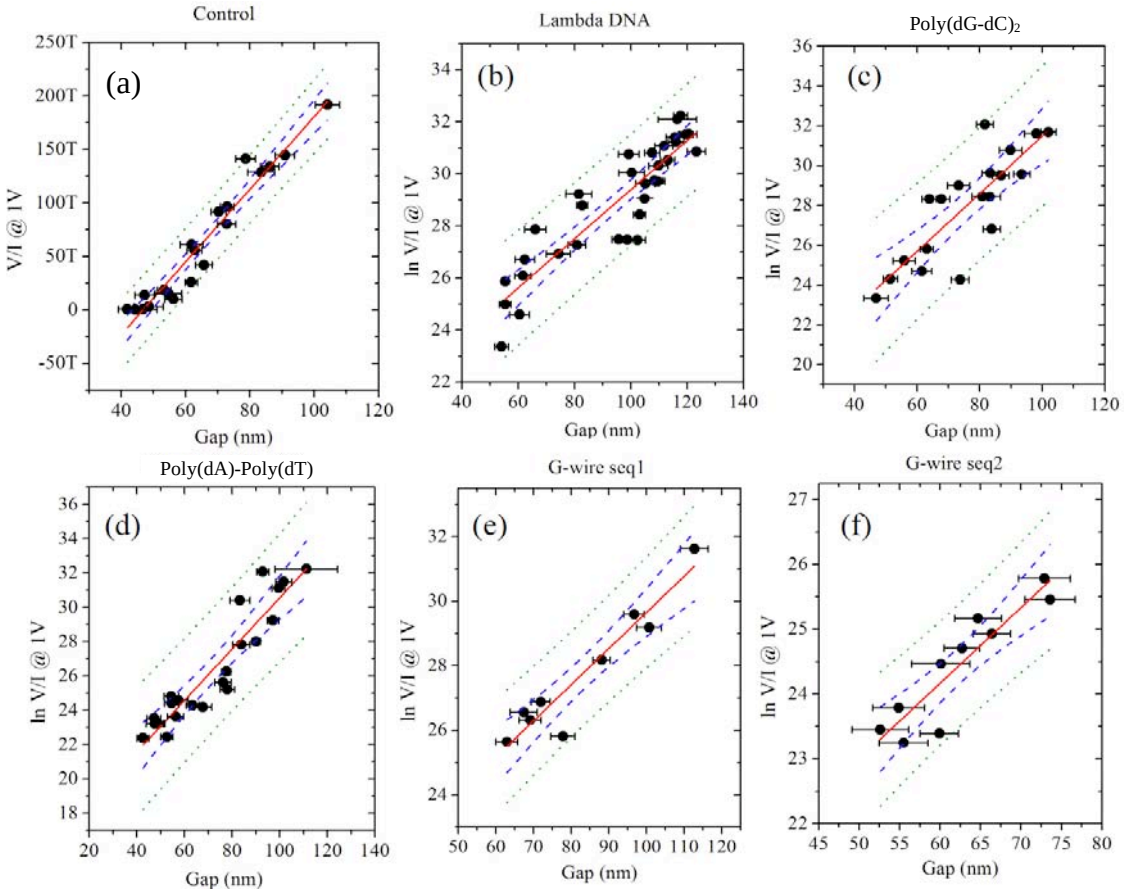

Figure 3.3-13
Correlation chart between resistance and distance between electrodes. (a) Control measurements (b) Lambda DNA (c) Poly(dG-dC)2 (d) Poly(dA)-Poly(dT) (e) G-wire (SEQ1) (f) G-wire (SEQ2). The straight line, dashed line and dotted line indicates averaged line calculated by least-squares method, confidence limits (95 %) and prediction limit (95 %), respectively.

On the other hand, *different* correlations are obtained for DNA presented samples. Figure (b), (c), (d), (e) and (f) show the results for Lambda DNA, Poly(dG-dC)$_2$, Poly(dA)-Poly(dT), G-wire (SEQ1) and G-wire (SEQ2), respectively. The straight line, dashed line and dotted line indicate averaged line calculated by least-squares method, confidence limits (95%) and prediction limit (95%), respectively. These results show that the ***exponential*** increase in resistance is measured with increasing the distance between electrodes. Moreover the value of resistance for all sequence of DNA is lower than that of control experiments. Therefore, it is conceivable that the measured electrical characteristics are originated from the DNA.

Then, correlations between the resistance and the distance for different DNA samples are compared each other. Figure 3.3-14 (a) shows the experimental data for all samples. For comparison, lines fitted by least-squares methods are plotted as shown in figure (b) and (c). Figure (b) shows the differences between lambda DNA, Poly(dG-dC)$_2$ and Poly(dA)-Poly(dT), while figure (c) shows the differences between lambda DNA, G-wire (SEQ1) and G-wire (SEQ2). The value of slope, intercept, adjusted $\sqrt{R^2}$ that are calculated by the least-squares method, and the number of samples for the electrical measurements is shown in Table 3.3-1.

	Slope	Intercept	Adjusted $\sqrt{R^2}$	Sample Number
Lambda DNA	0.094±0.008 ($MgCl_2$)	19.97	0.808	32
	0.072±0.013(NaCl)	22.04	0.812	8
Poly(dG-dC)$_2$	0.145±0.023 ($MgCl_2$)	17.01	0.681	19
	0.091±0.014(NaCl)	22.28	0.790	11
Poly(dA)-Poly(dT)	0.150±0.018	15.60	0.868	22
G-wire SEQ1	0.112±0.013	18.49	0.896	9
G-wire SEQ2	0.117±0.018	17.17	0.816	10

Table 3.3-1
Calculated values of slope, intercept and adjusted $\sqrt{R^2}$ by the least-squares method. The calculated data is plotted as shown in figure 3.3-14. The number of samples for the electrical measurement is also noted.

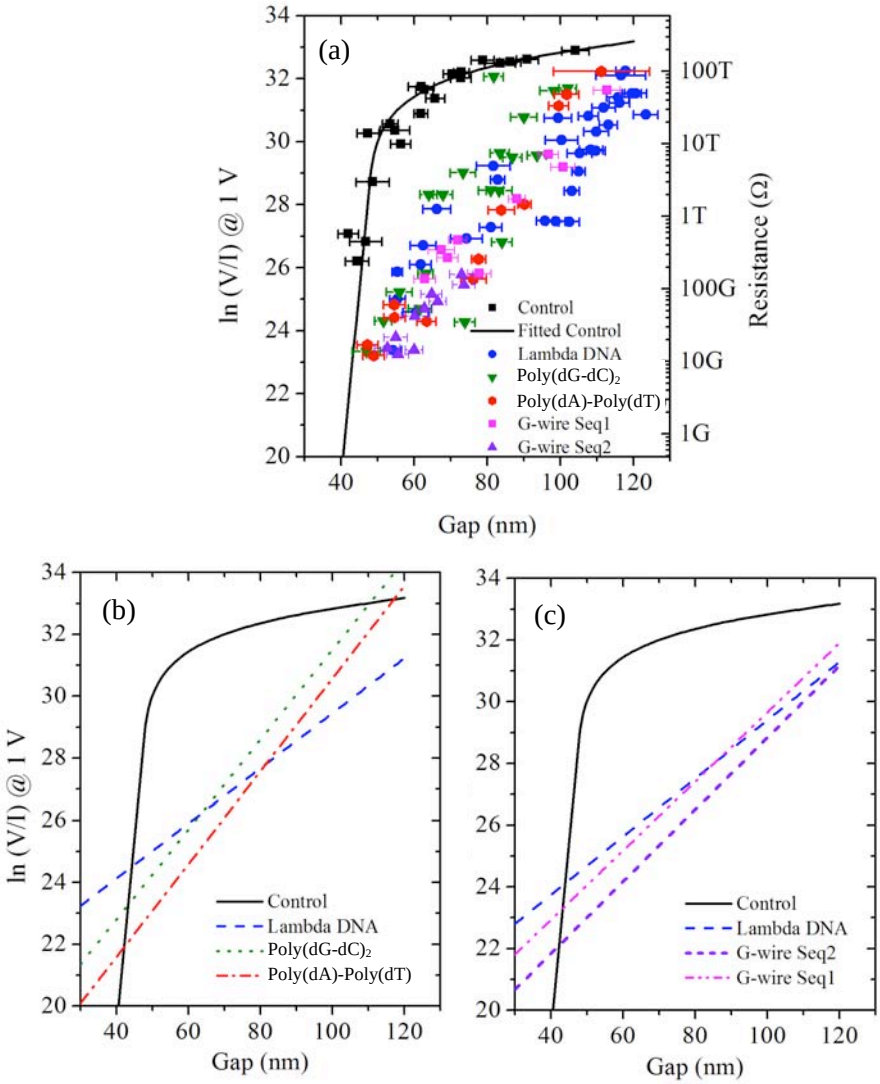

Figure 3.3-14
The relationship between the calculated resistance and distance between electrodes. (a) Experimental data. Fitted curve is also shown only for control experiment. (b), (c) Fitted data. All data is calculated by least-squares method.

As shown in figure (b), the difference between lambda DNA and both of Poly(dG-dC)$_2$ and Poly(dA)-Poly(dT) in the value of slope is clearly obtained. The value of slope for lambda DNA, Poly(dG-dC)$_2$ and Poly(dA)-Poly(dT) is 0.094 ± 0.008, 0.145 ± 0.023, 0.150 ± 0.018, respectively. These results indicate that the resistance of synthesized DNA (Poly(dG-dC)$_2$ and Poly(dA)-Poly(dT)) increases drastically compared to natural DNA (lambda DNA) with increasing the gap size. On the other hand, as shown in figure (c), the value of slope for lambda DNA, G-wire (SEQ1) and G-wire (SEQ2) is 0.094 ± 0.008, 0.112 ± 0.013 and 0.117 ± 0.018,

respectively. These results, again, indicate that the resistance of G-wire increases steeply compared to natural DNA.

Comparison between natural DNA and synthesized DNA

Then, the exponential increases in resistance for both of lambda DNA and synthesized DNA is discussed below.

As for the value of resistance, the intersecting point around 70 nm of gap size is found between synthesized and lambda DNA as shown in figure (b). This result would indicate that the origin of resistance is different between synthesized and natural DNA.

First, the difference of structure is discussed. The natural DNA is composed of nearly perfect double-stranded structure. On the other hand, the synthesized DNA is composed of small pieces of hybridized fragment of single DNA strands. Therefore, it is conceivable that larger number of defects such as nick exist along the double stranded structure of synthesized DNA.

The structural difference of DNA that supports this idea is confirmed as follows. Figure 3.3-15 shows the CD spectrum and absorbance spectrum of different DNA. Every DNA solutions are prepared by dissolving DNA molecules in the phosphate buffer (pH 7, 0.1 M). The

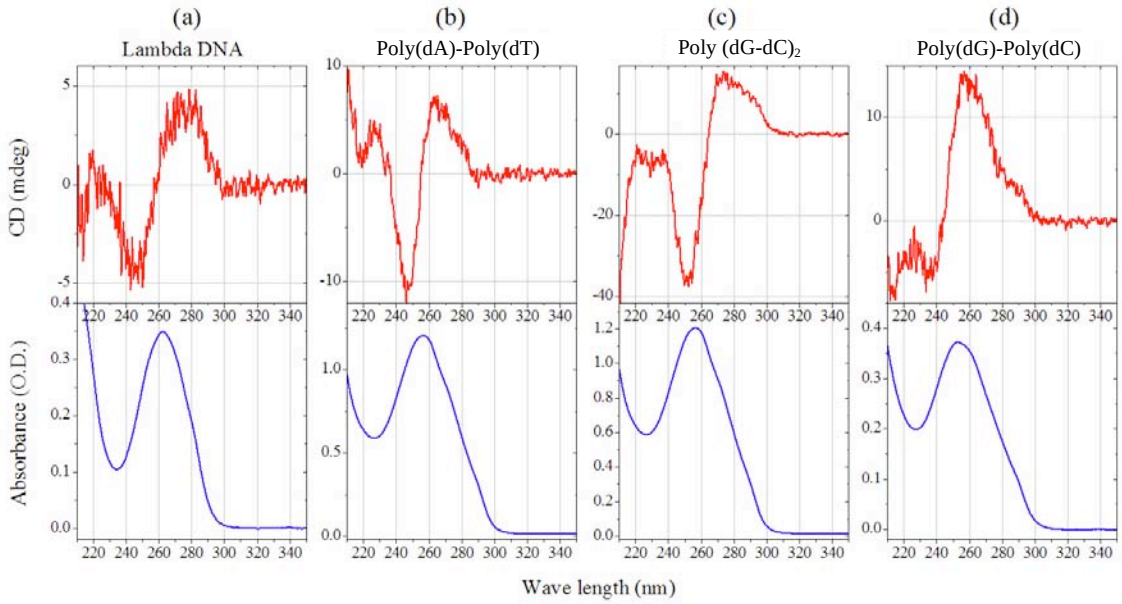

Figure 3.3-15
CD spectrum and absorbance spectrum for different sequence of DNA.

kind of DNA is also noted in images. The positive cotton effect is observed for all sequences, but the position of the peak is different each other. As shown in figure (a), the maximum and minimum peaks are measured around 280 nm and 250 nm, respectively. Therefore, it is confirmed that lambda DNA maintain the B-form structure in the solution. On other hand, as shown in figure (b) and (c), the maximum and minimum peaks are 260 nm and 246 nm for Poly(dA)-Poly(dT), 270 nm and 252 nm for Poly(dG-dC)$_2$, respectively. These results for synthesized DNA are in good agreement with the former result [46-49], and therefore, it is confirmed that Poly(dA)-Poly(dT) maintain the alternating B-form and Poly(dG-dC)$_2$ maintain B-form, respectively.

As shown in figure 3.3-14, the resistance of synthesized DNA increases drastically compared to natural DNA, and this would be due to the difference in structure. The difference is categorized by 2 cases. That is, the presence of nicks and the form of double strand. It also has been studied that the changes of the form affect the overlap between neighboring base molecules inside double helix, and electrical conductivity would be changed.

Comparing the “form” and “nicks”, it would be derived that the most effective parameter that affects the electrical property of DNA would be the “presence of nicks”. This is because the presence of nicks generates the “local defects in π–stacked structure”. That is, base molecule that form the conductive path is lacked, and hence the conductivity would decrease after all.

This assumption would be supported by the comparison between Poly(dA)-Poly(dT) and Poly(dG-dC)$_2$. As shown in figure 3.3-16, the fitted lines both of Poly(dA)-Poly(dT) and Poly(dG-dC)$_2$ by least-squares method are different each other, but the areas of confidence limit are overlapped each other. As for lambda DNA, both of the slope of line and the area of confidence are different from that of synthesized DNA. Therefore, it is impossible to confirm the presence of significant differences between Poly(dA)-Poly(dT) and Poly(dG-dC)$_2$. This identical correlation between the resistance and gap size of different synthesized DNA indicate that the increase in resistance is not due to the sequence, but to the structural matter that is common to both of synthesized DNA. That is, the structural defects as nicks along double stranded structure. Hence this discussion indicates that the electrical properties of synthesized DNA are strongly limited by the structural defect.

The reason why the resistance of lambda DNA is lower than that of synthesized DNA under the condition that gap size is more than 70 nm is the existence of structural defects. Even the synthesized DNA is composed of uniform sequence, the resistance is higher than lambda DNA due to the nicks. The sequence of lambda DNA is random, but the structure of double

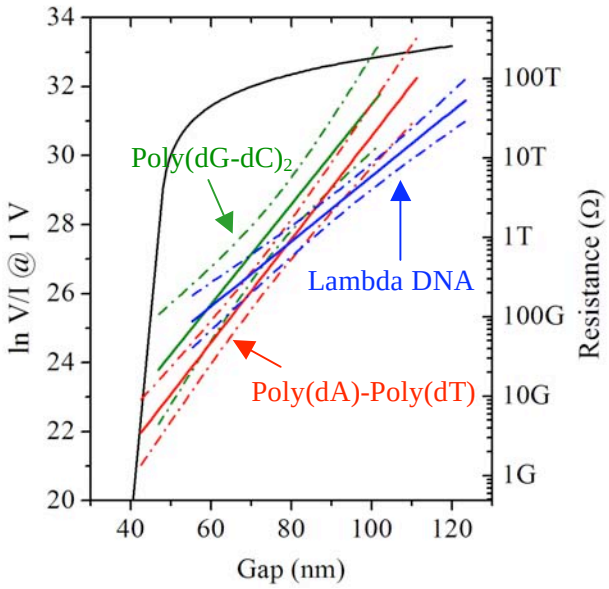

Figure 3.3-16
Comparison between resistance and distance between electrodes in order to discuss the significant difference. The straight line, double dashed line is the resistance calculated by least-squares method and confidence limit (95 %), respectively.

strand is stable because the DNA is taken from bacteria (lambda phage).

Nevertheless, the effect of base sequence on the electrical conductivity should be discussed. This is because both of Poly(dA)-Poly(dT) contain uniform base sequence, while lambda DNA contains random base sequence. The resistances both of Poly(dA)-Poly(dT) and Poly(dG-dC)$_2$ are lower than that of lambda DNA under the condition that the gap size is less than 70 nm. As the discussion about structural difference, the structural defects would cause the increase in resistance under this condition, as well. However, these lower resistances of synthesized DNA than lambda DNA would be originated from the difference of base sequence. That is, charge transport along DNA under smaller gap size is affected by not only structural defects but also base sequence. Hence, the resistance of synthesized DNA is lower than lambda DNA because of the uniform sequence. Uniform sequence would possess uniform electrical potential along π-stacked base molecules, while random sequence would cause potential difference and make electrical transport harder. As the comparison between Poly(dA)-Poly(dT) and Poly(dG-dC)$_2$ indicated no difference in conductivity between them, the reason is unclear yet, but it might be due to the structural defects. The effect of structural defect to scatter the conductive carrier might make the effect of uniformity of base sequence obscured.

Hence, it is found that the effective parameters that determine the charge transport along

DNA are 1, mainly structural defects under the condition that the range of gap size is over 70 nm, 2, base sequence and structural defects under the condition that the gap size is less than 70 nm.

Comparison between natural DNA and G-wire

Then the difference between lambda DNA and G-wire (SEQ1 and SEQ2) is discussed. Back to the figure 3.3-14 (c), the relationship between resistance and distance between electrodes indicate the exponential increase in resistance as for both of lambda DNA and G-wire (SEQ1 and SEQ2). The degree of increase in G-wire resistance is larger than that of lambda DNA as noted in the previous page, and this would be also due to the structural defects. Lambda DNA is composed of almost perfect double stranded structure, while G-wire contains gaps at intervals of 2-base T and 1-base T in SEQ1 and SEQ2, respectively. (See the "G-wire solution" in "Material and methods") Hence, the increase in resistance of G-wires would be attributed to the increase of structural defects along G-wire. The amount of defects would be increased with increasing the distance between electrodes. Moreover, the value of slope for both G-wire is similar, and thus this would indicate the effect of structural defects (gaps) is almost same in so far as the number of base in the gap is 1 or 2.

As for the value in resistance, SEQ2 is lower than both of lambda DNA and SEQ1. Then, comparison between lambda DNA and SEQ1 indicates that the intersecting point around 85 nm of gap size is found. The factor to occur this intersection would be again the structural defects. This comparison may indicate that the resistance of G-wire is lower than that of double stranded DNA, but the structural defects in G-wire act as parasitic resistance. Although the effect of the number of base in the gap of G-wire is trivial in the viewpoint of the degree of increase in resistance, the resistance of SEQ2 is about 5 times lower than SEQ1.

This would originate from the additional structural defects in G-wire. G-wire is formed by the hybridization of single strand DNA as shown in figure 3.3-6, ideally. However, the imperfect hybridization would occur because the hybridization process is limited by the self-assembly. As the primal length of synthesized DNA between SEQ1 (5'-gggg-TT-gggg-3') and SEQ2 (5'-ggggTggggTgggg-3') is different, it would be conceivable that the number of the additional structural defects of SEQ1 is larger than that of SEQ2. The structure of such defects is unclear, but the modification of base sequence is needed to reduce the structural defects and

enhance the electrical conductivity.

Calzolari et al. studied the first-principle study of the electronic and conduction properties of G-wire. [41] The atomic configuration of G-wire is obtained from the experimental results. The calculation showed that the high degree of charge delocalization along the long axis of G-wire, and G-wire may be described as good electron/hole channels for mobile charges compared to double-stranded DNA. The main difference between G-wire and double-stranded DNA was indicated to be the pathways for mobile charges. Two kinds of pathways are indicated. One originates from the component of the HOMO of guanine due to the base-base interaction. Other originates from the component of the HOMO that results from the K^+-guanine interaction. Hence the dimension of pathway of G-wire would be much larger than that of double stranded DNA. Moreover, the other difference between G-wire and double-stranded DNA is the rigidity of structure. As is measured by AFM, the height of SEQ1 is almost identical to the value measured by X-ray crystallography. On the other hand, the height of DNA molecules are often measured to be smaller by AFM than the ideal value (2 nm) proposed by Watson and Click. Hence, G-wire is more stable than double-stranded DNA such as lambda DNA on the substrate, and the electrical state would be maintained as indicated by this calculation.

Although the structural defects of G-wire should be controlled in the future to control and enhance the conductivity, these results would be the first direct electrical measurement of G-wire.

The effect of bias voltage on the exponential change of resistance

Next, the bias voltage dependency on the degree of increase in resistance is discussed. This is because as the I-V characteristics are not linear (Figure 3.3-12), the degree of increase in resistance under different bias voltage should be studied. As shown in the previous page (Figure 3.3-13, Figure 3.3-14), the difference of electrode-distance dependency on the degree of increase in resistance as for different sequence DNA is studied. The resistance is calculated by *V/I* only at the 1 V of bias voltage.

Figure 3.3-17 (a) shows the relationship between the applied bias voltage and the degree of increase in resistance. The degree of increase in resistance is calculated by the same method as figure 3.3-14 and table 3.3-1. That is, the correlation between the distance of electrodes and calculated resistance under different bias voltage is plotted, and the linear correlation is

calculated by least-squares method. Then the slope of fitted line for different bias voltage is calculated. The value of slope is correspond to the degree of increase in resistance under the condition that distance between electrodes is changed.

First, the difference of value of slope between each DNA is discussed. As shown in previous page, the slope calculated at 1V of bias voltage is increased in the order as;

Lambda DNA < G-wire (SEQ1) < G-wire (SEQ2) < Poly(dA)-Poly(dT) ~ Poly(dG-dC)$_2$.

This order is kept under all bias voltage as shown in figure 3.3-17 (a).

Then, the comparison of change of value for each bias voltage indicates the difference of increase for each DNA. The value of lambda DNA is increased with increasing the bias voltage, and kept almost constant over 1 V. The similar change is observed for both of G-wires, but the value is kept constant over 0.5 V. On the other hand, as for Poly(dA)-Poly(dT) and Poly(dG-dC)$_2$, the value is increased with increasing the bias voltage, and no constant value is observed. At lower bias voltage (V < 0.1V), the degree of increase is bigger than that of higher bias voltage (V > 0.1V). This indicates the degree of increase in resistance is bias-voltage-dependent and different mechanism would be involved that affect the electrical properties. Moreover, as the value under lower bias voltage is not 0, this means the resistance of every DNA calculated at lower bias voltage still increase exponentially with increasing the distance between electrodes. Hence, this is another evidence that the measured electrical properties are not the contact-limited (that is contact resistance between Au electrode and DNA controls the electrical properties.) but the sample-limited.

As for the mechanism that affect the amount of increase in resistance, the value of slope is plotted against ln$V$ as shown in figure 3.3-17 (b). While lambda DNA and both of G-wires indicate the value of slope increases with increasing bias voltage, and constant value is observed at higher bias voltage. The presence of constant value of slope would indicate that the bias voltage does not affect the electrical properties at higher bias voltage. On the other hand, Poly(dA)-Poly(dT) and Poly(dG-dC)$_2$ indicated the linear increase of slope and no constant value. This indicates that the bias voltage exponentially affects the degree of increase in resistance.

This difference would originate from the structural difference of DNA. As is noted in the previous page, the structural defects are involved in every DNA, but the amount is different. If the structural defects form the localized state, the conductive carriers would be trapped at the state. The mechanism of degree of increase in resistance is strongly affected by both of the localized state and the bias voltage. At lower bias voltage, the resistance would strongly

affected by the conductive carriers at the localized state that is originated from the structural defects. Hence, the value of slope is smaller at lower bias voltage.

With increasing the bias voltage, the potential barrier for conductive carriers is lowered. Hence the constant value at higher bias voltage shown as for lambda DNA and both of G-wires would be correspond to the phenomenon that the effect of structural defects is decreased due to the lowered potential at higher electric field.

As for both of G-wire, constant value is obtained, but the degree of increase at lower bias voltage is different. While the value is increased with increasing bias voltage for SEQ1, gradual increase for SEQ2 is obtained. This would indicate that the amount of structural defect in SEQ2 is lower than SEQ1. On the other hand, the increase in slope at higher bias voltage shown as for Poly(dA)-Poly(dT) and Poly(dG-dC)$_2$ would indicate that the electrical properties are still affected by the structural defects even the potential barriers are lowered. Hence, the amount of defects of Poly(dA)-Poly(dT) and Poly(dG-dC)$_2$ would be larger than other DNA.

Moreover, the structural deference between double-stranded DNA under vacuum condition would also affect the electrical properties, and the detail should be studied.

These results indicate that the electrical properties of DNA are strongly affected by the structure of DNA and bias voltage between electrodes. The detailed conduction mechanism is discussed in the next section.

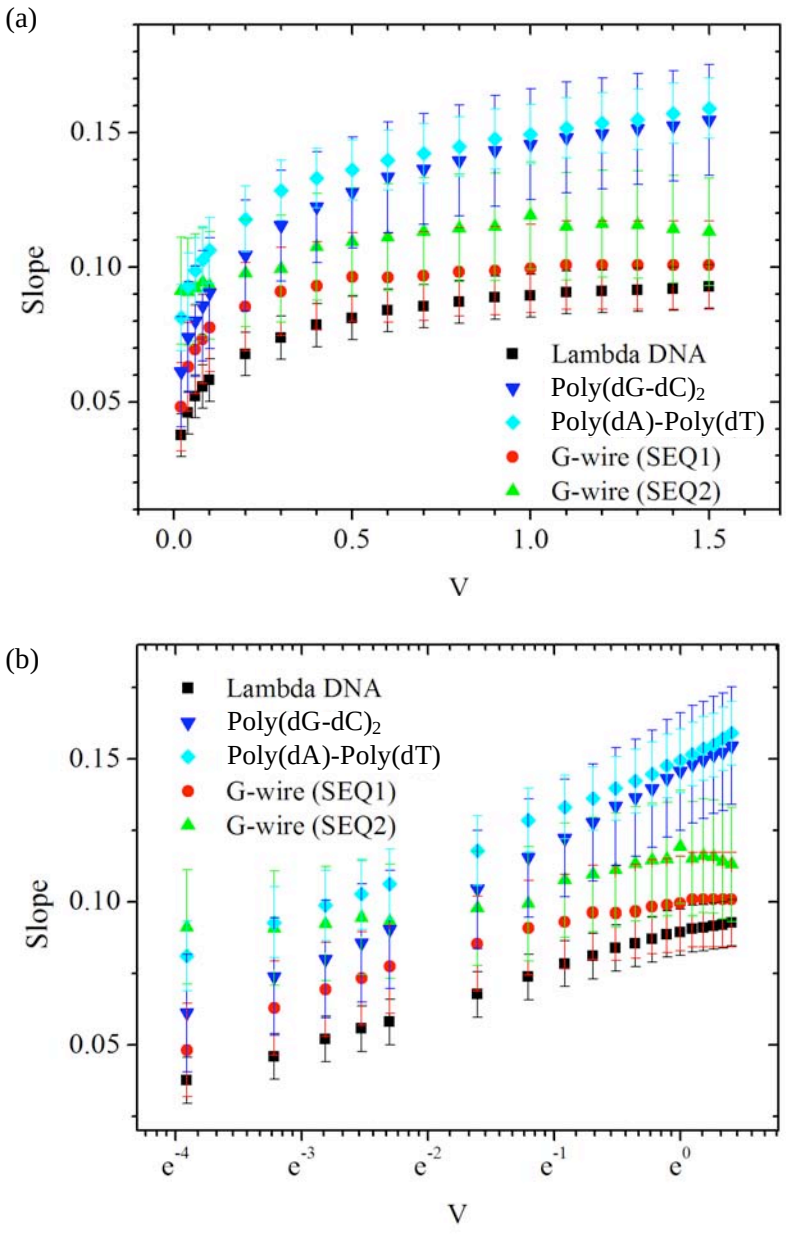

Figure 3.3-17
(a) Relationship between the applied bias voltage and the degree of increase in resistance. The slope is correspond to the degree of increase in resistance. The values are calculated as the same method as figure 3.3-14. (b) Value of slope vs ln*V* plot.

Temperature dependence on electrical property and conduction mechanisms

In order to study the conduction mechanism, *I-V* characteristics are measured at different temperature. Both of lambda DNA and G-wire (SEQ2) is employed for the measurements. Measurements are performed on three samples for both of DNA. The distances between electrodes is measured to be 54.1 nm, 55.4 nm and 80.9 nm for lambda DNA sample and 54.9 nm, 60.1 nm and 66.4 nm for G-wire sample, respectively.

Figure 3.3-18 shows the *I-V* characteristics of lambda DNA (a) and G-wire (SEQ2) (b). Each result shows the enhancement in current with increasing the temperature. Moreover, the temperature dependence on current is shown in figure 3.3-19. Same tendency is obtained; the current increased with increasing temperature. The amount of change in current is found to be varied by the bias voltage. The current measured under lower bias voltage changed linearly. On the other hand, the degree of change in current under higher bias voltage decreased with decreasing temperature. These results indicate that the electrical conduction is thermally activated process and bias-voltage dependent process.

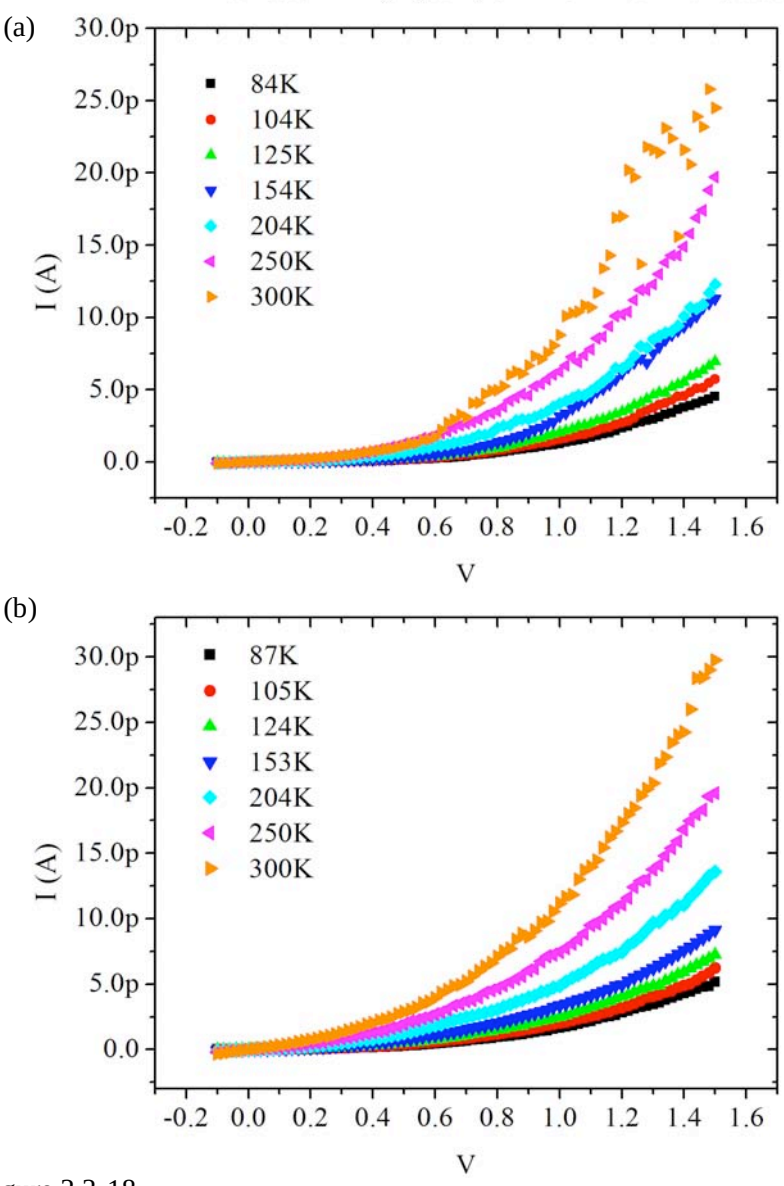

Figure 3.3-18
I-V characteristics measured at different temperature. (a) and (b) show the results of lambda DNA and G-wire (SEQ2), respectively.

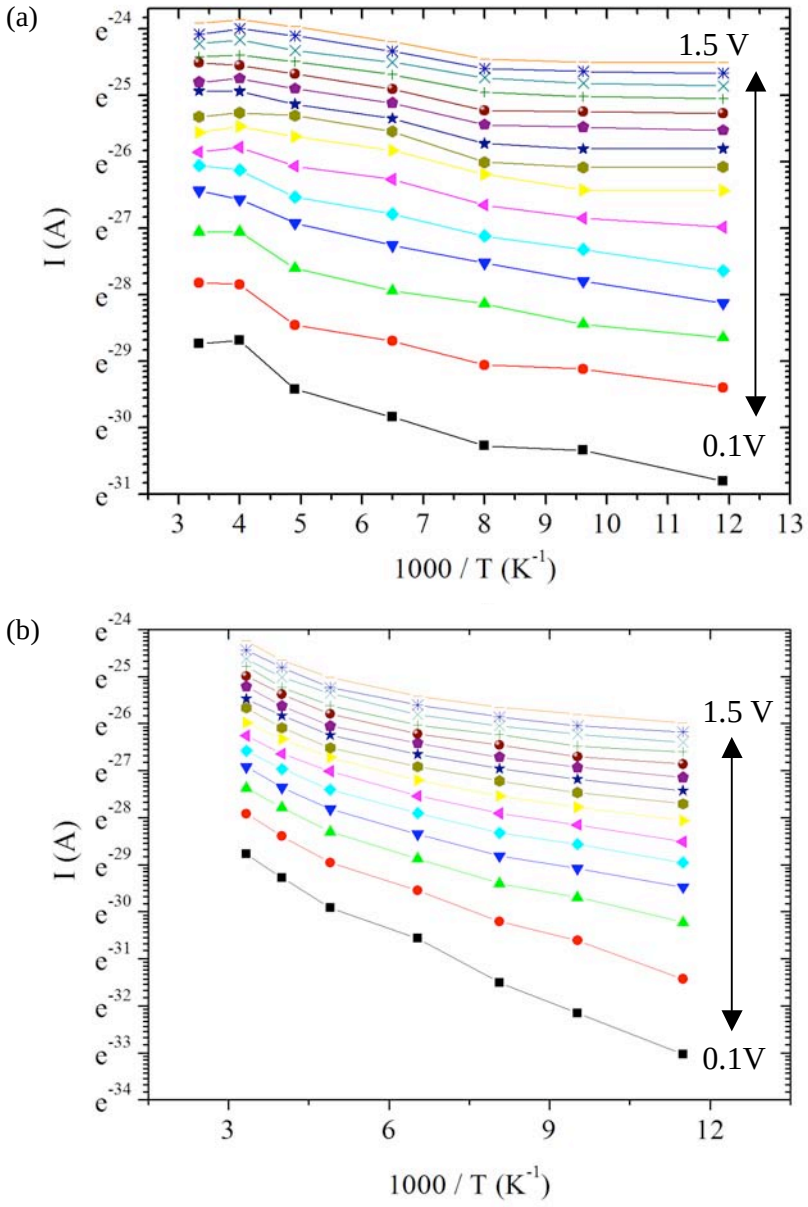

Figure 3.3-19
Temperature dependence of current. Current under specific bias voltage is plotted. Bias voltage is noted in the viewgraph. (a) and (b) show the results of lambda DNA and G-wire (SEQ2), respectively.

Then the conduction mechanism is discussed. The possible conduction mechanisms are shown in table 3.3-2 [50-52]. In case we study the conduction mechanisms, they should be classified whether they are based on the charge injection at the electrode/sample interface or charge transport along sample [53].

In this study, the relationship between resistance and distance between electrodes indicate that the charge transport is sample-limited-process. Hence, it would be unlikely that Schottky emission, Fowler-Nordheim tunneling and direct tunneling mechanisms can be employed for explanation of this result. Therefore, we herein discuss the possibility of explanation by hopping conduction, Frenkel-Poole emission and trap assisted tunneling mechanisms.

Concuction Mechanism	Expression	Proportionality relation	Schematic Illustration
Hopping Conduction	$I \sim V \exp(-\Delta E / kT)$	$\ln(I/V) \propto 1/T$ $I \propto V$	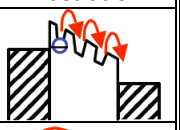
Schottky Emission	$J = A^* T^2 \exp\left[-q(\phi - \sqrt{qE/4\pi\varepsilon})/kT\right]$	$\ln(J/T^2) \propto 1/T$ $\ln J \propto E^{1/2}$	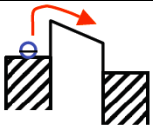
Frenkel-Poole Emission	$J = qN\mu(kT)^2 E \exp\left[(-q\phi + \beta E^{1/2})/kT\right]$	$\ln(J/T^2) \propto 1/T$ $\ln(J/E) \propto E^{1/2}$	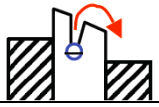
Direct Tunneling	$J = \frac{q^2 V\sqrt{2mq\phi}}{4\pi\hbar^2 d}\exp\left[-\frac{2d}{\hbar}\sqrt{2mq\phi}\right]$	$J \propto V$	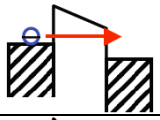
Fowler-Nordheim Tunneling	$J = \frac{q^2E^2}{8\pi h\phi}\exp(-\frac{8\pi(2m*\phi^3)^{1/2}}{3qh}\cdot\frac{1}{E})$	$\ln(J/E^2) \propto 1/E$	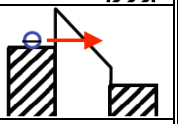
Trap Assisted Tunnling	$J \approx \exp\left(-\sqrt{E_0/E}\right)$	$\ln J \propto 1/E^{1/2}$	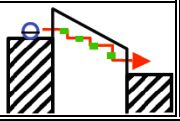

Table 3.3-2 List of possible conduction mechanism

1, Hopping conduction [54,55]

The thermally excited electrons hop from the isolated state to the neighboring isolated state. The current is strongly affected by temperature, and can be described as,

$$I \sim V \exp(-\Delta E / kT) \quad (1)$$

where Δ E is the activation energy. The expression can be transformed to,

$$\ln(I/V) \propto (-\Delta E / kT) \quad (2)$$

Hence, the proportionally relation following this expression can be obtained for the electrical property by hopping conduction.

2, Frenkel-Poole conduction [55-58]

The conductive carriers trapped at the localized state are moved to the neighboring localized state due to the field-enhanced thermal excitation. The current density is described as follows;

$$J = C \cdot E \exp\left[\frac{-q\phi + \beta E^{1/2}}{kT}\right] \quad (3)$$

where $\beta = (q^3 / \pi \varepsilon_o \varepsilon_d)^{1/2}$. This expression can be transformed to,

$$\ln(J/E) \propto E^{1/2} \quad (4)$$

Hence the proportionally relation following this expression can be obtained for the electrical property by Frenkel-Poole conduction.

3, Trap assisted tunneling conduction[51,52,59]

The conductive carriers trapped at the localized state are moved to the neighboring localized state as Frenkel-Poole conduction, but the moving process is by tunneling. This process is usually strongly dependent on film thickness and electrical field. The current density is described as follows;

$$J \approx \exp(-\sqrt{E_0 / E}) \quad (5)$$

This expression can be transformed to,

$$\ln J \propto 1/\sqrt{E} \quad (6)$$

Hence the proportionally relation following this expression can be obtained for the electrical property by trap assisted tunneling conduction.

The reason why each expression is transformed is that the fitting of obtained results to the transformed expression is the simplest way to outline the conduction mechanism. Next, the fitting results are shown.

Fitting by Hopping conduction mechanism

Figure 3.3-20 shows ln(*V/I*) vs. 1/T plot. (a) and (b) show the results of lambda DNA and G-wire (SEQ2), respectively. This is according to the expression (2). Experimental data (current) obtained at the bias voltage lower than 0.1 V is plotted. It is found that the linear correlation between ln(*V/I*) and 1/T at the temperature more than 150 K for both samples. This indicates that the I-V characteristics are linear, and ohmic characteristics are measured. The graph with the same correlation is plotted as for the data obtained at the bias voltage more than 0.1 V, but the linear correlation is not found for both samples.

These results indicate that the conduction mechanism under both of higher temperature ($T > 150$ K) and lower bias voltage ($V < 0.1$ V) can be interpreted as hopping conduction.

Fitting by Frenkel-Poole conduction mechanism

Figure 3.3-21 shows ln(J/E) vs. $E^{1/2}$ plot. (a) and (b) show the results of lambda DNA and G-wire (SEQ2), respectively. This is according to the expression (4). The linear correlations between ln(J/E) and $E^{1/2}$ are found with increasing $E^{1/2}$. Deviances from the linearity are found under both of the conditions that lower $E^{1/2}$ and lower temperature.

These results indicate that the conduction mechanism under both of higher temperature and higher electric field (that corresponds to bias voltage) can be interpreted as Frenkel-Poole conduction.

Fitting by trap assisted tunneling conduction mechanism

Figure 3.3-22 shows lnJ vs.$1/\sqrt{E}$ plot. (a) and (b) show the results of lambda DNA and G-wire (SEQ2), respectively. This is according to the expression (6). The linear correlations between lnJ and$1/\sqrt{E}$ are found with decreasing $1/\sqrt{E}$ (this is correspond to the increase of E). Deviances from the linearity are found under both of the condition that higher $1/\sqrt{E}$ (correspond to lower E) and higher temperature.

These results indicate that the conduction mechanism under both of lower temperature and higher electric field (that corresponds to bias voltage) can be interpreted as multi-step trap assisted tunneling conduction.

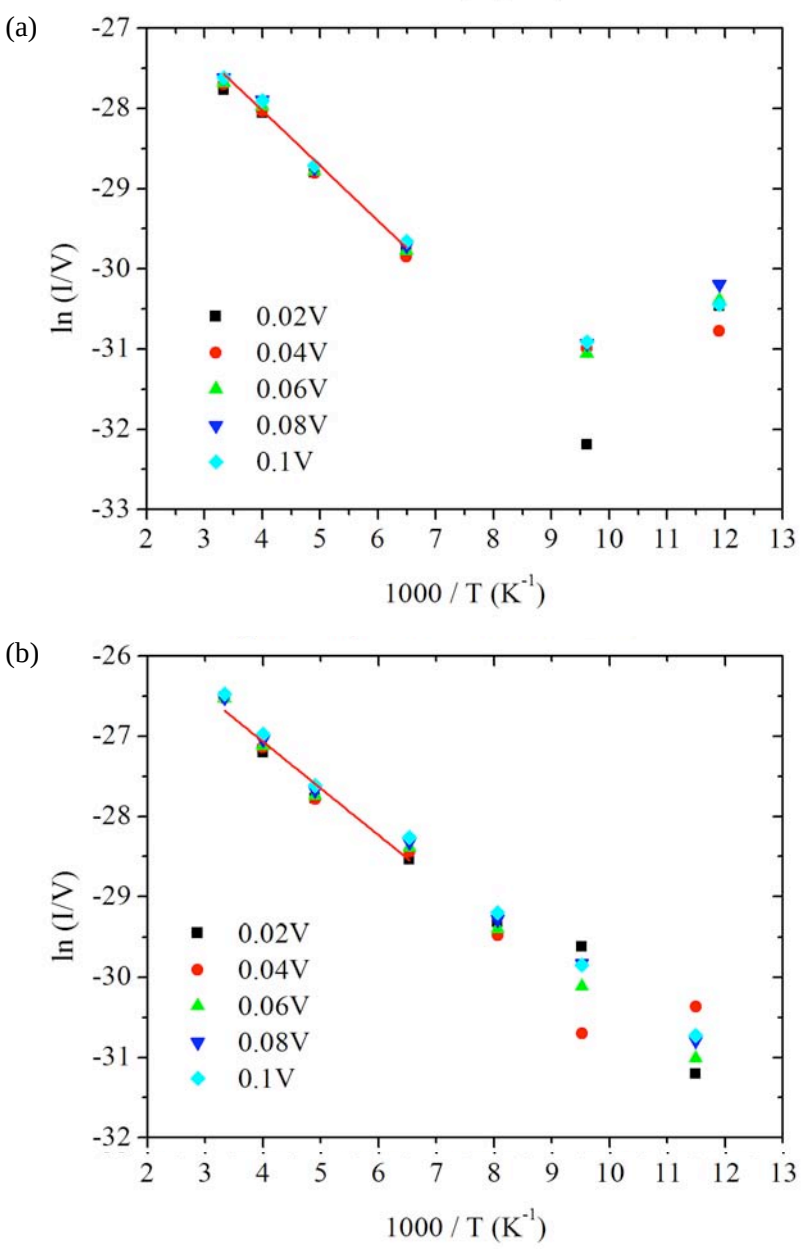

Figure 3.3-20 ln(*V/I*) vs. 1/T plot. (a) and (b) show the results of lambda DNA and G-wire (SEQ2), respectively.

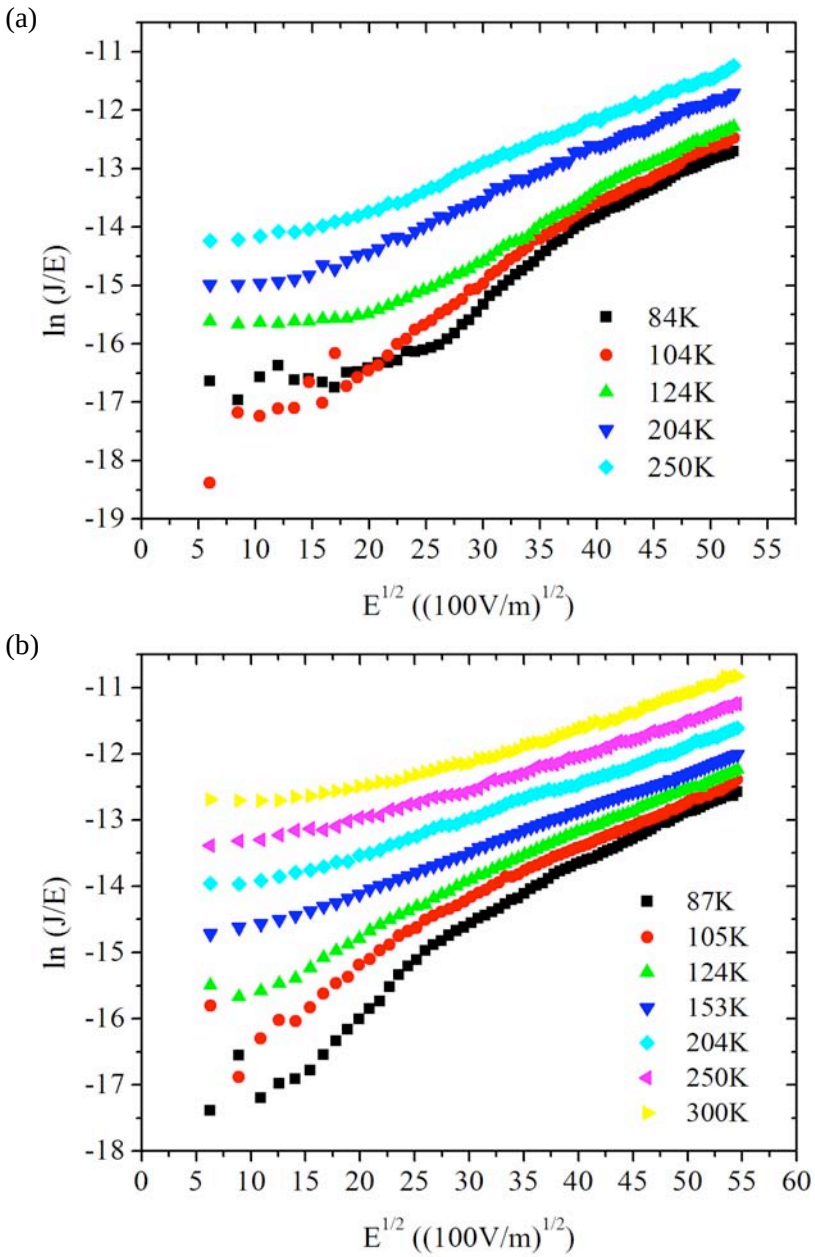

Figure 3.3-21
ln(J/E) vs $E^{1/2}$ plot. (a) and (b) show the results of lambda DNA and G-wire (SEQ2), respectively.

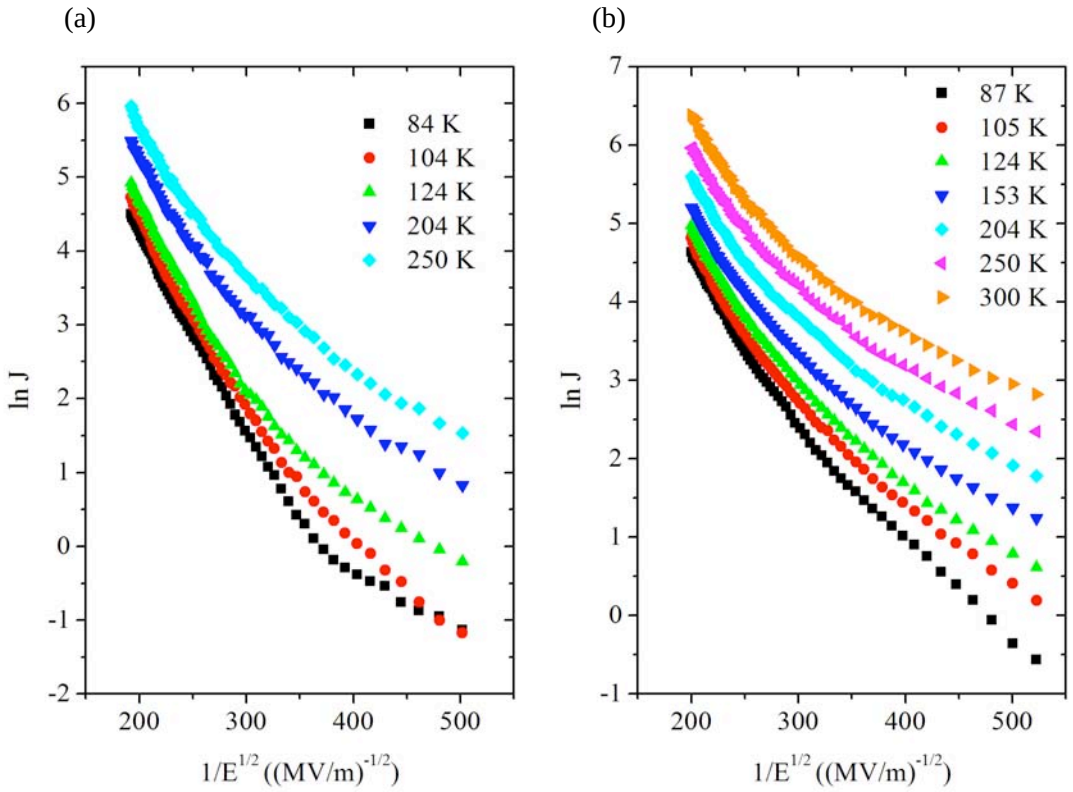

Figure 3.3-22
lnJ vs.1/√E plot. (a) and (b) show the results of lambda DNA and G-wire (SEQ2), respectively.

These fitting studies indicated that conduction mechanisms vary according to the temperature and applied bias voltage (electric field). The schematic illustrations in order to understand the different mechanism are shown in figure 3.3-23. (a) shows the situation without applying bias voltage (0V) between electrodes. As the bias voltage is applied between electrodes, the potential barriers both between DNA /Au and localized state along DNA are bent. In case the lower bias voltage (V < 0.1 V) is applied (b), the conductive carriers are transported from one-side electrode to another electrode through DNA localized state by hopping. As the hopping process is limited by the diffusion of thermally excited carriers [60], the current level is smaller.

As the bias voltage increasing (V > 0.1 V), the potential barriers are bent steeply and the effective potential barriers are lowered (c). The conductive carriers trapped at the localized state are transported along the strong electric field. The process of charge transport varies according to the temperature. At higher temperature, the thermally excited carriers are transported. (Frenkel-Poole conduction) As the effective potential barriers are lowered due to the higher

electric field [61] and the mobility of carriers are accelerated (left illustrations in (d)), the current level is larger than the hopping process. On the other hand, at lower temperature, the carriers are not thermally excited enough to overcome the potential barriers. The carriers are transported by the tunneling process at the effectively lowered potential barriers. (Trap assisted

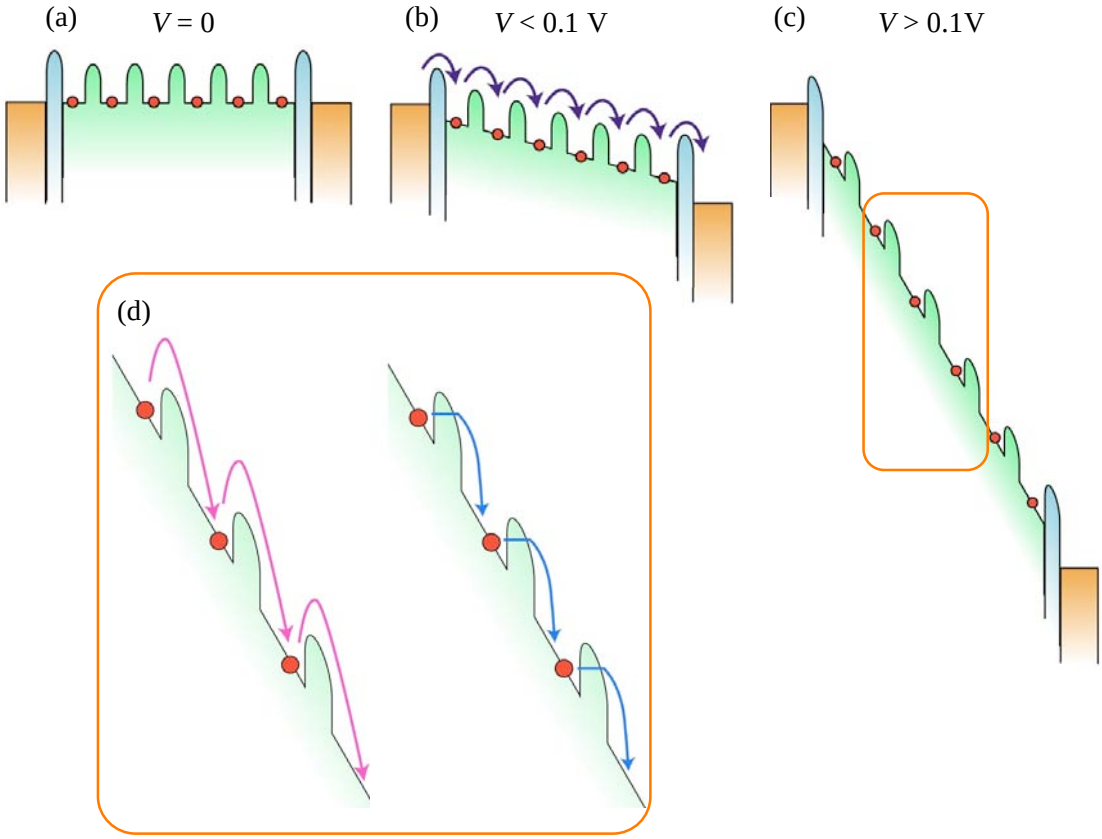

Figure 3.3-23
Schematic illustrations of conduction mechanism under different bias voltage are applied between electrodes. (a) $V = 0$, (b) $V < 0.1$ V, (c) $V > 0.1$ V. (d) Magnified image at the position shown in (c).

tunneling) (Right illustration in (d))

These results indicate the localized conductive carrier along both of lambda DNA and G-wire. Endres et al. studied the possible mechanism of generation of conductive carriers along double-stranded DNA [62]. The DFT calculation for four-base-pair-long B-DNA (5'-GAAT-3') indicates the formation of impurity state due to counter ions such as Na^+ and Mg^{2+} between the π state and π* state of DNA. The energy gap between the impurity state and π* state is calculated to be 62 meV and 500 meV as for Mg^{2+} and Na^+, respectively. Hence the effective hole doping to the π* state due to the impurity state of Mg^{2+} is suggested.

In this measurements, the resistance of Mg^{2+} added lambda DNA is lower than that of Na^+

added lambda DNA. (Table 3.3-1) The mechanism that generates these differences would be attributed to the formation of conductive carriers as suggested by Endres et al. After the conductive carriers are introduced to DNA, the carriers would be localized due to the random base sequences.

As for G-wire, Calzolari et al. suggested the charge delocalization along G-wire [41] as noted in the previous page. But the G-wire contains structural defects due to the gaps of T in the base sequence. Therefore, the localization of conductive carriers might be generated at such defects. However, the mechanism of the formation of conductive carriers has not been calculated yet.

Moreover, the structural bending might generate the electrical localization along base stacking. As the surface of SiO_2 substrate used in this study is not atomically flat, but mechanically polished amorphous surface, the structural deformation would occur.

Furthermore, the activation energy for hopping conduction and effective potential barrier for Poole-Frenkel conduction is calculated for the quantitative comparison. First, the activation energy is calculated from the slope of fitted line as shown in figure 3.3-20. The values are shown in table 3.3-2. The estimated activation energy by the hopping conduction mechanism was 60 – 70 meV. This value is much less than the HOMO-LUMO gap (~ 4 eV). Previous study [63] of the charge transport in polydiacetylene quasi 1D single crystals concluded the smaller activation energy (13 – 19 meV) than the energy-gap of crystal (~3.2 eV) originates from the thermally assisted nearest-neighbor hopping mechanism by self-localized excitations as small poralons characteristic of quasi-1D polymers [64]. Therefore, this calculated value might indicate the formation of small poralons along double-stranded DNA and G-wire.

Gap size	54.1 nm	55.4 nm	80.9 nm
Lambda DNA	0.067 eV	0.060±0.006 eV	0.055±0.016 eV
Gap size	54.9 nm	60.1 nm	66.4 nm
G-wire	0.058±0.012 eV	0.066±0.006 eV	0.075±0.005 eV

Table 3.3-3 Calculated activation energy

The formation of small poralons is previously reported by Yoo et al. They measured the electrical conductivity both of poly(dA)-poly(dT) and poly(dG)-poly(dC) with bottom-contacted geometry type electrodes separated by 20 nm. The calculated activation energy was 0.18 and 0.12 for poly(dA)-poly(dT) and poly(dG)-poly(dC), respectively. These values are

larger than this result. The origin of this difference is unclear, but the structure of DNA and/or electrical contact between electrodes and DNA might affect the electrical properties. As shown in the previous reports (also shown in figure 1.2-13), DNA molecules are immobilized between electrodes; hence the structure of DNA molecules would be bent more or less at the edge of electrodes. The structural bending would generate the fluctuation of π-stacking of base molecules and localize the electrical state, hence the activation energy would be increased.

Then, the potential barrier for Frenkel-Poole conduction is measured. As shown in figure 3.3-21 and its related sentence, the conduction mechanism under both of higher temperature and higher electric field. Here the barrier height for different DNA at room temperature is calculated. The calculation is performed as follows.

I-V characteristics both of different DNA and different distance between electrodes are plotted as ln(J/E) vs $E^{1/2}$ (Figure 3.3-24). Then the points with linear correlation (E > 9 MV/m) are fitted by least-squares method. As shown in equation (3), the current density with Poole-Frenkel conduction is described as,

$$J = C \cdot E \exp\left[\frac{-q\phi + \beta E^{1/2}}{kT}\right]$$

Then this expression can be transformed to

$$\ln\left(\frac{J}{E}\right) = \frac{\beta}{kT} E^{1/2} - \frac{q}{kT}\phi + C$$

C is corresponded to the current density at the lower electric field. As the current level of lower electric field (bias voltage) is much smaller than that of higher electric field (bias voltage), the value of intercept in ln(J/E) vs $E^{1/2}$ plot is corresponded to the potential barrier.

Figure 3.3-25 shows the relationship between calculated intercepts and distance between electrodes for different DNA. (a) shows the calculated data and (b) shows the fitted correlations by least-squares method. The calculated potential barrier is also shown in the right axis.

The calculated barrier height varies for different DNA. The amount of slope of fitted line increased in the order as,

Lambda DNA < G-wire (SEQ1 & SEQ2) < Poly(dA)-Poly(dT) ~ Poly(dG-dC)$_2$.

This tendency is similar to the amount of increase in resistance as shown in figure 3.3-14. The increase in barrier height with increasing distance between electrodes would indicate that the number of localized state between electrodes increases with increasing the gap size.

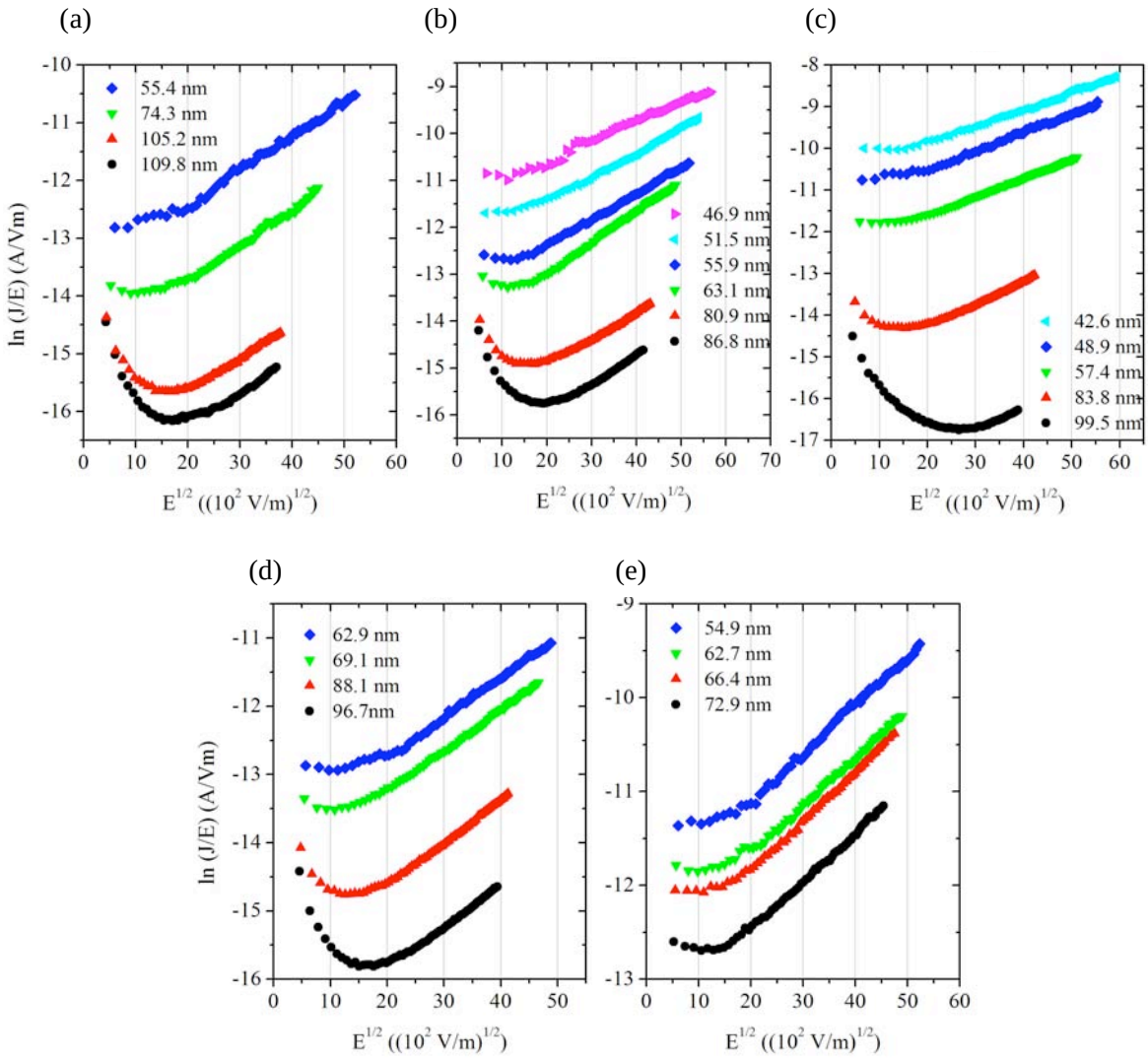

Figure 3.3-24
ln(J/E) vs $E^{1/2}$ plots for both of different DNA and different distance between electrodes. The distance between electrodes are noted in each graph. (a) Lambda DNA, (b) Poly(dG-dC)$_2$, (c) Poly(dA)-Poly(dT), (d) G-wire (SEQ1), (e) G-wire (SEQ2).

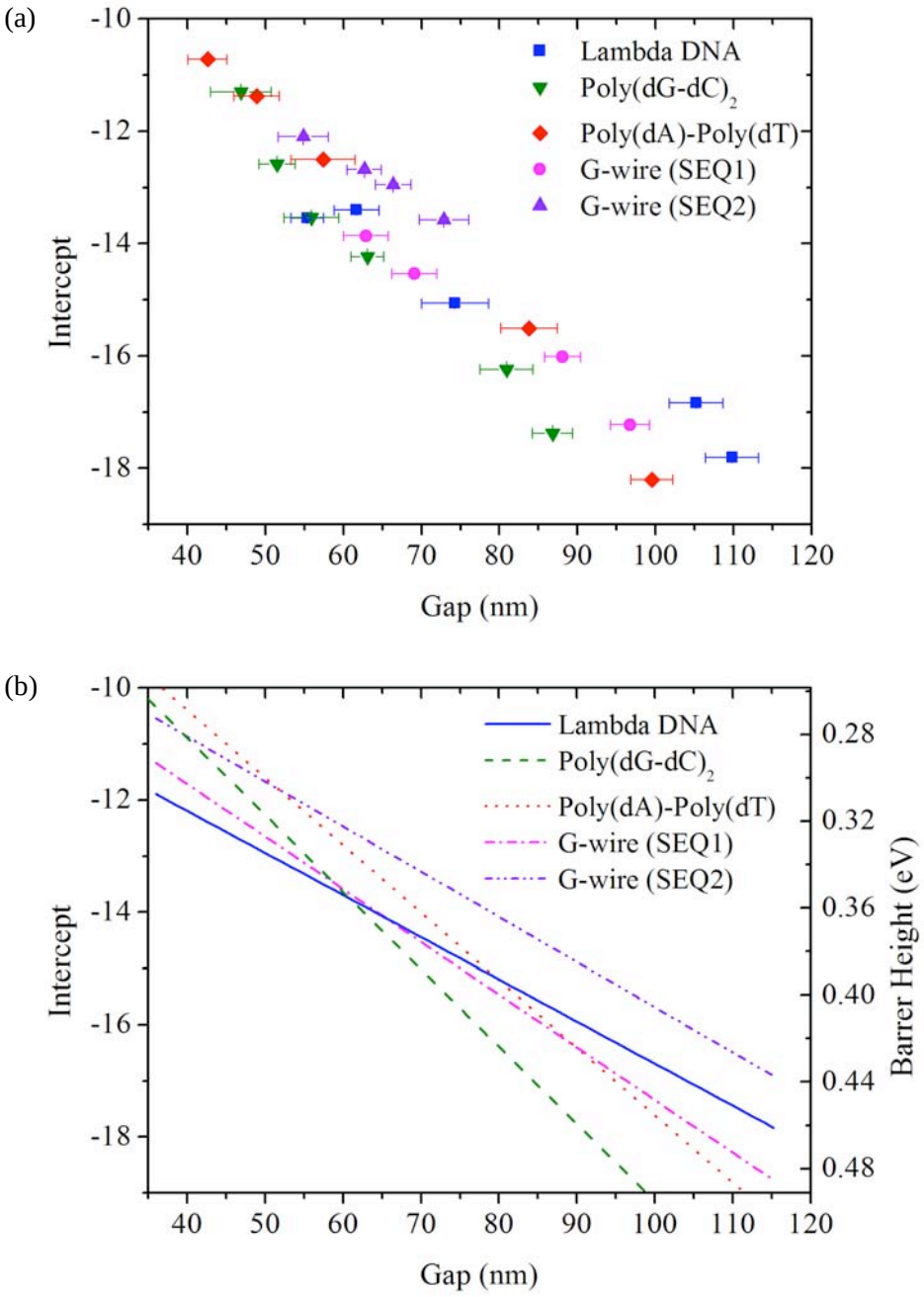

Figure 3.3-25
The relationship between calculated intercepts and distance between electrodes for different DNA. (a) Calculated data, (b) Fitted correlations by least-squares method.

Conclusion

The electrical conductivity of DNA is measured by 1: bottom-contacted geometry electrodes separated by 100 nm, 2: PCI-AFM at the distance between conductive tip and Au layer is more than 100 nm and 3: top-contacted geometry electrodes separated by 40 - 100 nm, respectively. As noted in chap 3.1, the electrical measurements of DNA film by method 1 show that the apparent resistance is strongly affected by the relative humidity around DNA. Next, as noted in chap 3.2, the measurements of DNA network by PCI-AFM show the effect of humidity as well. These results by method 1 and 2 indicated no electrical properties originate form DNA.

Finally, as shown in chap 3.3, the measurements by top-contacted geometry electrodes show the experimental results that indicate the charge transport along DNA under vacuum condition (10^{-5} Torr). The detailed study indicated the resistance of DNA is exponentially dependent of the distance between electrodes. The degree of increase in resistance of synthesized DNA that contain uniform base sequences is measured to be larger than that of lambda DNA that contains random base sequences. This results indicate the structural defect such as nick strongly affect electrical property. Moreover the comparison of resistance between lambda DNA and synthesized DNA indicate at smaller nanogap electrode (<70nm) indicate the conduction path would be π-stacked base molecules.

The electrical measurements at different temperatures also indicate the possible electrical conduction mechanism of DNA. It is suggested that the electrical conductivity originates from the localized conductive carrier along DNA, and this would be supported by the previous DFT calculation. Moreover, the electrical property of G-wire is also studied for the first time. The electrical conduction mechanism is similar to that of double-stranded DNA, but the value of resistance is about more than 5 times lower than lambda DNA. This would be due to the expanded and delocalized conductive path along G-wire as shown in the calculation results.

From the viewpoint obtained by top-contacted geometry electrode, it is concluded that the insulative characteristics shown in chapter 3.1 originate from the localization of conductive path of DNA due to the structural deformation at the edge of electrode, and that shown in chapter 3.2 originate from the measurement limitation of PCI-AFM because the distance between conductive tip and Au layer is limited to be more than about 100 nm for the sake of secure measurement. Therefore, it is suggested that the electrical measurements of

DNA requires the special care to minimize the structural deformation for electrical connection between DNA and electrodes.

References

[1] Y. Okahata, T. Kobayashi, K. Tanaka, M. Shimomura, *J. Am. Chem. Soc.* **120,** 6165 (1998).
[2] E. Braun, Y. Eichen, U. Sivan, G. B. Yoseph, *Nature* **391**, 775 (1998).
[3] K. Fukui, K. Tanaka, *Angew. Chem. Int. Ed.* **37**, 158 (1998).
[4] H. W. Fink, C. Scho¨nenberger, *Nature* **398**, 407 (1999).
[5] S. O. Kelly, J. K. Barton, *Science* **283**, 375 (1999).
[6] L. Cai, H. Tabata, T. Kawai, *Appl. Phys. Lett.* **77**, 3105 (2000).
[7] D. Porath, A. Bezryadln, S. de Vries , C. Dekker, *Nature* **403**, 635 (2000).
[8] J. Richter, M. Mertig, I. Mönch, H. K. Schackert, W. Pompe, *Appl. Phys. Lett.* **78**, 536 (2001).
[9] S. Priyadarshy, S. M. Risser, D. N. Beratan, *J. Phys. Chem.* **100**, 17678 (1996).
[10] G. Taubes, *Science* **275**, 1420 (1997).
[11] E. K. Wilson, *C&EN* **July 27**, 51(1998).
[12] J. Jortner, M. Bixon, T. Langenbacher, M. E. Michel-Beyerle, *Proc. Natl. Acad. Sci. U.S.A.* **95**, 12579 (1998).
[13] E. Meggers, M. E. Michael-Beyerle, B. Giese, *J. Am. Chem. Soc.* **120**, 12950 (1998).
[14] M. Bixon, B. Giese, S. Wessely, T. Langenbacher, M. E. Michel- Beyerle, J. Jortner, *Proc. Natl. Acad. Sci. U.S.A.* **96**, 11713 (1999).
[15] P. T. Henderson, D. Jones, G. Hampikian, Y. Kan, G. B. Schuster, *Proc. Natl. Acad. Sci. U.S.A.* 96, 8353 (1999).
[16] M. Ratner, *Nature* **397**, 480 (1999).
[17] P. Tran, B. Alavi, G. Gruner, *Phys. Rev. Lett.* **85**, 1564 (2000).
[18] W. Saenger, *Principles of Nucleic Acid Structure* (Springer-Verlag, Tokyo, 1987) p. 347 [in Japanese].
[19] O. K. Varghese, L. K. Malhotra, *J. Appl. Phys.* **87**, 7457 (2000).
[20] H. Tamura, Y. Matuda, *Gendai Denjkikagaku (Electrochemistry)* (Baifukan, Tokyo, 1977) p. 28 [in Japanese].
[21] G. Travot, P. Divetain, G. Sirand-Rey, *J. Appl. Phys.* **49**, 5680 (1978).
[22] O. K. Varghese, L. K. Malhotra, *J. Appl. Phys.* **87**, 7457 (2000).
[23] Y.Otsuka, H.-Y. Lee, J.-H. Gu, J.-O. Lee, K.-H. Yoo, H. Tanaka, H. Tabata, T. Kawai, *Jpn. J. Appl. Phys.* **41**, 891 (2002).
[24] J.A. Hackett, D.M. Felder, C.W. Greider, *Cell* **106**, 275 (2001)
[25] G.N. Parkinson, M.P.H. Lee, S. Neidle, *Nature* **417**, 876 (2002).
[26] E.H. Blackburn, *Nature* **350**, 569 (1991).
[27] J.R. Williamson, M.K. Raghuraman, T.R. Cech, *Cell* **59**, 871 (1989).
[28] T.C. Marsh, E. Henderson, *Biochemistry* **33**, 10718 (1994).
[29] T.C. Marsh, J. Vesenka, E. Henderson, *Nucl. Acid. Res.* **23**, 696 (1995).
[30] D. Sen, W. Gilbert, *Methods In Enzymology* **211**, 191 (1992).
[31] Y. Fang, J.H. Hoh, *Nucl. Acid. Res.* **26**, 588 (1998).
[32] L.A. Shlyakhtenko, A.A. Gall, J.J. Weimer, D.D.Hawn, Y.L. Lyubchenko, *Biophys. J.* **77**, 568 (1999).
[33] C.A.M Seidel, A. Schulz, M.H.M. Sauer, *J. Phys. Chem.* **100**, 5541 (1996).
[34] H. Fernando, G.A. Papadantonakis, N.S. Kim, P.R. LeBreton, *Proc. Natl. Acad. Sci. USA* **95**, 5550 (1998).
[35] A.A. Voityuk, J. Jortner, M. Bixon, N. Rösch, *Chem. Phys. Lett.* **324**, 430 (2000).
[36] D. Sen, W. Gilbert, *Methods In Enzymology* **211**, 191 (1992).
[37] C.C. Hardin, E. Henderson, T. Watson, J.K. Prosser. *Biochemistry* **30**, 4460 (1991).

[38] R.H. Shafter, *Progress In Nucleic Acid Research and Moleuclar Biology* **59**, 55 (1998).
[39] M. Lu, Q. Guo, N.R. Kallenbach, *Biochemistry* **32**, 598 (1993).
[40] C.C. Hardin, E. Henderson, T. Watson, J.K. Prosser. *Biochemistry* **30**, 4460 (1991).
[41] A. Calzolari, R.D. Felice, E. Molinari, A. Garbesi, *cond-mat* 041012 (2004).
[42] C.H. Kang, X. Zhang, R. Ratliff, R. Moyzis, A. Rich, *Nature* **356**, 126 (1992).
[43] G. Laughlan, A.I.H. Murchie, D.G. Norman, M.H. Moore, P.C.E. Moody, D.M. Lilley, B. Luisi, *Science* **265**, 520 (1994).
[44] Y. Fang, J.H. Hoh, *Nucl. Acid. Res.* **26**, 588 (1998).
[45] H.G. Hansma, D.E. Laney, *Biophys. J.* **70**, 1933 (1996).
[46] H. Vasmel, J. Greve, *Biopolymers* **20**, 1239 (1981).
[47] O.V. Davydova, I.A. Kuznetsov, V.L. Florentiev, *Biopolymers* **28**, 605 (1989).
[48] K. Nejedlý, J. Chládková, M. Vorlíćková, I. Hrabcová, J.Kypr, *Nucl. Acid. Res*. **33**, e5 (2005).
[49] K. Grzeskowiak, J. Onishi, V. Ivanov, *Nucleic Acids Symposium Series*, **49**, 249 (2005).
[50] C.A. Mead, *Phys. Rev.* **128**, 2088 (1962).
[51] D. Braun, *J. Poly. Sci. Part B* **41**, 2622 (2003).
[52] C.L. Henderson, *Semiconductor Reliability Manual* "The Dependent Dielectric Breakdown" (2002).
[53] J.G. Simmons, *Phys. Rev. Lett.* **166**, 912 (1968).
[54] S. Banerjee, B. Shen, I. Chen, J. Bohiman, G. Brown, R. Doering, *J. Appl. Phys.* **65**, 1140 (1989).
[55] S.M. Sze, *J. Appl. Phys*. **38**, 2951 (1967).
[56] W.D. Gill, *J. Appl. Phys*. **43**, 5033 (1972).
[57] A.A. El Tayyan, A. Khogali, *Chi. J. Phys.* **42**, 392 (2004).
[58] A.A. Dakhel, *Cryst. Res. Technol.* **38**, 968 (2003).
[59] M. Raikh, X. Wei, *Mol. Cryst. Liq. Cryst.* **256**, 563 (1994).
[60] I.I. Fishchuk, A.Kadashchuk, H. Bässler, M. Abkowitz, *Phys. Rev. B* **70**, 245212 (2004).
[61] J. Frenkel, *Phys. Rev.* **54**, 647 (1938).
[62] R. G. Endres, D.L. Cox, R.R.P. Singh, *Rev. Mod. Phys.* **76**, 195 (2004).
[63] A.N. Aleshin, J.Y. Lee, S.W. Chu, S.W. Lee, B. Kim, S.J.Ahn, Y.W. Park, *Phys. Rev. B.* **69**, 214203 (2004).
[64] A.J. Heeger, S. Kivelson, J.R. Shriefer, W.P. Su, *Rev. Mod. Phys.* **60**, 781 (1988).

Chapter4

Patterning DNA on the Surface Modified with Molecules

4.1. Introduction

The charge transport phenomenon of randomly immobilized DNA on the APS coated SiO_2 substrate with top-contacted geometry type nanogap electrode was studied in previous chapter. It was confirmed the charge transport is actually measured, and concluded that the origin of conductivity is the formation of conductive carrier at the localized state due to counter ions such as magnesium and potassium ions.

Although it was possible to study the detailed conduction mechanism, it seemed difficult to evaluate the precise resistivity because the random immobilization of DNA makes it difficult to decide the precise conduction path. It is conceivable the resistance of straight DNA molecules will be lower than that of bend DNA molecules because the structural deformation would cause the localization of electrical state along π-stacked base molecules. Therefore, it is necessary to measure the straight DNA molecules by top-contacted geometry type nanogap electrodes. (Figure 4-1)

The preparation method of straight DNA molecules has been studied previously. Various kinds of substrates such as mica, sapphire, polymer coated SiO_2, and HOPG has been used so far. [1-9]

In case of the electrical measurements of DNA molecules, it is necessary to use the insulative substrate whose conductivity is much lower than DNA molecules. Furthermore, it is also important to take care of ingredients in the DNA solution, namely only straight DNA molecules should be immobilized on the substrate without undesirable residues due to ions and buffers.

In order to fulfill these requirements, I have developed the new method to immobilize straight DNA molecules on the insulative substrate. I have employed the “patterned” surface with hydrophobic and hydrophilic area whose conductivity is much lower than DNA molecules.

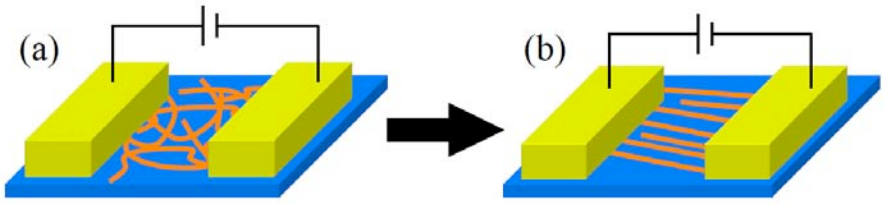

Figure 4-1
The schematic illustration of electrical measurements of DNA molecules by top-contacted geometry type electrodes. (a) and (b) shows the randomly immobilized DNA and straight DNA on insulative substrates, respectively.

The patterning of surface has been studied previously [10-15]. The organosilane molecules on the surface can be dissociated by the UV light irradiation. Hence it is possible to change the chemical properties of the surface by this process, and to pattern the surface by the metal mask pattern as light is irradiated. (Figure 4-2)

DNA molecules are immobilized on the patterned surface. It is found that straight DNA molecules are immobilized on the hydrophobic area by AFM. As DNA molecules are on the hydrophobic surface, it would be possible to measure electrical characteristics of DNA molecules without undesirable residues such as counter ions and buffers. This is because they have no interactions with hydrophobic surface, and they could be removed by rinsing the sample with ultra pure water.

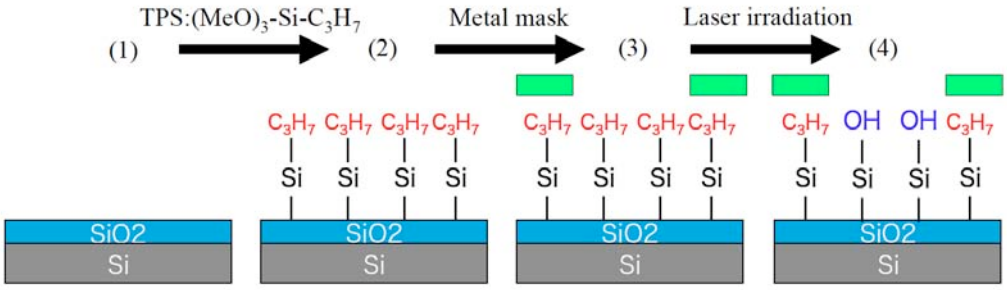

Figure 4-2
The schematic illustrations of the preparation methods of patterned surface.

4.2. Material and methods

Fabrication of hydrophobic surface

SiO_2 / Si (100) substrate (electronics and material corp.) is cleaned by UV-Ozone treatment (NL-UV253, Laser Techno, Japan) for 1 hour and it is reacted with trimethoxypropylsilane (TPS, Wako corp.) immediately. The substrate is placed in the sealed container with small vial. 20ul of TPS solution is put in the vial. The container is heated at 160 ℃ for 30 min. The substrate is picked up and washed with ethanol and ultra pure water for 3 min, successively. The surpass water is removed by dried nitrogen gas flow and the substrate is heated at 100 ℃ to remove water and promote the condensation of TPS molecules. The SiO_2 substrate reacted with TPS molecules (TPS-SiO_2) used for DNA immobilization as soon as

possible.

Patterning surface

The surface is patterned with hydrophobic and hydrophilic area as follows. The TPS-SiO_2 is irradiated with ArF eximer laser through the metal mask. The energy of laser, frequency and irradiation time is 50 mJ, 20 Hz and 10 min, respectively. Metal mask pattern is composed of combination of metal and glass line patterns. The width of metal and glass is 5 μm and 1 μm, respectively.

Surface energy measurements

The surface energy of hydrophobic and hydrophilic surface is measured by sessile drop method. Contact angle of water, diiodomethane and hexadecane on each surface are measured (KRÜSS DSA10 Mk2). The atmospheric temperature is kept to be 25 ℃ and the humidity is kept to be 40 %.

Immobilization of DNA molecules

Lambda DNA (Takara Bio), phosphate buffer (pH 7), $MgCl_2$ is mixed in a micro tube. The final concentration of Lambda DNA, phosphate buffer and $MgCl_2$ is 26.7 ng/μl, 0.1 M and 0.1 M, respectively. The mixture of phosphate buffer and $MgCl_2$ is voltexed, and DNA solution is added and mixed by pippetting gentry. The solution is incubated overnight at 4 degree centigrade before use.

The DNA solution (20 μl) is dropped on the patterned surface. After 20 min of incubation, the solution is blow up by dried nitrogen gas flow. The direction of gas flow is kept so as the interface between solution and substrate move vertical to the line pattern with hydrophobic and hydrophilic area. That is, interface moves hydrophobic and hydrophilic area alternately. The gas pressure is kept to be about 0.1 MPa and the angle of gas flow is about 80 degree.

Immediately after the surpass solution is removed, the surface is rinsed with double amount of pure water for 2 times. 40 μl of pure water is dropped on the surface, and it is blow up by dried nitrogen gas immediately. The condition of gas flow is the same as that of DNA solution.

AFM measurements

The patterned substrates with and without DNA molecules are observed by AFM (DI,

Nanoscope VI). Si probes (MPP-11100) is used. Measurements are performed under atmospheric condition by tapping mode.

Electrical measurements

The top-contacted nanogap electrodes are fabricated on the prepared DNA samples. The detailed procedure is noted in chapter 2.3 and 3.3. The electrical characteristics are measured by DC characterization system (Keithley SCS-4200) under the vacuum condition (about 10^{-5} Torr) and light shielded condition.

4.3. Results and Discussion

Surface free energy measurement

At first, it is confirmed that the hydrophobic surface is changed to the hydrophilic surface after ArF laser irradiation. Table 4-1 shows the contact angle of water, diiodomethane and hexadecane on the UV-ozone treated SiO_2, TPS-SiO_2 and laser irradiated TPS-SiO_2, respectively. The contact angle decreased on the laser irradiated TPS-SiO_2 for all solvents. These results indicate the hydrophobic surface (TPS-SiO_2) is actually changed to hydrophilic surface after laser irradiation. It is also to be noticed that the contact angle on the UV-Ozone treated SiO_2 is slightly higher than that of irradiated TPS-SiO_2, and this would indicate the laser irradiation is effective for the surface activation compared to conventional UV-Ozone treatment.

The surface free energy is calculated according to the Young-Dupre equation and extended Fowkes equation, [16]

$$W_{sl} = \gamma_l \left(1 + \cos\theta_{sl}\right)$$

	Water	Hexadecane	Diiodomethane
UV Ozone treated	31.4	15.5	53.3
TPS-SiO_2	61.7	21.9	59.0
Laser irradiated	27.6	12	51.1

Table 4-1
Contact angle of each solvents on the different type of substrate. Each angle is averaged for 3 tests. The unit is degree.

$$W_{sl}/2 = \left(\gamma_s^d \cdot \gamma_l^d\right)^{1/2} + \left(\gamma_s^p \cdot \gamma_l^p\right)^{1/2} + \left(\gamma_s^h \cdot \gamma_l^h\right)^{1/2}$$

where γ_s and γ_l are surface energy of solid and liquid, respectively. The superscripts noted as *d*, *p* and *h* show the component of dispersion force, dipole interaction and hydrogen bond.

As shown in the Figure 4-3, the total surface energy decreased for the TPS-SiO_2, but it is increased for the laser irradiated TPS-SiO_2. Comparing values in each component such as dispersion force, dipole interaction and hydrogen bond, the component of hydrogen bond increases dramatically for the irradiated TPS-SiO_2, and other components slightly increased meanwhile. Therefore, it is confirmed that the enhancement of surface free energy generates the

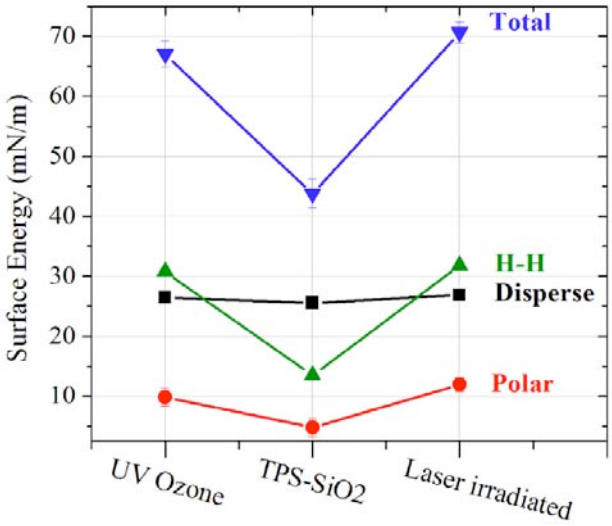

Figure 4-3
Estimated surface energy for each substrate.

hydrogen bond between substrate and solvents.

The modification of surface with light irradiation has been studied previously [10, 17]. The irradiation of light to molecular modified surface generates the chemical reaction. In this case, as the energy of ArF eximer laser (147 kcal/mol) is much more than the chemical bond such as Si-C and C-C (88 kcal/mol), alkyl chain of TPS molecules are dissociated. The dissociation produces the radicals, which can react with moisture in the atmosphere, hydroxyl group is formed in the front (Figure 4-2). It is conceivable that hydroxyl groups on the surface can react with solvents such as water and hydrogen bond is formed.

AFM observation

As it is confirmed that hydrophobic surface can be changed into hydrophilic surface after laser irradiation, patterned surface is fabricated, and observed AFM as shown in Figure 4-4. Figure 4-4 (a) shows the topography, (b) shows the phase image and (c) shows the metal mask pattern observed by optical microscopy.

Although flat surface structure is observed in the topography, distinct surface pattern is observed in the phase image. Moreover, the pattern in the phase image is quite similar to that of metal mask. As the width of metal part (5 μm) and glass part (1 μm) in the metal mask is different each other, the pattern in the phase image is correspond to the surface with and without laser irradiation (hydrophilic and hydrophobic area).

It is known that the phase image shows the phase lag between drive signal and actual cantilever oscillation. The phase lag is originated from the interaction between the tip surface and sample surface due to composition, adhesion, friction, and viscoelasticity of sample surface. Therefore, it is possible to distinguish the variations of surface properties. Although the identification of the value in phase image is quite complicated and out of this intent, the increase in phase lag on the hydrophobic surface would be originate from the repulsive interaction between tip and surface. As the tip is covered with naturally oxidized SiO_2 under atmospheric condition, the interaction between the hydrophobic surface and hydrophilic tip would be repulsive, whereas that of between the hydrophilic surface and hydrophilic tip would be attractive.

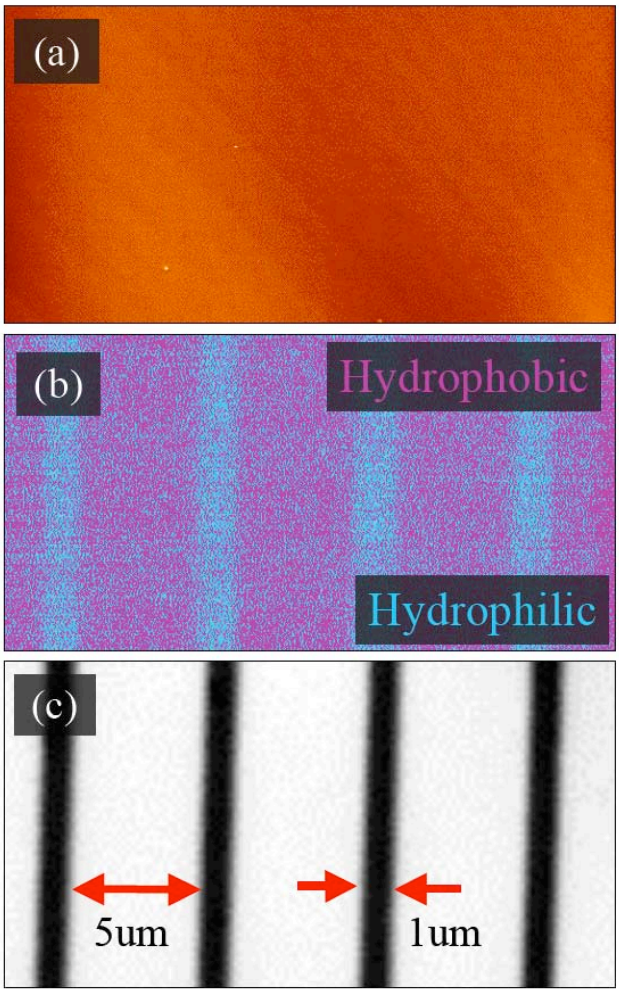

Figure 4-4
(a) and (b) Topographic image and phase image of patterned surface by AFM, respectively. (c) Metal mask pattern observed by optical microscope.

DNA immobilization

Figure 4-5 shows the topography of DNA immobilized sample on the patterned surface. Figure (a) shows the wide-ranging image and (b) shows the magnified image. The distinct pattern is observed over all and different morphology of immobilization is formed on the hydrophobic and hydrophilic surface.

As shown in the Figure 4-5 (b), region A and B are corresponding to the hydrophilic and hydrophobic area, respectively. On the region A, the hydrophilic area, DNA molecules are randomly immobilized over all. On the other hand, straight and bundled DNA molecules are immobilized on the region B, the hydrophobic area. The direction of bundled DNA molecules is identical to the nitrogen gas flow.

As is indicated from the surface free energy measurements, hydroxyl groups formed on the region A. The isoelectric point of SiOH is pH 2. In this study, the phosphate buffer with pH 7 is used. Therefore, SiOH is dissociated under this condition to form the SiO^- and H^+. The ionized SiO^- would be not only hydrated with water molecules but also reacted with DNA molecules through magnesium ion that is included in the solution by electrostatic force. An evidence to support this mechanism is obtained for the study that $MgCl_2$ is not added in the DNA solution. It is confirmed that DNA molecules doesn't adsorb effectively on the patterned surface.

Once DNA molecules immobilized on the region A, they are stretched on the surface due to the interfacial tension between substrate and solution by nitrogen gas flow. Then, stretched DNA molecules would be attached to the opposite region A, that is, DNA molecules bridge region B. As there is little interactions between DNA molecules and region B, DNA molecules don't adsorb on the surface firmly. As a consequence, DNA molecules adsorb each other in order to stabilize structure.

The height distribution is also measured, as shown in Figure 4-5 (c). The averaged height is estimated to be 1.6 nm. Comparing this averaged height to that of single lambda DNA molecule (0.6 nm), the number of DNA molecules in the bundle is estimated to be 7.

Electrical measurements

Electrical properties of bundled DNA molecules are studied by top-contacted geometry nanogap electrode. Figure 4-6 (a) shows the *I-V* characteristics. Non-linear and symmetrical *I-V*

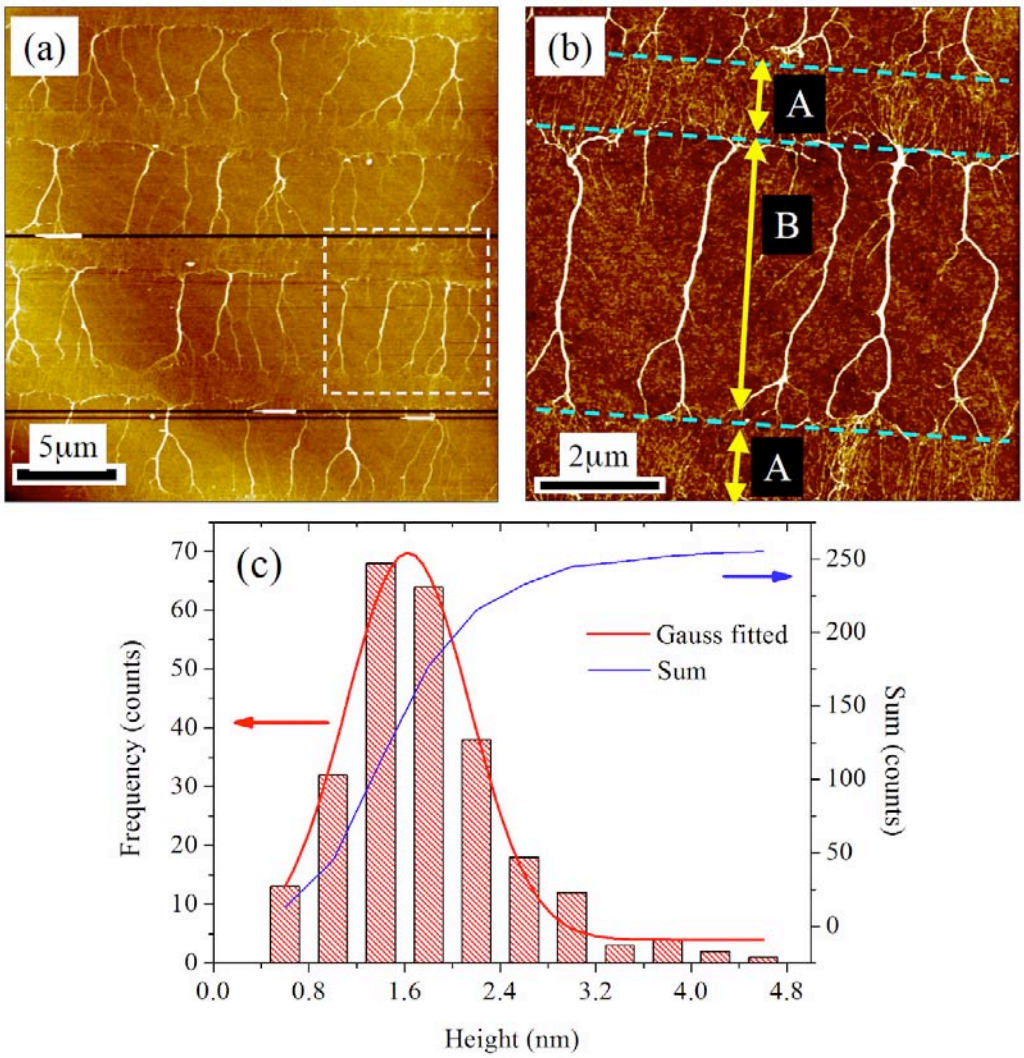

Figure 4-5
(a) AFM images of DNA molecules immobilized on the patterned surface. (b) Magnified AFM image for the area indicated as square with dotted line in (a). A and B shows the hydrophilic and hydrophobic area, respectively. (c) The height distribution of bundled DNA molecules. The fitted curve by Gaussian distribution and the sum of counts are also shown as well.

characteristics are measured for DNA molecules, but such kind of characteristics aren't measured for control experiments. As control experiments, *I-V* characteristics of three kinds of samples are also measured. They are 1: laser irradiated TPS-SiO_2 substrate, 2: Solution without DNA molecules ($MgCl_2$ and phosphate buffer) is dropped on the laser irradiated TPS-SiO_2 and 3: same solution as 2 is dropped on the TPS-SiO_2 substrate.

Next, the time course of current is measured as shown in figure 4-6 (b). Immediately after the specific bias voltage (+1V and -1V) is applied between electrodes, constant current is measured. The constant current is measured for more than 10 min.

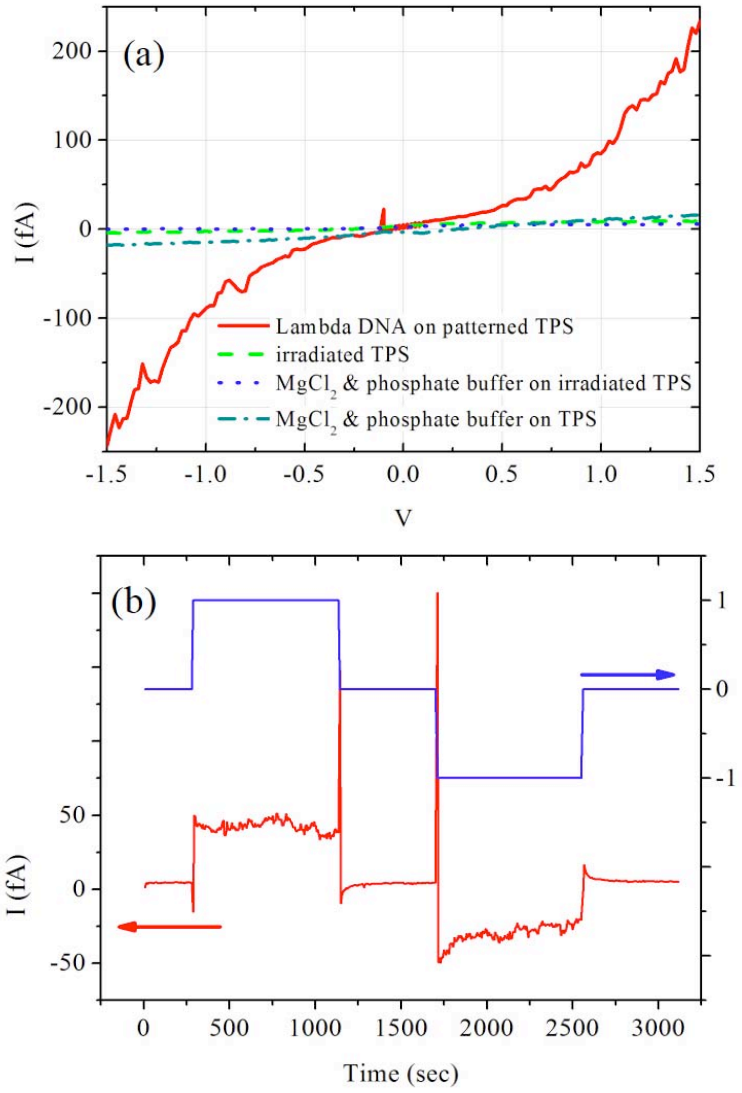

Figure 4-6
(a) *I-V* characteristics of bundled DNA molecules. Control measurements of laser irradiated TPS-SiO_2, counter ion and buffer solution (without DNA molecules) on the TPS-SiO_2 with and without laser irradiation are also shown. (b) The time course of current through bundled DNA molecules.

In order to calculate the resistivity, both of the surface structure and the distance between electrodes are observed. Figure 4-7 shows the AFM and SEM image of the sample near the electrode pair and between electrodes, respectively. The AFM image indicates the bundled DNA molecules are exist at the edge of electrode. As it is quite difficult to observe the structure between electrodes due to the convolution effect of the tip, the nanogap is measured to be 83 nm by SEM. From the distribution of bundled DNA on the surface ((a) and (d)), the number of bundles is estimated to be 40 between nanogap electrodes.

Table 4-2 indicates the comparisons of current, electrical current density J and resistivity ρ between randomly immobilized DNA samples and bundled DNA samples. For precise comparison, the results of electrical measurements by nanogap electrodes separated 80 nm fabricated on the randomly immobilized DNA molecules on APS coated SiO_2 is used [18].

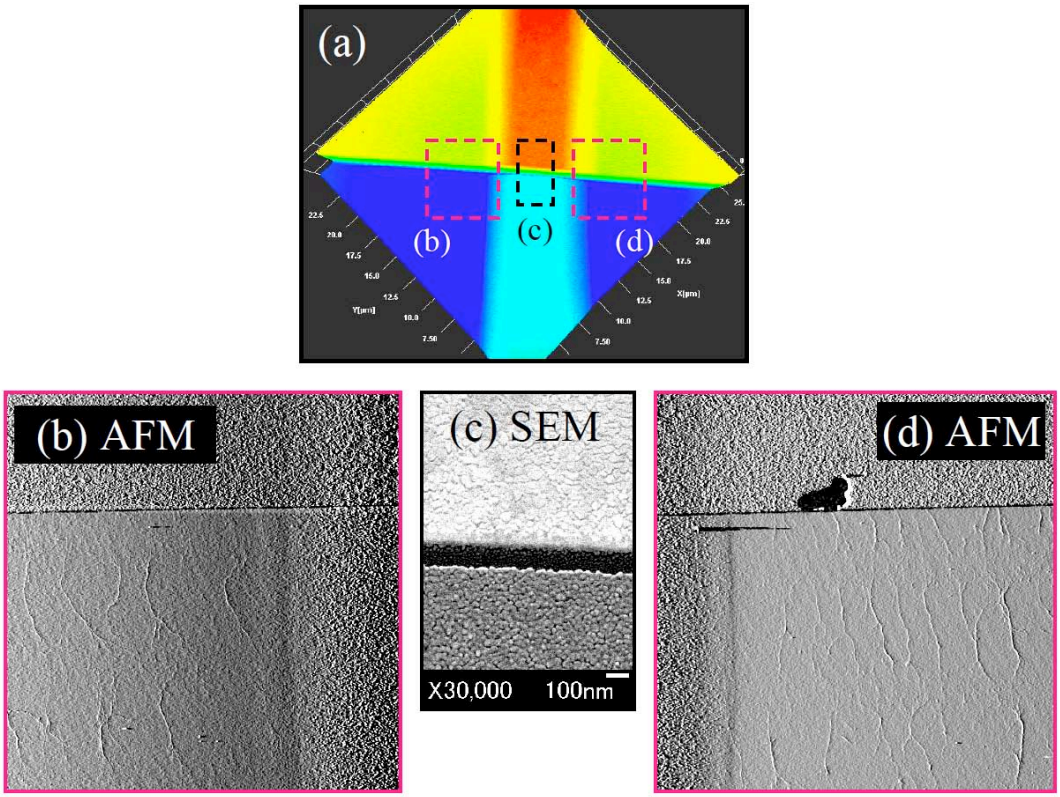

Figure 4-7
AFM and SEM image of sample structure around top-contacted geometry type nanogap electrode. (a) shows the 3D image obtained by AFM. (b),(c) and (d) shows the magnified image at the area noted in (a). (b) and (d) are topography by AFM, and (c) is SEM image of nanogap between electrodes.

The current level of randomly immobilized DNA is larger than that of bundled DNA, but the calculated J and ρ indicate about three orders magnitude each other.

These results indicate that the conduction path along randomly immobilized DNA is unclear, which is noted at the first part in this section. This is because it is quite difficult to observe the isolated DNA molecules for the randomly immobilized DNA (Figure 4-8 (a)), it is conceivable the surface is covered with DNA molecules all over. That is, the structure of DNA would be the mixture of bend and straight DNA molecules, and electrical conduction would occur along straight DNA molecules. Therefore, the estimated value in J and ρ of randomly immobilized DNA is overestimated. On the other hand, it is possible to calculate the value for bundled DNA molecules (Figure 4-8 (b)) because the number of straight DNA molecules is estimated.

Furthermore, this result was compared to the previously reported results. Table 4-3 shows the list of four kinds of results. [19-21] All results report the electrical conductivity measurements of lambda DNA molecules. In order to compare there results form various kind of parameters, kind of electrode geometry, electrode size, counter ion, buffer and electrical property are also listed.

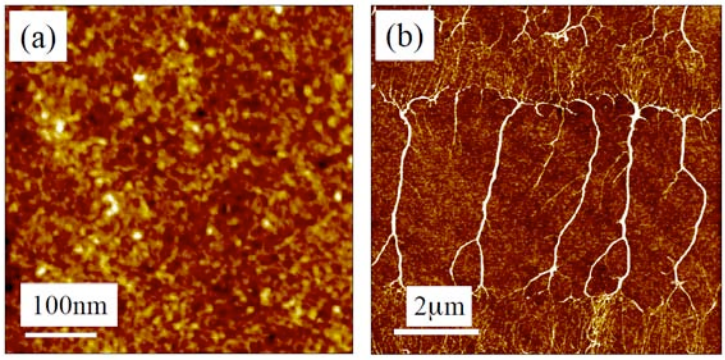

Figure 4-8
AFM image of DNA molecules on the substrate. (a) and (b) shows the randomly immobilized DNA on APS coated SiO_2 and bundled DNA on the patterned SiO_2, respectively.

	I (fA @1V)	J (A/m^2)	ρ (Ω・m)
Randomly immobilized DNA	202	4.1	3.0×10^6
Patterned DNA	85.2	3.3×10^3	3.6×10^3

Table 4-2
The comparison of current, current density and resistivity between randomly immobilized DNA and patterned DNA.

Comparing the type of electrode geometry, No,1 used the bottom-contacted geometry type electrode, whereas other used the top-contacted geometry type electrode. Even if nanogap separated 40 nm is used, No,1 reported electrical property is insulative. Next, in the top-contacted geometry electrode group, No,2 and No,4, this is my results, reported electrical property is conductive, but that of No,3 is insulative. Then comparing the counter ion, No,2 and No,4 used the $MgCl_2$, but No,3 didn't. Hence, it can be found out that both of the structure and presence of magnesium ion affect the DNA conductivity.

Next, the effect of structure of DNA is discussed. Previous results of the electrical measurements by top-contacted geometry type nanogap electrode separated less than 20nm shows that DNA is conductive (Figure 1.2-7, 1.2-13 and description related them). As DNA molecules are fixed on the electrode for top-contacted geometry type electrode, it is conceivable that DNA molecules bridge electrode and bend at the edge of electrode. If very small nanogap were used, the structural bending would be smaller, compared to the large nanogap (more than 40nm), hence electrical charge transport is emerged.

As for the effect of magnesium ion, previous theoretical calculation predict the formation of localized state of magnesium ion and it cause the electrical doping to the π^* state of base molecules due to the small energy gap between localized state and π^* state (~62 meV) [22]. In case the sodium ion is used, the localized state is formed as well, but the energy gap is bigger than that of magnesium ion (~500 meV). Moreover, previous study showed the effect of counter ions both of magnesium and sodium (chapter 3.3). Comparing the electrical properties, it is measured the resistance of DNA with magnesium ion is lower than that of DNA with sodium ion. Therefore, these results noted above indicate that the magnesium ion acts as electrical dopant.

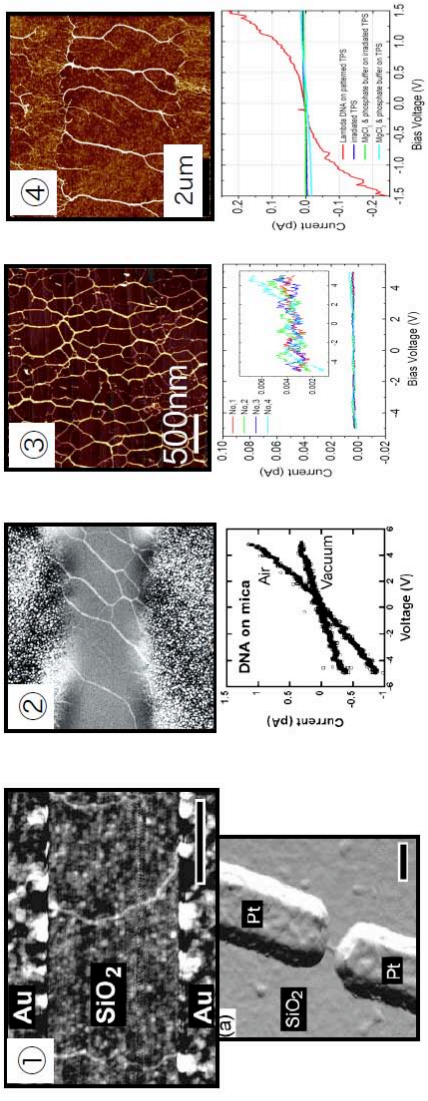

	① Strom et al. (2001, APL)	② Zhou et al. (2003, Nano Lett.)	③ Otsuka et al. (2004, Nanotech)	④ This result
DNA	λDNA, Isolated	λDNA Bundled	λDNA Bundled	λDNA Bundled
Electrode	Bottom Contact	Top Contact	Top Contact	Top Contact
Gap Size (nm)	40, 300	1000	65	83
Buffer	HEPES 20mM	Tris 10mM EDTA 1mM	Tris 1.25mM EDTA 0.13mM	Phosphate 100mM
Counter Ion	Mg^{2+}, 5mM	Mg^{2+}, 11mM	Dialyzed	Mg^{2+}, 100mM
Conductivity	Insulative	13 TΩ	Insulative	$3.6\times10^{3}\,\Omega\cdot m$

Table 4-3
List of four kinds of results. Electrical properties of lambda DNA are measured for all results. The kind of electrode geometry, electrode size, counter ion, buffer and electrical property are also listed.

4.4. Conclusion

The new method to immobilize straight DNA molecules on the substrate is developed. The patterned surface with hydrophobic / hydrophilic area enables us to control the structure of DNA on the surface. DNA molecules are immobilized on the hydrophilic surface randomly by electrostatic interaction, while straight and bundled DNA molecules are immobilized on the hydrophobic surface. Because the hydrophilic surfaces act as the "bounding DNA part", it is possible to immobilize DNA on the hydrophobic surface that has no interaction with DNA. The heights of bundles are almost same and about 7 molecules are estimated to be included.

The advantage in this sample fabrication method is that it is possible to measure the electrical properties of DNA undesirable residues such as buffers and counter ions and calculate the resitivity. The electrical measurements by top-contacted geometry electrodes show the charge transport along DNA is occurred. The I-V characteristics and time course of current indicate the same tendency as previous results of randomly immobilized DNA. The calculation of resistivity indicated the value of straight DNA molecules is $3.6\times10^{3}\ \Omega\cdot m$, and that of randomly immobilized DNA is overestimated because the conduction path cannot be decided precisely.

References

[1] H. Nakao, M. Gad, S. Sugiyama, K. Otobe, T. Ohtani, *J. Am. Chem. Soc.* **125**, 7162 (2003).
[2] J. Li, C. Bai, C. Wang, C. Zhu, Z. Lin, Q. Li, E. Cao, *Nucl. Acid. Res.* **4785** (1998).
[3] K.J. Kwak, H. Kudo, M. Fujihira, *Ultramicroscopy* **97**, 249 (2003).
[4] H. Yokota, F. Johnson, H. Lu, R.M. Robinson, A.M. Belu, M.D. Garrison, B.D. Ratner, B.J. Trask, D.L. Miller, *Nucl. Acid. Res.* **25**, 1064 (1997).
[5] X. Michalet, R. Ekong, F. Fougerousse, S. Rousseaux, C. Schurra, N. Hornigold, M.V. Slegtenhorst, J. Wolfe, S. Povey, J.S. Beckmann, A. Bensimon, *Science* **277**, 1518 (1997).
[6] A. Bensimon, A. Simon, A. Chiffaudel, V. Croquette, F. Heslot, D. Bensimon, *Science* 265, 2096 (1994).
[7] D. P. Allison, T. Thundat, K.B. Jacobson, L.A. Bottomley, R.J. Warmack, *J. Vac. Sci. Technol. A* **11**, 816 (1993).
[8] B. Oliveira, A. M. Chiorcea, *Langmuir* **19**, 3830 (2003).
[9] H. Nakao, H. Hayashi, T. Yoshino, S. Sugiyama, K. Otobe, T. Ohtani, *Nano Lett.* **2**, 475 (2002).
[10] D.A. Stenger, J.H. Georger, C.S. Dulcey, J.J. Hickman, A.S. Rudolph, T.B. Nielsen, S.M. McCort, J. M. Calvert, *J. Am. Chem. Soc.* **114**, 8435 (1992).
[11] W.J. Dressick, J.M. Calvert, *Jpn. J. Appl. Phys.* **32**, 5829 (1993).
[12] C.S. Dulcey, J.H. Georger, Jr., M.-S. Chen, S.W. McElvany, C.E. O'Ferrall, V.I. Benezra, J.M. Calvert, *Langmuir* **12**, 1638 (1996).
[13] M. Ishida, M. Kasuga, T. Kaneko, T. Shimoda, *Jpn. J. Appl. Phys.* **39**, L227 (2000).
[14] Y. Masuda, W.S. Seo, K. Koumoto, *Thin Solid Films* **382**, 183 (2001).
[15] Y. Masuda, W.S. Seo, K. Koumoto, *Solid State Ionics* **172**, 283 (2004)
[16] M.R. Alexander, G.E. Thompson, G. Beamson, *Surf. Interface Anal.* **29**, 468 (2000).
[17] R. Walsh, *Acc. Chem. Res.* **14**, 246 (1981).
[18] Please see chapter 3.3
[19] A.J. Storm, J. van Noort, S. de Vries, C. Dekker, *Appl. Phys. Lett.* **79**, 3881 (2001).
[20] Y.X. Zhou, A.T. Johnson, J. Hone, W.F. Smith, *Nano Lett.* 3, **1371** (2003).
[21] Y. Otsuka, Y. Naitoh, T. Matsumoto, W. Mizutani, H. Tabata, T. Kawai, *Nanotechnology* **15**, 1639 (2004).)
[22] R.G. Endres, D.L. Cox and R.R.P. Singh, *Rev. Mod. Phys.* **76**, 195 (2004).

Chapter5

Conclusion and Remark

The charge transport properties of DNA are studied by nanoscale electrical measurements. In case of electrical measurements with “electrode – DNA – electrode” configuration, different type of measurements can be employed. These are 1: top-contacted geometry type electrodes, 2: conductive probe AFM and 3: bottom-contacted geometry type electrodes. I have employed all measurements methods and measured the electrical properties of DNA.

In the chapter 1, introduction of the electrical property of DNA is noted. As the π-stacked base molecules along DNA are expected to be the conductive path, various results have been reported. However, different results that indicated the electrical properties of DNA vary from insulator to superconductor. Hence, it was shown that it is quite important to control parameters that affect electrical properties.

In the chapter 2, the development of nanoscale electrical measurement techniques is explained. Measurement techniques named PCI-AFM and the fabrication of bottom-contacted geometry type electrodes are developed. After they are developed, the electrical properties both of SWCNTs and porphyrin nanorods are measured by PCI-AFM and bottom-contacted geometry type electrodes, respectively. The results by PCI-AFM indicated the relationship between nanostructure and electrical conductivity along bundled SWCNTs. The results by bottom-contacted geometry type electrodes indicated the bending of nano-structured molecules at the edge of electrode in case top-contacted geometry type electrodes were employed would cause insulative properties.

In the chapter 3, the electrical properties of DNA measured by different methods were noted. The electrical properties measured by both of bottom-contacted geometry type electrodes and PCI-AFM indicated insulative characteristics of DNA. On the other hand, the results by top-contacted geometry type electrodes indicated the charge transport phenomenon along DNA under vacuum condition. The resistance of DNA increased exponentially with increasing the distance between electrodes. Comparison of the degree of increase in resitance between different DNAs (lambda DNA, Poly(dA)-Poly(dT), Poly(dG-dC)$_2$, G-wire (SEQ1) and G-wire (SEQ2)) indicated the structural defect such as nick strongly affect electrical property.

The electrical measurements at different temperatures also indicate the possible electrical conduction mechanism of DNA. It is suggested that the electrical conductivity originates from the localized conductive carrier along DNA, and this would be supported by the DFT

calculation. Moreover, the electrical property of G-wire is also studied for the first time. The electrical conduction mechanism is similar to that of double-stranded DNA, but the value of resistance is about 5 times lower than lambda DNA. This would be due to the expanded and delocalized conductive path along G-wire as shown in the calculation results.

Therefore, these results suggested that the electrical measurement of DNA requires the special care to minimize the structural deformation for electrical connection between DNA and electrodes.

In the chapter 4, the new method to immobilize straight and bundled DNA molecules on the hydrophobic surface is developed in order to measure the electrical properties of DNA without undesirable residues such as buffers and counter ions and calculate the resistance. The electrical measurements by top-contacted geometry type electrodes show that the charge transport along DNA is occurred. The I-V characteristics and time course of current indicate the same tendency as results of randomly immobilized DNA (Chapter 3). The calculation of resistivity indicated the value of straight DNA molecules is $3.6\times10^{3}\,\Omega\cdot$m, and that of randomly immobilized DNA is overestimated because of the conduction path cannot be decided precisely.

In all studies, I have studied the electrical properties of different DNA through different nanoscale electrical measurement methods. The results indicated that it is possible to measure the electrical conductivity along DNA under the condition that both of the structural deformation is prevented and electrical contacts is formed to DNA. The study of the conduction mechanism indicated the formation of conductive carriers by counter ions and they are transported through the localized state along DNA between electrodes by 3 types of mechanism. Moreover, the control of immobilization of DNA on the surface made it possible to calculate the electrical resistivity of DNA quantitatively.

Chapter6

Appendix 1

Direct Immobilization and Elongation of DNA on Sapphire Substrate

6.1. Introduction

The immobilization of DNA molecules on sapphire substrate treated with acid solution has been studied. The enhancement of adsorbed DNA molecules on treated surface was observed by atomic force microscopy, and we found that the concentration of solution affect the structure of DNA on surface. The increase of hydroxyl groups on acid treated sapphire surface is confirmed with infrared spectrum and contact angle measurements. Furthermore, we employed the APS coated glass substrate in order to verify the effectiveness of acid treatment. The fluorescence microscopy observation of DNA adsorbed on sapphire surface show the almost same data as that of APS treated one. This simple method is quite useful for applications such as structural observation of DNA molecules and DNA electronics.

6.2. Experimental

DNA is a functional molecule composed of four bases, sugars and phosphates. As DNA contains hereditary information for biological phenomenon such as disease, structure of DNA [1–3] and its complexes with biological molecules have been observed by scanning probe microscopy [4-7]. While as base molecules inside double helix form stacked structure, charge transport properties have been extremely studied [8-20] and it is controversial. This is because it is very important and difficult to measure the electrical characteristics under the condition that the structure of DNA is retained. Moreover, DNA has been proposed to use as a metallization template [8, 21-29].

When we study the structure of DNA and its complex or its electrical properties, it is important to immobilize or elongate DNA onto the atomically flat substrate in order to eliminate the effect of substrate structure. [30-38] Immobilization of DNA is well studied so far. Mica, glass, Au and HOPG are frequently used as substrates. Although Mica and HOPG can be cleaved very easily to obtain the atomically flat surface, additional cations such as magnesium or nickel ions are usually needed to fix the molecule on the surface [4, 39]. Glass substrate also needs surface modification. For instance, APS is used to immobilize DNA. As APS covers the glass surface and form positively charged surface with amino groups, DNA, which contains negative charged phosphate groups around double helix, adsorb on it with electrostatic force. Au surface can be used for thiol-terminated DNA because it forms covalent bond between Au and thiol group.

We herein report the simple immobilization and elongation method of DNA on sapphire (α -Al2O3 (0001)) substrate without chemical surface modification with other molecule such as APS treatment. The surface hydrophilicity of the substrate was improved by the enhancement of hydroxyl groups after treatment with acid solution. This simple method for cleaning sapphire substrate results in enhancement of immobilization and elongation of DNA. The sapphire contains some advantages compared to other substrate such as mica, glass and HOPG. 1) It is well established to get the atomically flat surface by thermal annealing in air. 2) The surface is very stable even at atmospheric condition. 3) Optically transparent for visible light. 4) Electrically insulator. 5) It is possible to get single crystals of high quality at a relatively low price due to its industrial use such as SAW elements. Therefore, there are a lot of potential for practical applications.

Sapphire substrate (shinkosya) used in this study was prepared as follows. Substrate was etched in boiling H_3PO_4 and rinsed with MilliQ. Then the substrate was annealed at 1200 ℃ for 1 hour in air in order to make the atomically smooth surface. [39-42] The surface of sapphire shows atomically flatted step structure after annealing treatment. The stepped substrate was then immersed in boiling acid solution (H_2O : HCl : H_2O_2 = 43 : 5 : 2) for 5 min and rinsed with MilliQ. Figure 6-1 shows the surface structure observed by atomic force microscopy (Nanoscope IV, DI Instruments) after the acid treatment. Notice that the stepped structure without structural change was measured after acid treatment.

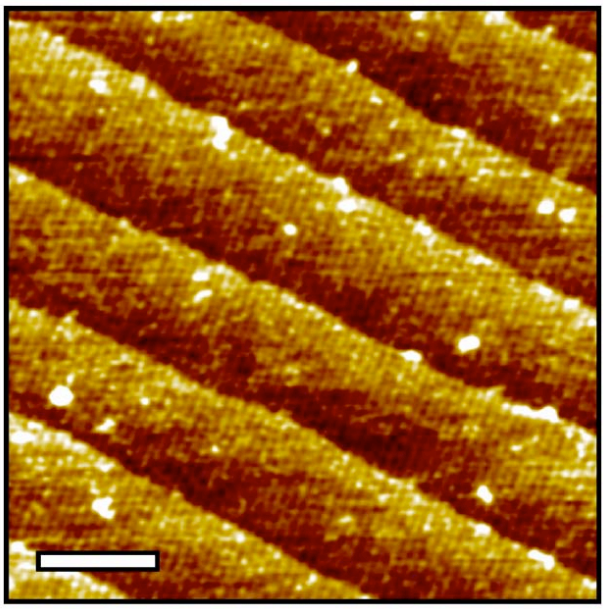

Figure 6-1.
AFM image of atomically smooth sapphire surface treated with acid solution. The scale bar shown inset is 100 nm.

For DNA immobilization and elongation, Lambda DNA solution (Takara corp.) was dropped on the substrate and the surpass solution was blown up by nitrogen gas after 1 min of adsorption time. The pressure of gas flow was controlled to be about 0.1 MPa, and the angle of flowing was about 45 degree against the surface. [31] DNA solution was dialyzed overnight before use. For comparison, we have employed substrates with and without acid treatment. Figure 6-2 shows the AFM images of the DNA immobilized on surface at varied DNA concentration. Figure 6-2 (a) and (b) show the results using acid treated substrate, and (c) shows the result using as annealed treatment. At low concentration of solution (3 μg /ml), isolated DNA molecules are elongated and immobilized on the surface (Figure 6-2 (a)). Furthermore, under high concentration condition (400 μg/ml), network-structured DNA molecules are observed (Figure 6-2 (b)). On the contrary, even under the high concentration as same as Figure 6-2 (b), only a few elongated DNA molecules were remained on the no-acid treated substrate (Figure 6-2 (c)).

These results indicated that DNA was strongly adsorbed on the surface with acid treatment and the structure of adsorbed DNA can be controlled by changing the concentration of solution. On the other hand, only a few DNA molecules were observed on the sapphire surface without acid treatment.

In order to study the effect of acid treatment to DNA immobilization and elongation in detail, infrared spectrum and contact angle with three kinds of solvent were measured. Figure 6-3 shows the difference infrared spectrum between before and after acid treatment. The

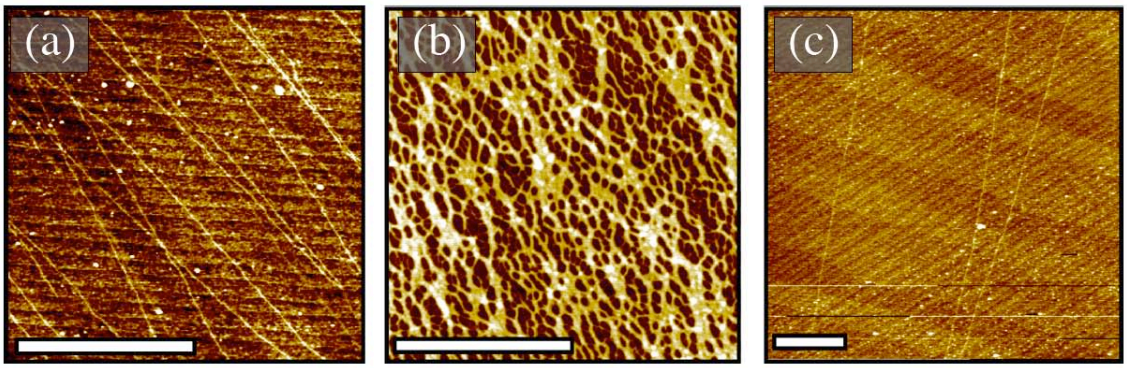

Figure 6-2
AFM images of the DNA on the acid treated sapphire substrate. (a) Elongated DNA molecules under low concentration condition. (b) network-structured DNA under high concentration condition (c) only a few stretched DNA molecules on the no-acid treated substrate under high concentration condition. The scale bars shown inset are 1 μm, respectively.

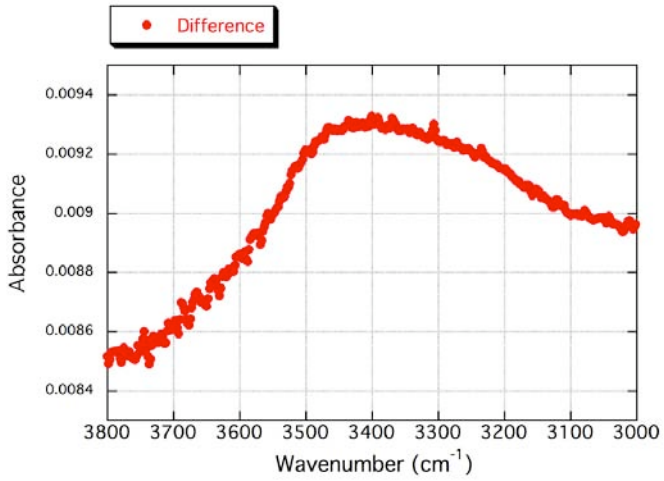

Figure 6-3
Difference spectrum of infrared ray measurements between before and after acid treatment. The absorbance peak at about 3500 cm^{-1} was measured which is attributed to the hydroxyl groups on the surface.

absorbance peak at about 3500 cm^{-1} was measured and this indicates the increase of associated hydroxyl groups on the surface. [43] This is corresponding to the previous results that showed the structural change occurred from Al-O-Al to Al-O-H. [44] We have tried to measure the spectrum originate in the phosphate groups of DNA molecules in order to study the detailed origin, but the signal was too small to detect.

Moreover, contact angle of sapphire substrate with water, diiodomethane and hexadecane was measured by sessile drop method in order to measure the surface energy (Kyowa interface science co., ltd.). The atmospheric temperature was kept to be 25 degree and the humidity was kept to be 40 %. Contact angle measurement with water, diiodomethane and hexadecane was averaged to be 5.8, 37.5 and 16.5 degree, respectively. The surface free energy was calculated according to the Young-Dupre equation and extended Fowkes equation. [45]

$$W_{sl} = \gamma_l\left(1+\cos\theta_{sl}\right)$$

$$W_{sl}/2 = \left(\gamma_s^d \cdot \gamma_l^d\right)^{1/2} + \left(\gamma_s^p \cdot \gamma_l^p\right)^{1/2} + \left(\gamma_s^h \cdot \gamma_l^h\right)^{1/2}$$

where γ_s and γ_l are surface energy of solid and liquid, respectively. The superscripts noted as *d*, *p* and *h* show the component of dispersion force, dipole interaction and hydrogen bond.

As shown in the Table 6-1, the chemically treated surface energies due to the component of dispersion force, dipole interaction and hydrogen bond were estimated to be 26.5, 26.8 and 35.8, respectively. Therefore, the total surface energy was estimated to be about 89.0. On the

other hand, the surface energies without treatment were estimated to be 27.4, 6.4 and 36.0, respectively. And the total surface energy was 69.8. This result indicates that the surface free energy was increased quantitatively due to the component of dipole interaction.

These measurements indicate that the surface was covered with associated hydroxyl groups due to both of the structural change and the removal of contaminants by acid treatment, and the surface energy was increased due to dipole interaction between hydroxyl groups. Therefore, the mechanism of immobilization might be due to the hydrogen bonds between hydroxyl groups on the surface and phosphate groups of DNA. As previous study indicated the octadecylphosphonic acid reacts strongly with sapphire surface to form a bulk (aluminoalkyl) phosphate, the Al-O-P bond may also be formed in our results. [46]

	Surface energy (mN/m)			
	Dispersion force	Dipole interaction	Hydrogen bond	Total
With treatment	26.5	26.8	35.8	89.1
Without treatment	27.4	6.4	36	69.8

Table 6-1

Surface energy of sapphire substrate both of untreated and treated with acid solution.

In order to verify the effectiveness of the acid treatment, we employed the APS coated glass substrate (Matsunami glass corp.). The APS treatment is widely used for immobilization of DNA molecules on the surface. As APS coated glass is covered with positively charged amino groups, DNA, which contains negative charged phosphate groups around double helix, adsorb on it with electrostatic force.

200 μl of lambda DNA solution (80 ng/μl) was mixed with 1ul of 1mM YO-PRO1 (Y-3603, Molecular probes inc.). The solution (20 μl) was deposited on both of the acid treated substrate and APS coated grass. Then the surplus solution was blown up by nitrogen gas within 1 minute of adsorption time and the fluorescence image was observed by optical microscopy (Olympus).

Figure 6-4 shows the results. Fluorescence images of DNA molecules on both of APS coated glass and acid treated sapphire substrate indicated that DNA was immobilized and elongated on the surfaces. It should be noted that the amount of DNA adsorbed on the sapphire substrate was almost same as the APS coated glass, although no chemical modification was

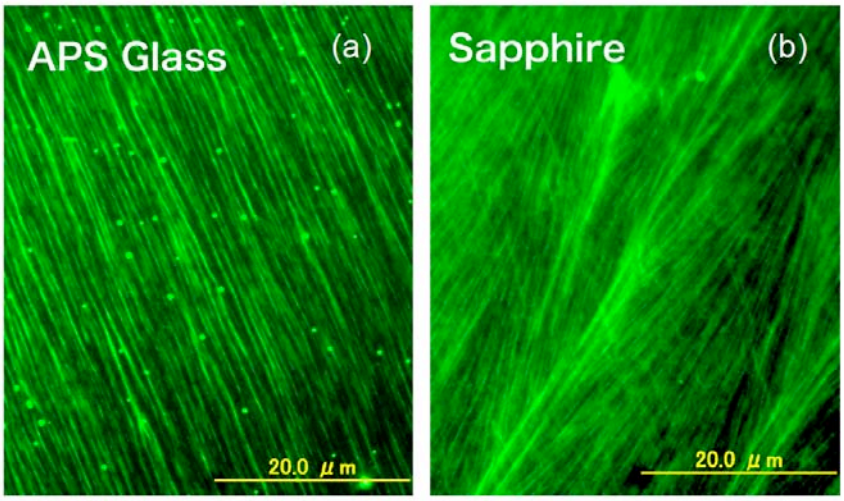

Figure 6-4
Fluorescence images of DNA molecules immobilized on (a) APS coated glass and (b) acid treated sapphire substrate.

performed.

In conclusion, we have immobilized and stretched DNA molecules on the atomically flat sapphire substrate by very simple treatment with acid solution. The treatment of surface with acid solution indicated the increased hydrophilicity and this would cause the enhancement in DNA immobilization onto the surface with hydrogen bond. As the structural deformation will be minimized due to the atomically flat surface and the sapphire substrate is optically transparent in the visible rays range and electrically insulative, this simple method will be useful as basic sample preparation technique for observation of DNA or its complex with such as proteins, and electrical transport measurements.

References

[1] J. M. Kim, T. Ohtani, S. Sugiyama, T. Hirose, H. Muramatsu, *Anal. Chem.* **73**, 5984 (2001).
[2] D.P. Allison, T. Thundat, K.B. Jacobson, L.A. Bottomley, R.J. Warmack, *J. Vac. Sci. Technol. A*, **11**, 816 (1993).
[3] A.M.O. Brett, A.M. Chiorcea, *Langmuir* **19**, 3830 (2003).
[4] X. Li, J. Sun, X. Zhou, G. Li, P. He, Y. Fang, M. Li, J. Hu, *J. Vac. Sci. Technol. B* **21**, 1070 (2003).
[5] L.I. Pietrasanta, B.L. Smith, M.C. MacLeod, *Chem. Res. Toxicol.* **13**, 351 (2000).
[6] A.T. Woolley, C. Guillemette, C.L. Cheung, D.E. Housman, C.M. Lieber, *Nature Biotechnology* **18**, 760 (2000).
[7] K. Uemura, J. Komatsu, T. Uchihashi, N. Choi, S. Ikawa, T. Nishinaka, T. Shibata, Y. Nakayama, S. Katsura, A. Mizuno, H. Tokumoto, M. Ishikawa, R. Kuroda, *Biochem. Biophys. Res. Comm.* **281**, 390 (2001).
[8] E. Braun, Y. Eichen, U. Sivan, G. Ben-Yoseph, *Nature* **391**, 775 (1998).
[9] H.W. Fink, C. Schenberger, *Nature* **398**, 407 (1999).
[10] D. Porath, A. Bezryadin, S.D. Vries, C. Dekker, *Nature* **403**, 635 (2000).
[11] P. Tran, B. Alavi, G. Gruner, *Phys. Rev. Lett.* **85**, 1564 (2000).
[12] P.J. de Pablo, F.M Herrero, J. Colchero, J.G. Herrero, P. Herrero, A,M, Baró, P. Ordejón, M.S. Soler, E. Artacho, *Phys. Rev. Lett.* **85**, 4992 (2000).
[13] L.T. Cai, H. Tabata, T. Kawai, *Appl. Phys. Lett.* **77**, 3105 (2002).
[14] A.Y. Kasumov, M. Kociak, S. Guéron, B. Reulet, V.T. Volkov, D.V. Klinov, H. Bouchiat, *Science* **291**, 280 (2001).
[15] A.J. Strom, J.V. Noort, S.D. Vries, C. Dekker, *Appl. Phys. Lett.* **79**, 3881 (2001).
[16] K.H. Yoo, D.H. Ha, J.O. Lee, J.W. Park, J. Kim, J.J. Kim, H. Lee, T. Kawai, H. Choi, Y. Wa, *Phys. Rev. Lett.* **87**, 198102 (2001).
[17] H. Watanabe, C. Manabe, T. Shigematsu, K. Shimotani, M. Shimizu, *Appl. Phys. Lett.* **79**, 2462 (2001).
[18] J. Gu, S. Tanaka, Y. Otsuka, H. Tabata, T. Kawai, *Appl. Phys. Lett.* **80**, 688 (2002).
[19] J.S. Hwang, K.J. Kong, D. Ahn, G.S. Lee, D.J. Ahn, S.W. Hwang, *Appl. Phys. Lett.* **81**, 1134 (2002)).
[20] Y. Zhang, R.H. Austin, J. Kraeft, E.C. Cox, N.P. Ong, *Phys. Rev. Lett.* **89**, 198102 (2002).
[21] H. Nakao, H. Shiigi, Y. Yamamoto, S. Tokonami, T. Nagaoka, S. Sugiyama, T. Ohtani, *Nano Lett.* **10**, 1391 (2003).
[22] C.F. Monson, A.T. Woolley, *Nano Lett.* **3**, 359 (2003).
[23] J. Richter, M. Mertig, W. Pompe, I. Mönch, H.K. Schackert, *Appl. Phys. Lett.* **78**, 536 (2002).
[24] J. Richter, R. Seidel, R. Kirsch, M. Mertig, W. Pompe, J. Plaschke, H.K. Schackert, *Adv. Mater.* **12**, 507 (2000).
[25] W.E. Ford, O. Harnack, A. Yasuda, J.M. Wessels, *Adv. Mater.***13**, 1793 (2002).
[26] M. Mertig, C. Ciacchi, R. Seidel, W. Pompe, A. De Vita, *Nano Lett.* **2**, 841 (2002).
[27] A. Kumar, M. Pattarkine, M. Bhadbhade, A.B. Mandale, K.N. Ganesh, S.S. Datar, C.V. Dharmadhikari, M. Sastry, *Adv. Mater.* **13**, 341 (2001).
[28] M. Sastry, A. Kumar, S. Datar, C.V. Dharmadhikari, K.N. Ganesh, *Appl. Phys. Lett.* **78**, 2943 (2001).
[29] Harneck, W.E. Ford, A. Yasuda, J.M. Wessels, *Nano Lett.* **2**, 919 (2002).
[30] H. Nakao, M. Gad, S. Sugiyama, K. Otobe, T. Ohtani, *J. Am. Chem. Soc.* **125**, 7162 (2003).
[31] J. Li, C. Bai, C. Wang, C. Zhu, Z. Lin, Q. Li, E. Cao, *Nucl. Acid. Res.* **4785** (1998).
[32] K.J. Kwak, H. Kudo, M. Fujihira, *Ultramicroscopy* **97**, 249 (2003).
[33] H. Yokota, F. Johnson, H. Lu, R.M. Robinson, A.M. Belu, M.D. Garrison, B.D. Ratner, B.J. Trask, D.L. Miller, *Nucl. Acid. Res.* **25**, 1064 (1997).
[34] X. Michalet, R. Ekong, F. Fougerousse, S. Rousseaux, C. Schurra, N. Hornigold, M.V. Slegtenhorst, J. Wolfe, S. Povey, J.S. Beckmann, A. Bensimon, *Science* **277**, 1518 (1997).
[35] A. Bensimon, A. Simon, A. Chiffaudel, V. Croquette, F. Heslot, D. Bensimon, *Science* **265**, 2096 (1994).
[36] D. P. Allison, T. Thundat, K.B. Jacobson, L.A. Bottomley, R.J. Warmack, *J. Vac. Sci. Technol. A* **11**, 816 (1993).

[37] B. Oliveira, A. M. Chiorcea, *Langmuir* **19**, 3830 (2003).
[38] H. Nakao, H. Hayashi, T. Yoshino, S. Sugiyama, K. Otobe, T. Ohtani, *Nano Lett.* **2**, 475 (2002).
[39] S. Tanaka, L.T. Cai, H. Tabata, T. Kawai, *Jpn. J. Appl. Phys.* **40**, L407 (2001).
[40] L.P. Van, O. Kurnosikov, J. Cousty, *Surf. Sci.* **411**, 263 (1998).
[41] M. Yoshimoto, T. Maeda, T. Ohnishi, H. Koinuma, O. Ihiyama, M. Shinohara, M. Kubo, R. Miura, A. Miyamoto, *Appl. Phys. Lett.* **67**, 2615 (1995).
[42] J.R. Heffelfinger, M.W. Bench, C.B. Carter, *Surf. Sci.* **370**, 168 (1997).
[43] Kurnosikov, L. Pham Van, J. Cousty, *Surf. Sci.* **459**, 256 (2000)
[44] D.B. Mawhinney, J.A. Rossin, K. Gerhart, J.T. Yates Jr., *Langmuir* **16**, 2237 (2000).
[45] M.R. Alexander, G.E. Thompson, G. Beamson, *Surf. Interface Anal.* **29**, 468 (2000).
[46] W. Gao, L. Dickinson, C. Grozinger, F.G. Morin, L. Reven, *Langmuir* **12**, 6429 (1996).

Chapter7

Appendix 2

“Profiles of Achievements”

Oral Presentations (International Meeting)

1, "Nanoscale Electrical Characterization techniques for molecular nanoelectronics"
21st COE Student Seminar 2003 (Finland, Tempare and Turku Univ., Finland)
January 2004
Yoichi Otsuka

2, "Fabrication of Nano-gap Electrodes Without Lithography Technique & Electrical Characteristics of Nano- Structured Molecules"
APS March Meeting (Montreal, Canada)
March 2004
Yoichi Otsuka, Takuya Matumoto, Hitoshi Tabata, Tomoji Kawai,
Yasuhisa Naitoh, Wataru Mizutani

3, "Fabrication Method of Nano-gap Electrodes without Wet Process and Electrical Measurement of Nano-structured Molecules"
8th International Conference on Nanometer-Scale Science and Technology
June, 2004 (Venice, Italy)
Yoichi Otsuka, Takuya Matumoto, Hitoshi Tabata, Tomoji Kawai,
Yasuhisa Naitoh, Wataru Mizutani

4, "A Simple Fabrication Method of Nanogap Electrodes for Top-Contacted Geometry: Application to Porphyrin Nanorods and a DNA Network"
The 12th International Colloquium on Scanning Probe Microscopy
December, 2004 (Atagawa, Japan)
Y. Otsuka, Y. Naitoh, T. Matsumoto, W. Mizutani, H. Tabata and T. Kawai

5, "Structure and electrical property of DNA molecules immobilized on the patterned self-assembled monolayers,"
APS March Meeting 2005 (Los Angeles, USA)
March, 2005
Yoichi Otsuka, Kaoru Ojima, Takuya Matsumoto, Hitoshi Tabata, Tomoji Kawai

6, "Structure and electrical property of DNA molecules immobilized on the patterned hydrophobic / hydrophilic surface"
13th international Conference on Scanning Tunneling Microscopy / Spectoscopy and Related Techniques (Sapporo, Japan)
July, 2005
Yoichi Otsuka, Kaoru Ojima, Takuya Matsumoto, Hitoshi Tabata, Tomoji Kawai

Poster Presentation (International Meeting)

1, "Atomospheric effect on the conductivity of DNA by using nano-gap electrode"
The 8th Workshop on Oxide Electronics
September, 2001
Yoichi Otsuka, Hea-Yeon Lee, Masateru Taniguchi, Jian-hua Gu, Jeory-O Lee、Kyung-Hwa Yoo, Hidekazu Tanaka, Hitoshi Tabata, Tomoji Kawai

2, “Tunneling junctions in bundled Single-walled Carbon Nanotubes by Point Contact Current imaging AFM Measurement”
7th International Conference on Nanometer-Scale Science and Technology
June, 2003
Yoichi Otsuka, Yasuhisa Naitoh, Takuya Matsumoto and Tomoji Kawai

3, ”Fabrication of Nano-gap Electrodes Without Lithography Technique and Electrical Characteristics of Nano Structured Molecules”
International Symposium on Scientific and Industrial Nanotechnology
December, 2003
Yoichi Otsuka, Yasuhisa Naitoh, Takuya Matsumoto, Wataru Mizutani, Hitoshi Tabata and Tomoji Kawai

4, “Measuring Electrical Conductivity of Molecules with Nano-gap Electrodes”
The 11th International Colloquium on Scanning Probe Microscopy
December, 2003
Yoichi Otsuka, Yasuhisa Naitoh, Takuya Matsumoto, Wataru Mizutani, Hitoshi Tabata and Tomoji Kawai

5, “Immobilization of DNA Molecules on the Patterned Self-assembled Monolayers and Electrical Properties of DNA molecules by Top-contacted Nanogap Electrodes”
International Symposium on Surface Science and Nanotechnology (Saitama, Japan)
November, 2005
Yoichi Otsuka, Takuya Matsumoto, Hitoshi Tabata, Tomoji Kawai

6, “Electrical Properties of DNA molecules by Top-contacted Nanogap Electrodes and Immobilization of DNA Molecules on the Patterned Self-assembled Monolayers”
2005 MRS Fall Meeting (Boston, USA)
November, 2005
Yoichi Otsuka, Takuya Matsumoto, Hitoshi Tabata, Tomoji Kawai

Published Paper (First author is indicated as underline part)

1, "Influence of Humidity on the Electrical Conductivity of Synthesized DNA film on Nanogap Electrode"
Jpn. J. Appl. Phys. **41**, 891 (2002).
Yoichi Otsuka, Hea-Yeon Lee, Jian-hua Gu, Jeory-O Lee, Kyung-Hwa Yoo, Hidekazu Tanaka, Hitoshi Tabata, Tomoji Kawai.

2, "Control of electrical conduction in DNA using oxygen hole doping"
Appl. Phys. Lett. **80**, 1670 (2002).
Hea-Yeon Lee, Hidekazu Tanaka, Yoichi Otsuka, Kyung-Hwa Yoo, Jeong-O Lee, Tomoji Kawai.

3, "Self-assembled dye-DNA network and its photoinduced electrical conductivity"
Appl. Phys. Lett. **80**, 688 (2002).
Jianhua Gu, Shin-ichi Tanaka, Yoichi Otsuka, Hitoshi Tabata, Tomoji Kawai.

4, "Electric Conductivity of Dye Modified DNA films with and without Light Irradiation in Various Humidities"
J. Appl. Phys. **92**, 2816 (2002).
Jianhua Gu, Shin-ichi Tanaka, Yoichi Otsuka, Hitoshi Tabata, Tomoji Kawai.

5, "Toward the DNA electronics"
Synthetic Metals **9480**,1 (2002).
Hitoshi Tabata, Lin Tao Cai, Jianhua Gu, Shin-ichi Tanaka, Yoichi Otsuka, Yutaka Sacho, Masateru Taniguchi, Tomoji Kawai.

6, "Point-contact current-imaging atomic force microscopy: Measurement of contact resistance between single-walled carbon nanotubes in a bundle"
Appl. Phys. Lett. **82**, 1944 (2003).
Yoichi Otsuka, Yasuhisa Naitoh, Takuya Matsumoto, Tomoji Kawai.

7, "A Nano tester: A new technique for nanoscale electrical characterization by point-contact current-imaging atomic force microscopy"
Jpn. J. Appl. Phys. **41**, L742 (2002).
Yoichi Otsuka, Yasuhisa Naitoh, Takuya Matsumoto, Tomoji Kawai.

8, "DNA エレクトロニクス"
表面科学 **24**, 677 (2003).
田畑仁、谷口正輝、田中裕行、大塚洋一、田中慎一、川合知二

9, "点接触電流イメージング原子間力顕微鏡の開発"
表面科学 **24**, 573 (2003).
大塚洋一、内藤泰久、寺脇歩、松本卓也、川合知二

10, "Humidity Dependence of Electrical Resistivity in Poly(dG)･Poly(dC) DNA Thin Film"
Jpn. J. Appl. Phys. **42**, 6629 (2003).
Masateru Taniguchi, Yoichi Otsuka, Hitoshi Tabata, Tomoji Kawai

11, “A simple fabrication method of nanogap electrodes fortop-contacted geometry: application to porphyrin nanorod and DNA network”
Nanotechnology **15**, 1639 (2004).
Yoichi Otsuka, Yasuhisa Naitoh, Takuya Matsumoto,
Wataru Mizutani, Hitoshi Tabata, Tomoji Kawai,

12, ”Conductance measurement of a DNA network in nanoscale by point contact current imaging atomic force microscopy”
Appl. Phys. Lett. **86** (2005) 113901.
Ayumu Terawaki, Yoichi Otsuka, HeaYeon Lee,
Takuya Matsumoto, Hidekazu Tanaka, and Tomoji Kawai

13, “Printing electrode for top-contact molecular junction”
Appl. Phys. Lett. **87**, 234110 (2005).
Kaoru Ojima, Yoichi Otsuka, Takuya Matsumoto, and Tomoji Kawai

Patent (in Japanese)

１，探針装置
発明者）松本卓也、大塚洋一、内藤泰久、川合知二
出願番号）特願 2002-245811

２，ナノギャップ電極の製造方法及び該方法により製造されたナノギャップ電極を用いた素子
発明者）内藤泰久、大塚洋一、松本卓也、川西祐司、水谷亘、田畑仁、川合知二
出願番号）特願 2003-412356

３，自己組織化材料または微粒子を基板上に固定化する方法、および当該方法を用いて作成した基板
発明者）川合知二、田畑仁、大塚洋一、山田郁彦、松本卓也
出願番号）特願 2004-381549

４，自己組織化材料を配列させた基板およびその作製方法
発明者）大塚洋一、川合知二
出願番号）特願 2005-080602

Grant (in Japanese)

2003　新世代研究所　海外派遣助成費
「原子間力顕微鏡によるナノスケール分子回路の電気伝導性測定」

2004　大阪大学産業科学研究所　21COE ナノマテリアル研究グループ学生セミナー 海外派遣助成

2005　(財)産業科学研究協会資金による海外派遣助成

2005~2006　学術振興会　特別研究員（ＤＣ２）